

ORIGINAL PAPER

Open Access



Re-description of the sauropod dinosaur *Amanzia* (“*Ornithopsis/Cetiosauriscus*”) *greppini* n. gen. and other vertebrate remains from the Kimmeridgian (Late Jurassic) Reuchenette Formation of Moutier, Switzerland

Daniela Schwarz^{1*} , Philip D. Mannion² , Oliver Wings³  and Christian A. Meyer⁴ 

Abstract

Dinosaur remains were discovered in the 1860's in the Kimmeridgian (Late Jurassic) Reuchenette Formation of Moutier, northwestern Switzerland. In the 1920's, these were identified as a new species of sauropod, *Ornithopsis greppini*, before being reclassified as a species of *Cetiosauriscus* (*C. greppini*), otherwise known from the type species (*C. stewarti*) from the late Middle Jurassic (Callovian) of the UK. The syntype of “*C. greppini*” consists of skeletal elements from all body regions, and at least four individuals of different sizes can be distinguished. Here we fully re-describe this material, and re-evaluate its taxonomy and systematic placement. The Moutier locality also yielded a theropod tooth, and fragmentary cranial and vertebral remains of a crocodylomorph, also re-described here. “*C. greppini*” is a small-sized (not more than 10 m long) non-neosauropod eusauropod. *Cetiosauriscus stewarti* and “*C. greppini*” differ from each other in: (1) size; (2) the neural spine morphology and diapophyseal laminae of the anterior caudal vertebrae; (3) the length-to-height proportion in the middle caudal vertebrae; (4) the presence or absence of ridges and crests on the middle caudal centra; and (5) the shape and proportions of the coracoid, humerus, and femur. These anatomical differences, combined with their discrepancy in stratigraphic age, make it unlikely that *C. stewarti* and “*C. greppini*” belong to the same genus, as also supported through our phylogenetic analysis. “*C. greppini*” cannot be assigned to any other contemporaneous sauropod taxon from Europe, but is diagnosed by an autapomorphic rugosity on the posteromedial margin of the humerus, as well as a unique combination of features. As such, we erect the new genus name *Amanzia* for the Swiss taxon “*Ornithopsis*” *greppini*, augmenting the growing diversity of Late Jurassic European sauropods. Our phylogenetic analysis places it outside of Neosauropoda, either as the sister taxon to that clade, or as a member of Turiasauria.

Keywords: Dinosauria, Neosauropoda, Late Jurassic, Switzerland, Mesozoic, Europe, Palaeontology

1 Introduction

Over the last 30 years, Switzerland has seen an impressive increase in dinosaur research (for reviews see: Meyer and Thüring 2003; Meyer and Marty 2014; Marty et al.

2017). Although the Late Jurassic record of Swiss dinosaur tracks has steadily grown, the record of dinosaur body fossils is still rather limited. Up to now, body fossil remains of theropods (teeth), stegosaurs, and sauropods are known, but most of these are fragmentary (e.g. Meyer and Lockley 1996; Meyer and Hunt 1998; Meyer and Thüring 2003). Among these Swiss body fossils, the finds documented herein are therefore exceptional.

Editorial handling: M.J. Benton.

*Correspondence: daniela.schwarz@mfn.berlin

¹ Museum für Naturkunde, Leibniz Institute for Evolution and Biodiversity Science, Invalidenstraße 43, 10115 Berlin, Germany

Full list of author information is available at the end of the article



© The Author(s) 2020. This article is licensed under a Creative Commons Attribution 4.0 International License, which permits use, sharing, adaptation, distribution and reproduction in any medium or format, as long as you give appropriate credit to the original author(s) and the source, provide a link to the Creative Commons licence, and indicate if changes were made. The images or other third party material in this article are included in the article's Creative Commons licence, unless indicated otherwise in a credit line to the material. If material is not included in the article's Creative Commons licence and your intended use is not permitted by statutory regulation or exceeds the permitted use, you will need to obtain permission directly from the copyright holder. To view a copy of this licence, visit <http://creativecommons.org/licenses/by/4.0/>.

In the 1860s, an accumulation of fossil reptilian bones was discovered in a limestone quarry in the Basse Montagne, near the city of Moutier, Bern, northwestern Switzerland (Fig. 1). The first bones appearing in the quarry had already been privately sold when the Swiss geologist Jean-Baptiste Greppin got notice of the find. Greppin recognized the material to be mostly dinosaurian, and saved the remaining bones for the Natural History Museum in Basel (Naturhistorisches Museum Basel [NMB]). Subsequently, he described and figured the bones as a faunal component of the “Virgulien” of the Jura Mountains in the region of Bern (Greppin 1870). The only mention of the original site can be found in his monograph where he stated (p. 339): , Le squelette entier de ce gigantesque reptile a été trouvé dans la carrière hypovirgulienne de la basse montagne de Moutier, d’où l’ on a retiré les pierres pour la construction du temple. Une grande partie de ce squelette bien curieux avec une dent bien conservée se trouve au Musée de Bâle“ [“The whole skeleton of this gigantic reptile was found in the “Hypovirgulien” of a quarry of the Basse Montagne of Moutier, from which the stones were removed for the construction of the temple. Much of this peculiar skeleton with a well-preserved tooth can be found at the Basel Museum”]. On the basis of a theropod tooth found with the material (Tables 1, 2), and in the context of the still poor knowledge about dinosaurs in the middle of the nineteenth century, Greppin

assigned all of the bones to the theropod dinosaur *Megalosaurus*, and erected the species “*Megalosaurus meriani*” in honour of one of the patrons of the NMB.

In 1920, Berlin vertebrate palaeontologist Janensch mentioned the theropod tooth from Moutier in his publication on the theropod dinosaur *Elaphrosaurus* from Tendaguru, Tanzania, and re-classified it as *Labrosaurus* (Janensch 1920). In a letter to Freiherr von Huene (Huene 1922), Janensch pointed out the sauropodian nature of the vertebrae figured by Greppin (1870). This stirred Huene’s interest and, invited by Hans Georg Stählin, the then director of the NMB, Huene examined and re-described the material from Moutier. Huene assigned the majority of the bones to the British sauropod genus *Ornithopsis* and named a new species “*Ornithopsis greppini*” (Huene 1922). Following Janensch (1920), Huene regarded the single theropod tooth as “*Labrosaurus meriani*” (Huene 1922, 1926), and identified four vertebrae from the material as belonging to a crocodylomorph (Huene 1922) (Table 2).

Some years later, Huene (1927a) erected the new genus *Cetiosauriscus* for the partial sauropod skeleton NHMUK (previously BMNH) R3078 (=“*Cetiosaurus leedsi*”, Woodward 1905). Huene also included “*Ornithopsis greppini*” in this new genus, thus re-combining the British and Swiss species as *Cetiosauriscus leedsi* and *Cetiosauriscus greppini*, respectively (Huene 1927a, b). Unfortunately, the

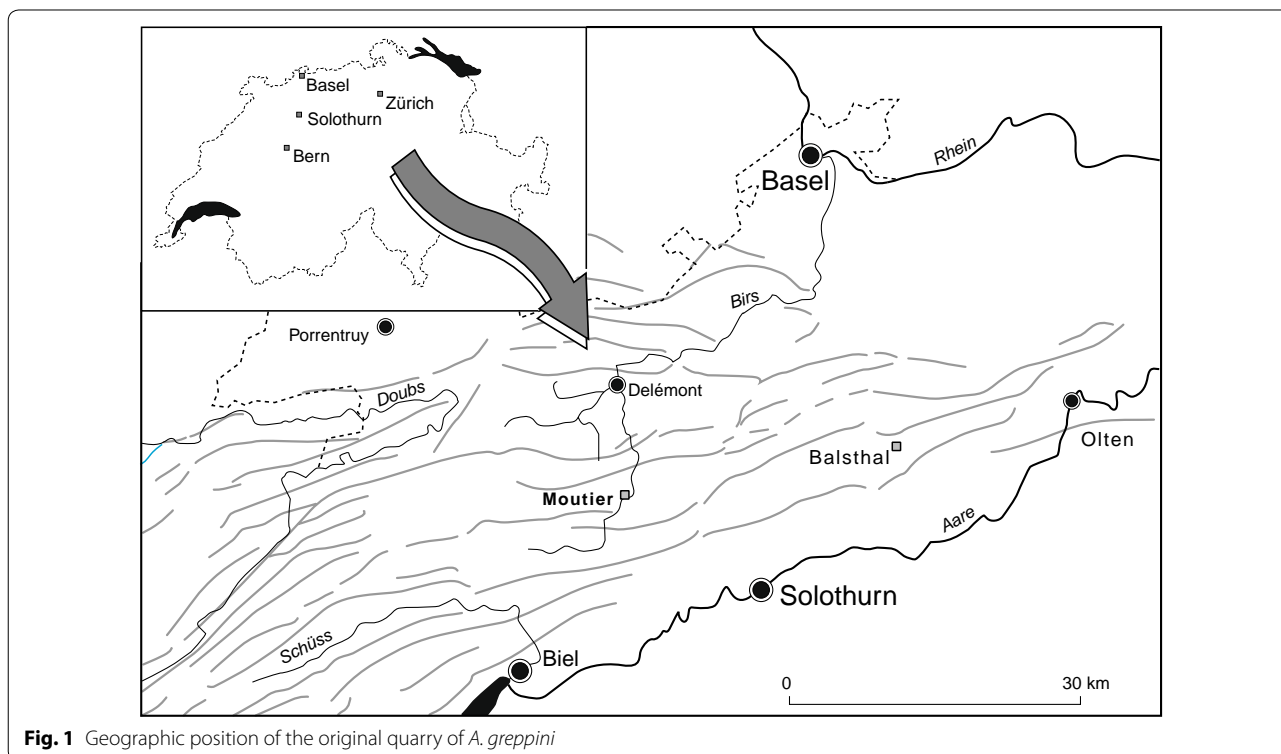


Fig. 1 Geographic position of the original quarry of *A. greppini*

Table 1 Complete list of material that can be assigned to *A. greppini*

Collection no.	Material	Assignment to type series	Previous mention	Individual	Annotations
M.H. 206	Bone fragment	No	None	Not assigned	None
M.H. 209	Bone fragment	No	None	Not assigned	None
M.H. 221	(8th) Caudal vertebra	No	None	Individual A	None
M.H. 235	Caudal vertebra	Syntype	Huene (1922: p. 82)	No assignment possible	17 cm long, 10 high, Bone is missing
M.H. 238	Caudal vertebra, mid-caudal region	No	None	Individual C	Bone fragment M.H. 357 was glued to this specimen in 2005
M.H. 239	Caudal vertebra, mid-caudal region	Syntype	Huene (1922: p. 82, fig. 5)	Individual C	None
M.H. 240	Caudal vertebra, mid-caudal region	No	None	Individual C	None
M.H. 241	Caudal vertebra	Syntype	Huene (1922: p. 82)	No assignment possible	12.5 cm long, 8.5 cm high, Bone is missing
M.H. 242	(17th) Caudal vertebra	No	None	Individual A	Pathologic, CT study performed in 2007
M.H. 243	Caudal vertebra, mid-caudal region	No	None	Individual D	None
M.H. 244	(27th) Caudal vertebra	No	None	Individual A	None
M.H. 245	(28th) Caudal vertebra	Syntype	Huene (1922: p. 82)	Individual A	None
M.H. 246	(Possibly fourth) metatarsal	Syntype	Huene (1922: p. 82, fig. 8)	Individual A	Determined as posterior caudal vertebra by Huene (1922)
M.H. 248	(18th) Caudal vertebra	No	None	Individual A	Pathologic, CT study performed in 2007
M.H. 249	(20th) Caudal vertebra with remnant of transverse process	No	None	Individual A	None
M.H. 250	(25th) Caudal vertebra	No	None	Individual A	None
M.H. 251	Caudal vertebra, mid-caudal region	No	None	Individual C	None
M.H. 252	Caudal vertebra, mid-caudal region	Syntype	Huene (1922: p. 82, fig. 6)	Individual C	None
M.H. 253	(26th) Caudal vertebra	Syntype	Huene (1922: p. 82)	Individual A	None
M.H. 254	(22nd) Caudal vertebra	Syntype	Huene (1922: p. 82)	Individual A	None
M.H. 255	Caudal vertebra, mid-caudal region	No	None	Individual D	None
M.H. 256	(24th) Caudal vertebra	No	None	Individual A	Pathologic
M.H. 257	(19th) Caudal vertebra	No	None	Individual A	None
M.H. 258	(21st) Caudal vertebra	Syntype	Huene (1922: p. 82, fig. 7)	Individual A	Bone fragment M.H. 324 was glued to this specimen in 2005
M.H. 259	Right ulna	Syntype	Huene (1922: p. 85)	Individual C	Determined as radius or tibia by Huene (1922)
M.H. 260	Right humerus	Syntype	Huene (1922: p. 83, Text-fig. A: b, c), Schwarz et al. (2007a, b, c)	Individual A	Distal articular cartilage capsule preserved
M.H. 261	Long bone shaft fragment	No	Huene (1922: p. 84)	Not assigned	Bone used for thin section
M.H. 262	Right femur, shaft fragment	Syntype	Huene (1922: p. 85)	Individual C	None
M.H. 263	Long bone shaft fragment	No	None	Not assigned	None
M.H. 264	Left radius	Syntype	Huene (1922: p. 85, fig. 18)	Individual C	Determined as metacarpal by Huene (1922)

Table 1 (continued)

Collection no.	Material	Assignment to type series	Previous mention	Individual	Annotations
M.H. 265	Cervical vertebra, mid-cervical region	Syntype	Huene (1922: p. 82)	Individual A	CT study performed in 2007
M.H. 266	Left prezygapophysis, mid-cervical region	Syntype	Huene (1922: p. 82)	Individual A	None
M.H. 267	Cervical vertebra, position, mid-cervical region	Syntype	Huene (1922: p. 82)	Individual A or D	CT study performed in 2007
M.H. 268	Cervical vertebra, fragment of caudal articular cotyla	Syntype	Greppin (1870: p. 339, Pl. 1 fig. 4), Huene (1922: p. 82)	Individual A	Originally preserved together with M.H. 365, both determined as scutes by Greppin (1870), and found to be lost by Huene (1922), although he mentions this specimen
M.H. 269	Pollex claw (manus unguis phalanx)	Syntype	Huene (1922: p. 86)	Individual A	Huene (1922: fig. 4) erroneously referred to this number the neural spine M.H. 369
M.H. 270	Pedal unguis phalanx, cast	Syntype	Greppin (1870: Pl. 1 fig. 5), Huene (1922: p. 86, fig. 23a, b)	Individual C	Preserved is only the cast, the original bone is missing
M.H. 271	(3rd) Caudal vertebra	Syntype	Huene (1922: p. 81)	Individual A	None
M.H. 272	(5th) Caudal vertebra	No	None	Individual A	None
M.H. 273	(6th) Caudal vertebra	No	None	Individual A	None
M.H. 274	(9th) Caudal vertebra	No	None	Individual A	None
M.H. 275	(12th) Caudal vertebra	Syntype	Huene (1922: p. 81)	Individual A	None
M.H. 276	(11th) Caudal vertebra	Syntype	Greppin (1870: Pl. 1, fig. 3), Huene (1922: p. 81, fig. 2)	Individual A	Transverse process incorrectly figured by Huene (1922)
M.H. 277	(4th) Caudal vertebra	Syntype	Huene (1922: p. 81, fig. 1a, b), Meyer and Thüring (2003: fig. 7b)	Individual A	Strongly simplified drawing in Huene (1922), wrong collection number (M.H. 280) in Meyer and Thüring (2003)
M.H. 278	First caudal (postsacral) vertebra	Syntype	Huene (1922: p. 81)	Individual A	None
M.H. 279	(7th) Caudal vertebra	Syntype	Huene (1922: p. 81)	Individual A	None
M.H. 280	(2nd) Caudal vertebra	Syntype	Greppin (1870: Pl. 1, fig. 2), Huene (1922: p. 81), Meyer and Thüring (2003: fig. 7a)	Individual A	Wrong collection number (M.H. 277) in Meyer and Thüring (2003) and transverse process is lacking in this figure
M.H. 282	Left fibula	Syntype	Huene (1922: p. 85)	Individual C	Determined as femur fragment by Huene (1922)
M.H. 283	Girdle or long bone cortex fragment	No	None	Not assigned	None
M.H. 284	Right coracoid	Syntype	Huene (1922: p. 86, fig. 22)	Individual A	Determined as metatarsal by Huene (1922)
M.H. 285	Long bone cortex fragment	Syntype	Huene (1922: p. 85)	Not assigned	Determined as femur fragment by Huene (1922)
M.H. 286	Neural spine of mid-caudal vertebra	Syntype	Huene (1922: p. 81)	Individual A	None
M.H. 287	Girdle or long bone cortex fragment	No	None	Not assigned	None
M.H. 288	Caudal vertebra, mid-caudal region	No	None	Individual C	None

Table 1 (continued)

Collection no.	Material	Assignment to type series	Previous mention	Individual	Annotations
M.H. 289	Girdle or long bone cortex fragment	No	None	Not assigned	None
M.H. 290	Bone fragment	No	None	Not assigned	None
M.H. 291	Dorsal rib, fragment	Syntype	Huene (1922: p. 82, fig. 9)	Individual A	Possible impact/bite marks
M.H. 292	Dorsal rib, fragment	No	None	Individual A	None
M.H. 293	Dorsal rib, fragment	No	None	Individual A	None
M.H. 294	Metapodium shaft fragment	No	None	Not assigned	None
M.H. 295	Caudal vertebra, fragment	No	None	Not assigned	None
M.H. 297	Caudal vertebra, fragment	Syntype	Huene (1922: p. 85, fig. 17)	Not assigned	None
M.H. 299	Dorsal vertebra, fragment	No	None	Not assigned	None
M.H. 300	Anterior caudal neural spine	Syntype	Huene (1922: p. 81)	Individual A	Could from its size and morphology belong to the caudal vertebra M.H. 277
M.H. 301	Left maxilla	No	None	Individual A	None
M.H. 302	(10th) Caudal vertebra	No	None	Individual A	None
M.H. 304	Fragment of mid-caudal neural spine	Syntype	None	Not assigned	None
M.H. 305	Bone fragment	No	None	Not assigned	None
M.H. 306	Dorsal rib, fragment	Syntype	Huene (1922: p. 82, fig. 10)	Individual A	None
M.H. 307	Dorsal rib, fragment	No	None	Individual A	None
M.H. 308	Bone fragment	No	None	Not assigned	None
M.H. 310	Small cortex fragment	No	None	Not assigned	None
M.H. 311	Bone fragment	No	None	Not assigned	None
M.H. 312	Bone fragment	No	None	Not assigned	None
M.H. 313	Left postorbital	No	None	Not assigned	None
M.H. 314	Cortex fragment	No	None	Individual A	Determination uncertain
M.H. 315	Bone fragment	No	None	Not assigned	None
M.H. 316	Dorsal rib, fragment	No	None	Individual A	None
M.H. 317	Bone fragment	No	None	Not assigned	None
M.H. 318	Bone fragment	No	None	Not assigned	None
M.H. 319	Bone fragment	No	None	Not assigned	None
M.H. 320	Tiny cortex chip	No	None	Not assigned	None
M.H. 321	Cortex fragment	No	None	Not assigned	None
M.H. 323	Metapodium shaft	No	None	Individual A	Possible impact/bite marks
M.H. 324	(21 st) Caudal vertebral neural spine, belongs to M.H.258	Syntype	Huene (1922: p. 82, fig. 7)	Individual A	Was glued to M.H. 258 in 2005

Table 1 (continued)

Collection no.	Material	Assignment to type series	Previous mention	Individual	Annotations
M.H. 325	Bone fragment	No	None	Not assigned	None
M.H. 326	Bone fragment	No	None	Not assigned	None
M.H. 327	Incomplete bone, possibly calcaneum	No	None	Not assigned	None
M.H. 328	Dorsal rib, fragment	No	None	Individual A	None
M.H. 330	Bone fragment	No	None	Not assigned	None
M.H. 331	Bone fragment, possibly from skull	No	None	Not assigned	None
M.H. 332	Bone fragment, possibly from skull	Syntype	Huene (1922: p. 82)	Not assigned	None
M.H. 333	Bone fragment	No	None	Not assigned	None
M.H. 334	Dorsal rib, fragment	No	None	Individual A	None
M.H. 335	Dorsal rib, fragment	No	None	Not assigned	None
M.H. 336	Dorsal rib, fragment	No	None	Not assigned	None
M.H. 337	Tiny bone fragment	No	None	Not assigned	None
M.H. 338	Bone fragment	No	None	Not assigned	None
M.H. 339	Left tibia	Syntype	Huene (1922: p. 85, fig. 20)	Individual A	Figured in Huene (1922) with complete proximal margin
M.H. 340	Left ulna	Syntype	Huene (1922: p. 84, fig. 16)	Individual C	None
M.H. 341	Left humerus	Syntype	Huene (1922: p. 83)	Individual C	None
M.H. 342	Right tibia	Syntype	Huene (1922: p. 85, fig. 20)	Individual A	None
M.H. 344	Right Scapula, shaft fragment	Syntype	Huene (1922: p. 82, fig. 11b)	Individual A	None
M.H. 345	Right fibula, distal fragment with rugosity	Syntype	Huene (1922: fig. 25)	Individual A	Huene (1922: fig. 25) erroneously referred to this number the figure of another caudal vertebra M.H. 354
M.H. 346	Left Pubis, shaft fragment	Syntype	Huene (1922: p. 83), fig. 13	Individual A	None
M.H. 347	Left Pubis, shaft fragment	Syntype	Huene (1922: p. 83, fig. 14)	Individual B	None
M.H. 348	Long bone fragment	No	None	Not assigned	None
M.H. 349	Left femur	Syntype	Huene (1922: p. 85), Meyer and Thüring (2003: fig. 6b)	Individual A	Wrong collection number (M.H. 372) in Meyer and Thüring (2003); possible impact/bite marks
M.H. 353	Caudal vertebra, mid-caudal region	Syntype	Huene (1922: p. 89)	Individual B	None
M.H. 354	Caudal vertebra, mid-caudal region	Syntype	Huene (1922: p. 89, fig. 25)	Individual B	Huene (1922) gives a wrong collection number (M.H. 345) to this specimen and determines it as crocodylomorph vertebra
M.H. 355	Fragment of mid-caudal vertebra	Syntype	Huene (1922: p. 89)	Individual B	Is glued to M.H. 354
M.H. 357	Fragment of caudal vertebra	No	None	Individual C	Is glued to M.H. 238

Table 1 (continued)

Collection no.	Material	Assignment to type series	Previous mention	Individual	Annotations
M.H. 358	Left ischium, proximal part	Syntype	None	Individual A	None
M.H. 359	Left pubis, fragment	Syntype	Huene (1922: p. 83, fig. 12)	Individual A	Possible impact/bite marks
M.H. 360	Long bone fragment	No	None	Not assigned	None
M.H. 361	Long bone fragment	No	None	Not assigned	None
M.H. 362	Long bone fragment	No	None	Not assigned	None
M.H. 363	Long bone fragment	No	None	Not assigned	None
M.H. 364	Long bone fragment	No	None	Not assigned	None
M.H. 365	Cervical vertebra, fragment of caudal articular cotyla	No	Greppin (1870: Pl. 1 fig. 4)	Individual A	Originally preserved together with M.H. 268, both determined as scutes by Greppin (1870), and found to be lost by Huene (1922)
M.H. 366	Bone fragment	No	None	Not assigned	None
M.H. 367	Long bone fragment	No	None	Not assigned	None
M.H. 368	Left scapula, proximal shaft fragment	Syntype	Huene (1922: p. 82, fig. 11a)	Individual C	Possible impact/bite marks
M.H. 369	Neural spine of cranial caudal vertebra	Syntype	Huene (1922: p. 81, fig. 4)	Individual A	Could from its size and morphology belong to the caudal vertebra M.H. 280
M.H. 371	Neural spine of cranial caudal vertebra	Syntype	Huene (1922: p. 81)	Individual A	Could from its size and morphology belong to the caudal vertebra M.H. 278
M.H. 372	Left femur	Syntype	Huene (1922: p. 85, fig. 19), Meyer and Thüring: fig. 6a	Individual C	Wrong collection number (M.H. 349) in Meyer and Thüring (2003)
M.H. 373	Left fibula	Syntype	Huene (1922: p. 86, fig. 21)	Individual A	None
M.H. 374	Left fibula fragment	Syntype	Huene (1922: text-fig. A-a)	Individual C	Is glued to M.H. 387
M.H. 378	Dorsal rib, fragment	No	None	Individual A	None
M.H. 386	Left fibula fragment	Syntype	Huene (1922: text-fig. A-a)	Individual C	Is glued to M.H. 387
M.H. 387	Left fibula	Syntype	Huene (1922: p. 83, text-fig. A-a)	Individual C	Bone is composed by the two glued fragments M.H. 374 and M.H. 386. Huene (1922) described and figured this bone as ischium with the number M.H. 386, whereas he referred M.H. 387 to be a left tibia, which is lost.
M.H. 449	(16th) caudal vertebra	No	None	Individual A	None
M.H. 450	Neural spine of mid-caudal vertebra	No	None	Individual A	None
M.H. 451	Tooth	No	None	Individual A	None
No collection number	Mid-caudal vertebra	No	None	Individual D	None

Those parts of the complete material that were mentioned in Huene's (1922) original description, represent the type material or syntype. Additional and unpublished material is referred to *A. greppini* in this paper. Size differences and double elements make it possible to distinguish between at least four individuals in three different size classes; these are indicated in the table as individuals A–D, or, if too fragmentary, are not assigned to one of these individuals. Caudal vertebrae assigned to individual A have been tentatively determined to their anatomical position in accordance with the skeletal reconstruction

Table 2 List of other vertebrate material from Moutier, Switzerland, found together with *A. greppini*

Collection no.	Material	Taxonomic assignment	Previous mention	Annotations
M.H. 350	Tooth	<i>Ceratosauria</i>	Greppin (1870: p. 339, Pl. 1, fig. 1a–c), Huene (1922: p. 80)	On the basis of this tooth, the material of <i>C. greppini</i> was initially assigned to a theropod dinosaur “ <i>Megalosaurus meriani</i> ”
M.H. 247	Vertebra	Teleosauridae	None	None
M.H. 303	Fragment of right premaxilla	Teleosauridae	None	
M.H. 309	Bone fragment, possibly vertebral fragment	Teleosauridae	None	Determination uncertain
M.H. 329	Mandibular remain, possibly fragmentary articular	Teleosauridae	None	None
M.H. 351	Caudal vertebra with small fragment of transverse process	Teleosauridae	Huene (1922: p. 89)	None
M.H. 352	Dorsal vertebra	Teleosauridae	Huene (1922: p. 89, fig. 24a–c)	Described by Huene (1922) as cervical vertebra.
M.H. 370	Fragment of left premaxilla	Teleosauridae	Huene (1922: p. 81, fig. 3)	Described by Huene (1922) as neural spine of a mid-caudal vertebra

holotype of *Cetiosaurus leedsi* (NHMUK R1988) is not referable to the same taxon as NHMUK R3078. Thus, in a revision of British sauropod material, Charig (1980) noted that referral of NHMUK R3078 to the species “*C. leedsi*” was not supported, and consequently renamed it *Cetiosauriscus stewarti*. NHMUK R3078 was later established as the type specimen for the genus *Cetiosauriscus* (Charig 1993).

Despite its relevance to this convoluted taxonomic history, the material of “*Cetiosauriscus*” *greppini* has received very little attention since Huene’s (1922, 1927a, b) work. On the rare occasions that it has been mentioned, “*Cetiosauriscus*” *greppini* is generally considered a nomen dubium, with little further discussion (e.g. Glut 1997; Upchurch et al. 2004), despite the material being relatively well preserved. However, “*Cetiosauriscus*” *greppini* represents the only skeletal find of a sauropod dinosaur from Switzerland (Meyer and Thüring 2003), and is among the few well-preserved Late Jurassic central European sauropod skeletons. Since its brief mention by Meyer and Thüring (2003), further work was carried out, including the complete preparation of all bones that are curated in the collection of the NMB. A publication describing the preservation of cartilage in this specimen (Schwarz et al. 2007b) was followed by an abstract in which the systematics of “*Cetiosauriscus*” *greppini* were first approached (Schwarz et al. 2007c). These latter authors proposed that the Swiss species is distinct from *C. stewarti* and likely represents a new genus of non-neosauropod eusauropod. The material was also subject to an unpublished master thesis (Hofer 2005).

Here, we present an extended monograph including the full re-description of all of the remains of “*Cetiosauriscus*” *greppini* from the type locality, in addition to

placing the taxon into a revised systematic framework. We also document its historical background, as well as reconstruct the taphonomic, sedimentological, and chrono- and biostratigraphic assignment of the type locality.

1.1 Geological framework

All of the material described here was found in the 1860’s in the Basse Montagne in a quarry near Moutier, north-western Switzerland (Fig. 1; Swiss coordinates: 123753 (N)/259535 (E); WGS84: 47° 17′ 19.04″ N 7° 22′ 37.66″ E) (Greppin 1870; Huene 1922, 1927b). The now abandoned quarry was in long-term use by the Swiss Army and no entry was possible until the late 1990’s. Today, only about 10 m of the former stratigraphic section can be seen: it consists of a series of grey limestones, with the uppermost part preserving micrites with bird’s-eye structures. This part can be correlated with the section in the nearby Combe du Pont (Gorge de Moutier), from which three levels with sauropod footprints are known from a few meters below (Meyer and Lockley 1996; Meyer and Marty 2014). The surfaces at the Combe du Pont are only a couple of meters below the Banné Marls, which can be assigned to the *divisum* ammonite biochron (Jank et al. 2006). Therefore, the sediments at both localities belong to the lower part of the Reuchenette Formation (of which the Banné Marls and the *divisum* ammonite biochron are important features), and are of early Kimmeridgian age (Meyer and Thüring 2003). Further northwest, in the area of Courtedoux, these layers have been extensively excavated and yield the most abundant dinosaur track assemblages from the Late Jurassic worldwide (Marty et al. 2017; Razzolini et al. 2017).

The skeletal remains at the quarry in Moutier were found within a greenish lens of marls and limestone

(Huene 1922; Jank 2004; Razzolini et al. 2017). Matrix collected from the specimens reveals charcoal remains (fusite), as well as fist-sized brecciated nodules with rhizolite traces, indicating deposition in a freshwater environment, on top of a paleosol. Screen-washing of the matrix resulted in a small sample of ostracods, which can be identified as *Cetacella inermis* (upper Oxfordian to Kimmeridgian), and a poorly preserved taxon from the *Cytheropteron-Eocytheropteron*-group (Oxfordian to Tithonian) (Ulla Schudack and the late Michael Schudack, pers. comm.). As such, it is not possible to constrain the early Kimmeridgian age further. Ecologically, these ostracods suggest a mixed, brackish environment, but not a pure freshwater environment. Thus, the bones were probably deposited in an ephemeral lake without current activity close to the sea.

1.2 Preservation

The material was found disarticulated and comprises at least four incomplete sauropod skeletons, as well as isolated remains of crocodylomorphs, and a single theropod tooth. Neither the theropod tooth (NMB M.H. 350), nor the single preserved sauropod tooth (NMB M.H. 451), are diagenetically compressed, but most of the bones have been strongly compressed and flattened. In most of the vertebrae, the more fragile parts (i.e. neural spines, zygapophyses, and transverse processes) have been broken off, and only a few of these are preserved separately. Most of the long bones exhibit incomplete articular ends, with some of the breakage areas on the bones appearing to be recent, rather than taphonomic: a possible result of poor excavation methods. It is plausible that several of the bones were broken during their removal from the quarry and that more fragile parts—which might have been present as isolated bone remains—were simply left behind.

Several small bone fragments cannot be attributed to the other skeletal remains. These fragments mainly preserve parts of the cortex and underlying spongiosa, rather than complete pieces of bones. At least one of the bone fragments, NMB M.H. 315, is unprepared and preserved within matrix, demonstrating that it must already have been embedded as an isolated fragment. None of the bones shows direct indication of transport.

Most of the bones have a darkish brown to grey color, whereas some are light brown in colour. These colour differences are attributed to slight differences in the pore water concentration and composition. The bone surface shows several cracks and fractures, which are filled with marl matrix. In places, the compact bone has been abraded, exposing the internal spongy bone. Pore spaces within the meshwork of the spongy bone are filled by matrix. Additionally, some of the bones, such as the pubis (NMB M.H.

346), bear deep scratches on their surfaces that are more likely traces of the preparation than of scavenging.

2 Methods

At the time of the description by Huene (1922), none of the material had undergone either cleaning or preparation. All available material was first cleaned and re-prepared where necessary, and final cleaning was carried out in an ultrasonic bath. Matrix was screen washed after soaking in H₂O₂ for 24 h.

Only one long bone fragment (NMB M.H. 261) was permitted to be sampled for bone histology. Following standard preparation procedures (Völkel 1967), a thin section and a polished cross section were produced from NMB M.H. 261.

The two cervical vertebrae NMB M.H. 265 and M.H. 267, the pathologic caudal vertebrae NMB M.H. 242 and M.H. 256, and the caudal vertebra NMB M.H. 238, were scanned with x-ray computed tomography at the Department of Medical Radiology of the University Hospital Basel. The scans were performed with a Multi-detector CT-scanner (Somatom Sensation 16, Siemens, Erlangen; Germany). The vertebrae were scanned along their long-axis with a parameter setting of 140 kV and 400 mAs. The raw data were reconstructed applying a standard algorithm for human osseous structures (B80s ultra sharp kernel), using a standard CT imaging processor with the imaging software version VA 70C. The data were reconstructed in all orthogonal planes at 3 mm thickness.

Terminology: The nomenclature of the external laminae in sauropod vertebrae follows that of Wilson (1999). Terminology of pneumatic structures follows Wedel et al. (2000) and Wilson et al. (2011).

Institutional Abbreviations: NMB, Naturhistorisches Museum Basel, Switzerland; NHMUK (formerly BMNH), Natural History Museum London, UK.

3 Systematic palaeontology

SAURISCHIA Seeley 1887a

SAUROPODOMORPHA von Huene 1932

SAUROPODA Marsh 1878

EUSAUROPODA Upchurch 1995

Amanzia *gen. nov.*

Etymology: The genus is named in honor of the well-known Swiss geologist Amanz Gressly (1814–1865) who introduced the term “facies” into geology and discovered the first dinosaur fossil from Switzerland in 1856.

Type Species: *Ornithopsis greppini* (Huene, 1922, figs. A, B, Plate IV)

Included Species: Type species only (syntype series as described by Huene (1922), comprising postcranial bones of a minimum of four individuals, see Table 1)

Stratigraphical Range: Lower part of the Reuchenette Formation (*divisum* zone), early Kimmeridgian (Late Jurassic).

Genus Diagnosis: As for the type and only known species.

***Amanzia greppini* (= *Ornithopsis greppini* Huene, 1922)**

Synonymy:

v 1870 *Megalosaurus meriani* Greppin: p. 118, Pl. I figs. 1–6 (partim)

v 1922 *Ornithopsis greppini* Huene: p. 89, figs. A, B, Plate IV

v 1927a *Cetiosauriscus greppini* Huene: p. 122

v 1990 *Cetiosauriscus greppini* McIntosh: p. 350

v 1997 *Cetiosauriscus greppini* Glut: p. 271

v 2003 *Cetiosauriscus greppini* Meyer and Thüring: p. 108, figs. 5, 6, 7

v 2004 *Ornithopsis greppini* Upchurch, Barrett and Dodson: p. 271

Syntype: NMB M.H. 265 (cervical vertebra), NMB M.H. 266 (prezygapophysis of cervical vertebra), NMB M.H. 267–268 (cervical vertebrae), NMB M.H. 239 (caudal vertebra), NMB M.H. 245 (caudal vertebra), NMB M.H. 252–254 (caudal vertebrae), NMB M.H. 258 (caudal vertebra), NMB M.H. 271 (caudal vertebra), NMB M.H. 275–280 (caudal vertebrae), NMB M.H. 297 (caudal vertebra), NMB M.H. 324 (caudal vertebra), NMB M.H. 353–355 (caudal vertebrae), NMB M.H. 286 (caudal neural spine), NMB M.H. 300 (caudal neural spine), NMB M.H. 369–370 (caudal neural spines), NMB M.H. 291 (dorsal rib), NMB M.H. 306 (dorsal rib), NMB M.H. 344 (scapula), NMB M.H. 368 (scapula), NMB M.H. 284 (coracoid), NMB M.H. 260 (humerus), NMB M.H. 341 (humerus), NMB M.H. 259 (ulna), NMB M.H. 340 (ulna), NMB M.H. 264 (radius), NMB M.H. 346–347 (pubes), NMB M.H. 359 (pubis), NMB M.H. 358 (ischium), NMB M.H. 262 (femur), NMB M.H. 349 (femur), NMB M.H. 372 (femur), NMB M.H. 339 (tibia), NMB M.H. 342 (tibia), NMB M.H. 282 (fibula), NMB M.H. 373 (fibula), NMB M.H. 387 (fibula, ex NMB M.H. 374 and NMB M.H. 386), NMB M.H. 246 (metatarsal), NMB M.H. 269–270 (ungual phalanges), NMB M.H. 285 (long bone

fragment), NMB M.H. 332 (bone fragment), NMB M.H. 345 (long bone fragment).

Referred Specimens: NMB M.H. 451 (tooth), NMB M.H. 301 (maxilla), NMB M.H. 313 (postorbital), NMB M.H. 365 (cervical vertebra), NMB M.H. 221 (caudal vertebra), NMB M.H. 238 (caudal vertebra), NMB M.H. 240 (caudal vertebra), NMB M.H. 242–244 (caudal vertebrae), NMB M.H. 248–251 (caudal vertebrae), NMB M.H. 255–257 (caudal vertebrae), NMB M.H. 272–274 (caudal vertebrae), NMB M.H. 288 (caudal vertebra), NMB M.H. 295 (caudal vertebra), NMB M.H. 299 (caudal vertebra), NMB M.H. 302 (caudal vertebra), NMB M.H. 357 (caudal vertebra), NMB M.H. 449 (caudal vertebra), NMB M.H. 450 (caudal neural spine), NMB M.H. 292–293 (dorsal ribs), NMB M.H. 307 (dorsal ribs), NMB M.H. 316 (dorsal rib), NMB M.H. 328 (dorsal rib), NMB M.H. 334–336 (dorsal ribs), NMB M.H. 378 (dorsal rib), NMB M.H. 294 (metapodium), NMB M.H. 323 (metapodium), NMB M.H. 206 (bone fragment), NMB M.H. 209 (bone fragment), NMB M.H. 261 (long bone fragment), NMB M.H. 263 (long bone fragment), NMB M.H. 283 (bone fragment), NMB M.H. 287 (bone fragment), NMB M.H. 289–290 (bone fragments), NMB M.H. 304–305 (bone fragments), NMB M.H. 308–312 (bone fragments), NMB M.H. 314–315 (bone fragment), NMB M.H. 317–321 (bone fragments), NMB M.H. 325–326 (bone fragments), NMB M.H. 327 (undetermined bone), NMB M.H. 330–331 (bone fragments), NMB M.H. 333 (bone fragment), NMB M.H. 337–338 (bone fragments), NMB M.H. 348 (long bone fragment), NMB M.H. 360–364 (long bone fragments), NMB M.H. 366–367 (long bone fragments).

Type Locality: near the city of Moutier in northwestern Switzerland. All of the referred material is also from the type locality.

Diagnosis: *Amanzia greppini* can be diagnosed by one autapomorphy (marked with an asterisk), as well as a unique combination of features: (1) lateral fossa at the base of the prezygapophyseal process in middle cervical vertebrae; (2) anterior and posterior centrodiapophyseal laminae present in anteriormost caudal vertebrae; (3) anterior–middle caudal centra pierced by vascular foramina; (4) elongate middle caudal centra; (5) mediolaterally broad proximal end of humerus relative to proximodistal length; (6) rugosity on the medial margin of the posterior surface of the humerus, level with the deltopectoral crest*; (7) rugosity on the lateral margin of the posterior surface of the humerus, level with the deltopectoral crest; (8) fibular condyle of femur much broader than tibial condyle; (9) lateral muscle scar on fibula formed from two ridges; and (10) shaft of fibula sinuous in lateral view.

Table 3 Measurements of bones of *A. greppini*, and other fossil vertebrates from Moutier, Switzerland: Skull fragments

	Preserved length	Preserved height	Preserved breadth
M.H. 301, left maxilla	51	37	14
M.H. 313, left postorbital	39	54	21
M.H. 451, tooth	11.4	8.3	5.3

Remarks: Huene (1922) listed 49 diagnostic bones with collection numbers on which he based his original taxon “*Ornithopsis*” *greppini* (Table 1). Because no holotype was defined in Huene’s (1922) original description, the published material corresponds to a type series (ICZN Art. 72.1.1.) and is therefore regarded as the syntype of *A. greppini*. This syntype contains a few previously misinterpreted bones and descriptions and figures with wrong

specimen numbers (see Table 1), which are corrected in this work. 75 additional collection numbers for the material from the type locality of Moutier have been referred to *Amanzia*, although they were not mentioned by Huene (1922). This additional material is listed under ‘Referred specimens’ and, together with the syntype, comprises a total of 124 bones attributed to *Amanzia*. The material of *Amanzia* belongs to at least four individuals, which can be distinguished by size differences and/or duplicated elements (Table 2).

3.1 Description and comparisons

Maxilla The incomplete left maxilla NMB M.H. 301 is a mediolaterally flattened, anteroposteriorly elongate bone fragment (Table 3), from which the base of a stout, rounded narial process projects steeply posterodorsally (Fig. 2a, b). Most of the anterior, posterior,

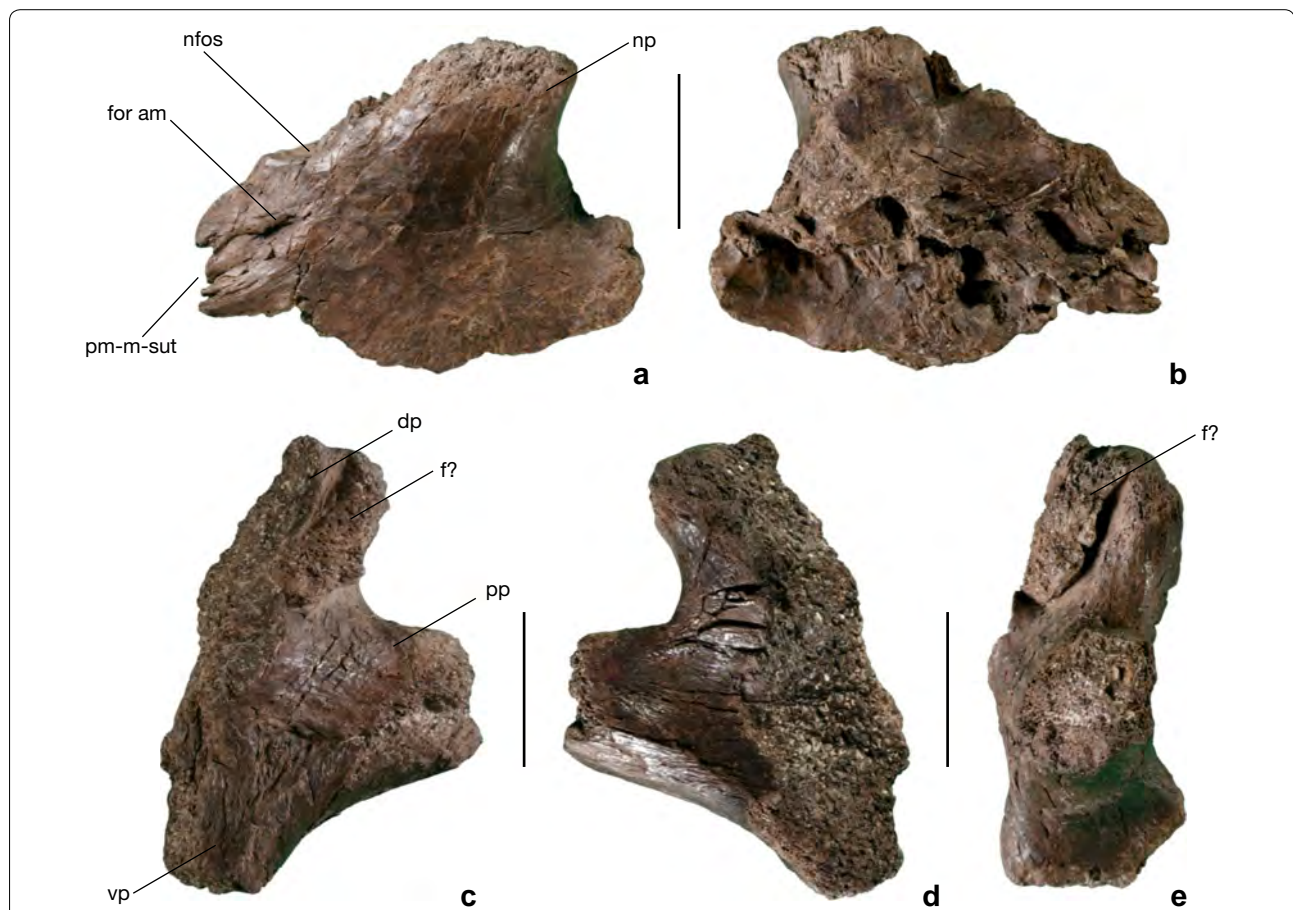


Fig. 2 Skull fragments of *A. greppini*. NMB M.H. 301, left maxilla in **a** lateral and **b** medial aspect. NMB M.H. 313, tentatively assigned left postorbital in **c** lateral, **d** medial and **e** posterior aspect. Scale bar is 20 mm. *dp* dorsal process, *f* frontal (determination questionable), *for am* anterior maxillary foramen, *nfos* narial fossa, *np* narial process, *pm-m-sut* premaxillo-maxillary suture, *pp* posterior process, *vp* ventral process

dorsal (narial process) and ventral margins of the maxilla are broken off. Where preserved, the anterior margin of the maxilla is jagged and might represent a part of the premaxillo-maxillary suture. The lateral surface of the maxilla is smooth, whereas the crushed medial surface is irregular, and possibly represents a part of the articular surface for the palatine (Fig. 2b). The base of the narial process is perforated by an anteroposteriorly elongate anterior maxillary foramen (Fig. 2a). A longitudinal depression is situated dorsal to this foramen and marks the posterolateral part of the narial fossa (Fig. 2a). An antorbital fossa is absent, and there is no evidence for a preantorbital fenestra. The presence of the latter opening characterises most neosauropods, whereas it is absent in basal eusauropods such as *Shunosaurus* and *Jobaria* (Upchurch 1998; Wilson and Sereno 1998). In comparison with the maxillae of other sauropods [e.g. *Diplodocus* (Berman and McIntosh 1978; Holland 1924), *Camarasaurus* (Madsen et al. 1995), *Abydosaurus* (Chure et al. 2010)], NMB M.H. 301 is proportionally most similar to *Camarasaurus*, indicating that the maxillary border of the external nares in *Amanzia* was probably long, likely comprising more than one-third of the narial perimeter. No teeth are preserved in this element.

Postorbital NMB M.H. 313 is a triradiate bone fragment that is tentatively identified as a fragment of a left postorbital (Table 3). Ventral, dorsal and posterior processes branch out from the central part of the postorbital (Fig. 2c–e). Most parts of these three processes, as well as the anterior margin of the postorbital, are broken off. The dorsal and posterior processes are oriented at an angle of ca. 80° to one another, forming a rounded concavity in between them. The margin between the posterior and ventral processes is slightly concave. As is the case in most derived eusauropods (Wilson and Sereno 1998; Upchurch et al. 2004), the ventral process is broader mediolaterally than anteroposteriorly. In lateral view, the posterior process bears a deep furrow that extends anteroventrally from its posteriormost point to the transition between the posterior and ventral processes. The dorsal two-thirds of the dorsal process are concealed by a rugose, elongate patch of bone that possibly represents the ventralmost part of the frontal (Fig. 2c–e). In medial view, the postorbital bears a longitudinal depression at approximately midheight (Fig. 2d).

Tooth NMB M.H. 451 is the undistorted base of a tooth crown (Fig. 3), with most of the root and crown broken

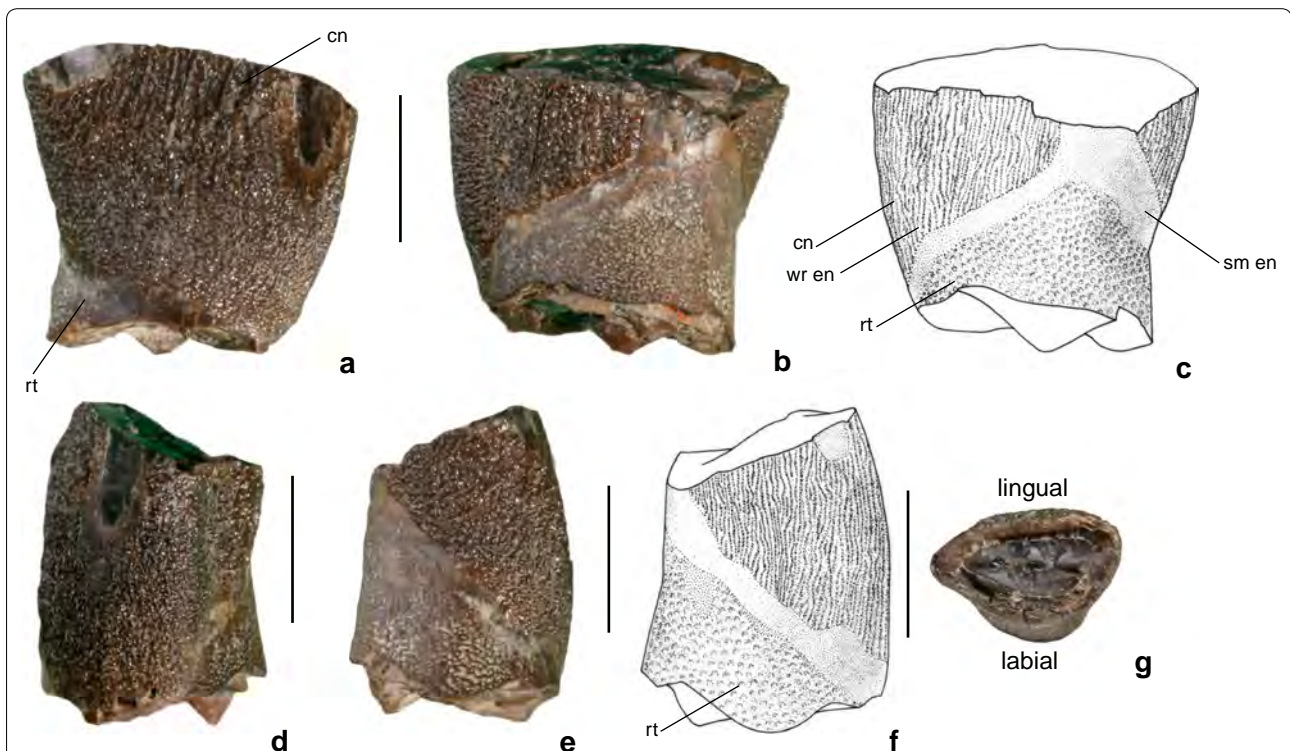


Fig. 3 Tooth NMB M.H. 451 of *A. greppini*. **a** lingual, **b** labial aspect, **c** line drawing of labial aspect, **d** distal (?) aspect, **e** mesial (?) aspect, **f** line drawing of same mesial (?) aspect, **g** apical view showing outline in cross-section. Scale bar is 5 mm. Drawings by Serafin Padzera. *cn* tooth crown, *rt* tooth root, *sm en* smooth enamel, *wr en* wrinkled enamel

away (Table 3). The crown is slightly labiolingually compressed, with a D-shaped cross section (Fig. 3g). Its lingual face is fairly flat, whereas the labial face of the base of the tooth crown and root are convex. The mesial and distal margins of the tooth crown diverge apically, so that the tooth rapidly increases in mesiodistal width above the root, as in most non-neosauropod eusauropods (Upchurch 1998), such as *Turiasaurus* (Royo-Torres et al. 2006), but also in some *Camarasaurus* teeth (Madsen et al. 1995). The enamel forms close-standing, apico-basally oriented wrinkles (Fig. 3). The surface of the enamel wrinkles themselves is interrupted by small incisions, giving them a strongly irregular appearance. Labially, the wrinkled crown enamel ends in an ‘inverted V-shaped’ incision (Fig. 3b, c) that is paralleled by a small bend of smooth enamel. The preserved portion of the root bears a network of close-standing small pores on its lingual surface. In comparison with the teeth of other sauropods, the D-shaped, spatulate tooth-crown of *Amanzia* is most similar to that of ‘basal’ eusauropods, contrasting with the parallel-sided tooth crowns that characterise most neosauropods (Upchurch 1998; Wilson and Sereno 1998; Chure et al. 2010).

Cervical vertebrae Two incomplete cervical vertebrae of different sizes are preserved (Table 4), as well as an isolated prezygapophysis. Cervical vertebra NMB M.H.

265 preserves the anterior half of a vertebral centrum, with an incomplete condyle, and basal parts of the neural arch (Fig. 4). The ventralmost part of the centrum is also broken off, and some fragmentary bone debris and matrix remains are attached to the neural arch. The vertebra is strongly mediolaterally compressed and slightly dorsoventrally distorted. In places, the cortical bone of the condyle is broken off, revealing a dense network of subcircular pneumatic camellae (see below). There is full synostosis between the centrum and the neural arch, such that the neurocentral suture is no longer detectable.

In lateral view, the outline of the condyle of NMB M.H. 265 can be reconstructed to be hemispherical, indicating an opisthocoelous vertebral articulation. Only on the left side of the centrum (Fig. 4a, b), the base of the parapophysis is preserved as a posteroventrally directed ‘stump’. The anterodorsal surface of the parapophysis bears two parallel, dorsoventrally elongate fossae. Dorsally, the parapophysis is perforated by a pneumatic foramen leading into a canal that hollows out the dorsal surface of the parapophysis. A dorsally excavated parapophysis is consistent with the cervical anatomy of most eusauropods, with the exception of somphospondylans and some dicraeosaurids (Upchurch 1998). Posterior and dorsal to the parapophysis, the anterior two-thirds of the lateral surface of the centrum is occupied by a pneumatic fossa, which is developed both on the right (Fig. 4c, d) and left (Fig. 4a,

Table 4 Measurements of bones of *A. greppini*, from Moutier, Switzerland: Presacral vertebrae, dorsal ribs

	CL	CHd	CH	CW	HD	LD	VH
M.H. 265, cervical vertebra	186 ^a	70 ^a	61 ^a	25 ^a	64 ^a	24	171 ^a
M.H. 267, cervical vertebra	141 ^a	71 ^a	57	16 ^a	–	–	71 ^a
M.H. 268, cervical vertebral cotyla	–	–	48 ^a	87 ^a	–	–	–
M.H. 299, dorsal vertebral centrum	78 ^a	–	86 ^a	27 ^a	–	–	84 ^a
M.H. 365, cervical vertebral cotyla	–	–	51 ^a	53 ^a	–	–	–
	BA	LA	PH	PL	PW		
M.H. 266, presacral left prezygapophysis	22	42	59 ^a	111 ^a	21 ^a		
	PDW	PL	WH				
M.H. 291, dorsal rib	30	87 ^a	51 ^a				
M.H. 292, dorsal rib	21	71	–				
M.H. 293, dorsal rib	12 ^a	119 ^a	–				
M.H. 306, dorsal rib	9 ^a	96 ^a	–				
M.H. 316, dorsal rib	19 ^a	27 ^a	–				
M.H. 328, dorsal rib	14 ^a	53 ^a	–				
M.H. 334, dorsal rib	16 ^a	58 ^a	–				

CL centrum length, CHd centrum height at diapophysis, CH centrum height at condylus/preserved height of vertebral cotyla, CW centrum width at condylus/preserved width of vertebral cotyla, HD preserved dorsoventral height of diapophysis, LD minimum (distal) craniocaudal length of diapophysis, VH total vertebral height, BA maximum breadth of articular surface, LA length of articular surface, PH preserved height, PL preserved length, PW preserved width, PDW preserved distalmost shaft width, PL preserved length, WH width at rib head. All measurement are in mm

^a Indicates that the measurements refers only to preserved dimension at the incomplete and compressed bone

b) sides. This fossa is oval-shaped in outline: it is almost as dorsoventrally high as the vertebral centrum in its anterior part, but tapers posteriorly to a narrow ending. The fossa is dorsally bounded by a rounded and prominent posterior centrodiapophyseal lamina (pcdl), and ventrally bounded by another lamina that bears resemblance to the apcdl reported for mamenchisaurid vertebrae (Wings et al. 2011). Its internal surface is irregular and bumpy, with pneumatic foramina penetrating dorsally, ventrally, and anteriorly into the vertebra.

The left diapophysis has been anteriorly displaced and is pressed against the lateral pneumatic fossa. The diapophysis is rectangular in outline and about 2.5 times as high dorsoventrally as it is long anteroposteriorly. It ends distally with a straight margin and has a smooth surface. Posterior to the prezygapophyseal region is an area of broken bone on the left side that represents the original attachment area of the diapophysis. The diapophysis of the right side is broken away, which exposes some small crests dorsal to the lateral pneumatic fossa that most probably represent the remnants of the walls of pneumatic camellae. On the left body side, on the anterior margin of the neural arch, dorsal to the condyle, the prezygapophyseal pedestal is preserved with its centroprezygapophyseal lamina (cp1). Posterolaterally, the neural arch on the left and right side is excavated by a postzygapophyseal centrodiapophyseal fossa (pocdf) that is pierced posteriorly by a large pneumatic foramen. The pocdf is bounded dorsally by a stout, rounded postzygo-diapophyseal lamina (podl) and divided by a thin median lamina on the right side.

Although strongly compressed mediolaterally, many details of the internal pneumatic cavity system of NMB M.H. 265 were revealed by computer tomography (CT). The pneumatic cavity system of this vertebra can be characterized as semicamellate (sensu Wedel et al. 2000), with a few pneumatic camerae and a dominance of small camellae (Fig. 4e). The vertebral condyle is hollowed out by two or three pneumatic camerae that are surrounded by camellae, separated from one another by thick bone walls. The camerae transition posteriorly into a network of small camellae. Further posteriorly, these camellae unite to form one large camera. The neural arch bears a median pneumatic camera in the diapophyseal region that branches out into smaller camerae posteriorly. Four internal camerae lie in the diapophyseal region, their thick bone walls hollowed out by camellae. The separating bone walls are much thinner in the vertebral centrum and neural arch than in the vertebral condyle. Remnants of a thin median bone strut are visible in the vertebral centrum and the neural arch, interrupted by the neural canal. The neural canal is surrounded by camellae. As such, the internal tissue structure of NMB M.H. 265 is

most similar to that of 'basal' titanosauriforms (Wedel 2003).

The second cervical vertebra, NMB M.H. 267, is another anterior part of a centrum. It possesses a hemispherical condyle and a prominent lamina separating the lateral pneumatic fossa in the anterior half of the vertebral centrum from the rest of the lateral surface of the centrum (Fig. 5), as in NMB M.H. 265. Posterodorsal to the parapophysis, the lateral pneumatic fossa bears two anteroposteriorly elongate pneumatic foramina, which penetrate ventrally into the bone (Fig. 5). The posteroventral part of the fossa is separated by a narrow ridge from the ventral surface of the vertebra. This ridge forms a sort of aperture for another pneumatic foramen that penetrates posteroventrally into the fossa where the bounding lamina reaches its ventral end. As in NMB M.H. 265, the lateral pneumatic fossa is oval-shaped and has an irregularly wavy surface.

The pneumatic cavity system of NMB M.H. 267, visible in the CT sections, is simpler than in NMB M.H. 265 and can be characterized as polycamerate (sensu Wedel et al. 2000) (Fig. 5). Consequently, NMB M.H. 267 more closely resembles the non-titanosauriform pneumatic condition. The vertebral condyle is hollowed out by two or three pneumatic camerae, but camellae are absent. The camerae are separated from each other by thick bone walls. The vertebral centrum bears a thick median bone strut that separates the two lateral pneumatic fossae from one another. The base of the neural canal is surrounded by smaller camerae, but the separating bone walls and the median bone struts are massive.

NMB M.H. 267 is only one third of the size of NMB M.H. 265 (Table 4). It has a pneumatic fossa that is restricted to the anterior half of the vertebral centrum and pneumatic structures less well-developed in its lateral pneumatic fossa. The exact position of both vertebrae in the neck cannot be determined with certainty. The size and proportions of NMB M.H. 265 indicate a position in the posterior third of the neck (see also Fig. 13). NMB M.H. 267 represents either a more anteriorly-positioned cervical vertebra of a similar-sized individual as NMB M.H. 265, and/or belongs to a smaller individual. The latter interpretation is probably more consistent with the 'simpler' internal tissue structure of NMB M.H. 267, given that the degree of pneumaticity increases with ontogeny in sauropods (e.g. Schwarz et al. 2007a; Carballido and Sander 2014).

An isolated left prezygapophysis (NMB M.H. 266) likely belongs to a posterior cervical, probably situated further along the sequence than NMB M.H. 265 or 267 (Fig. 6a–c, Table 4) as compared to the size of these specimens. In its posterior half, the lateral face of the prezygapophyseal pedestal is covered by bone debris. The anteroventral

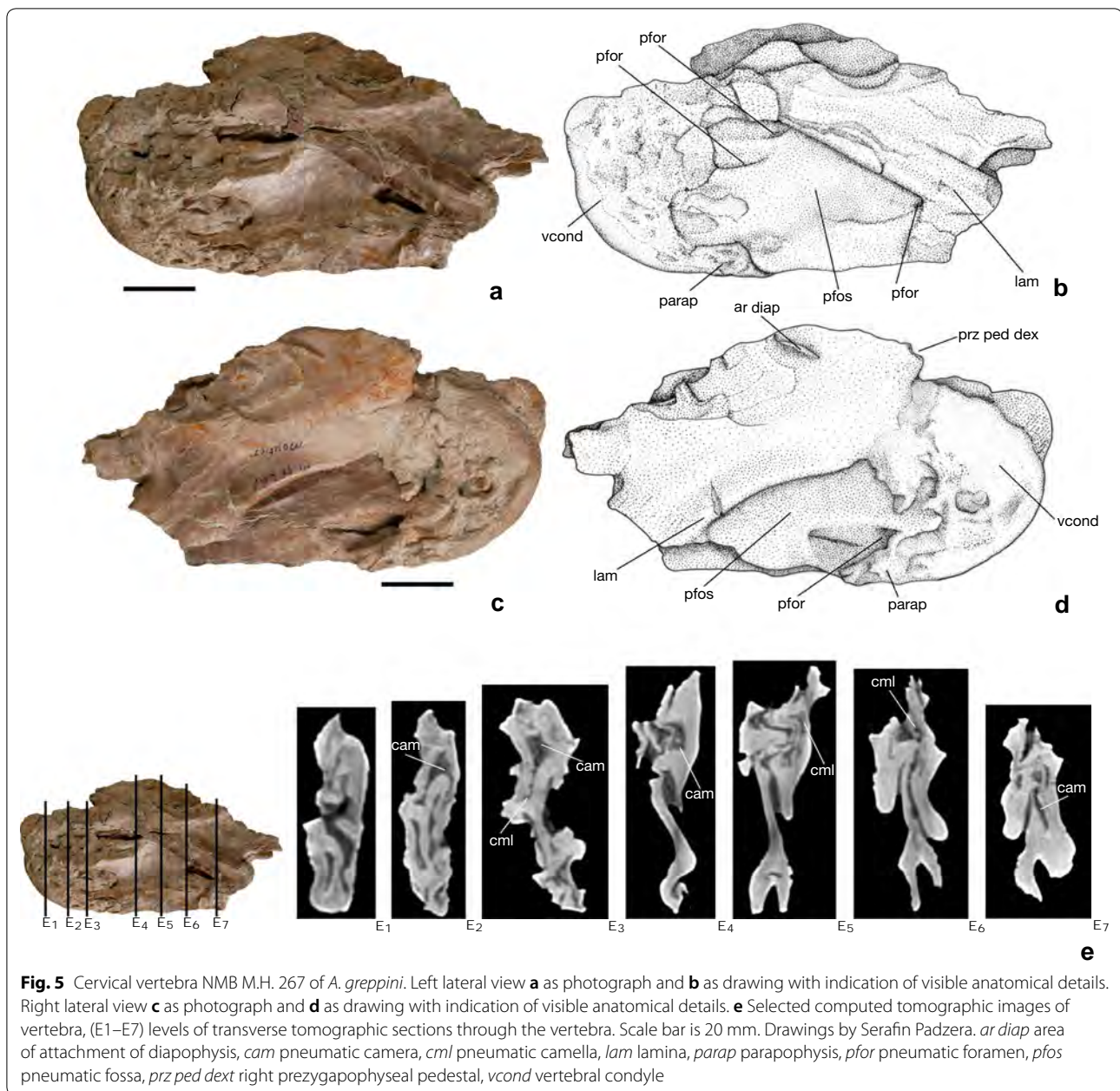
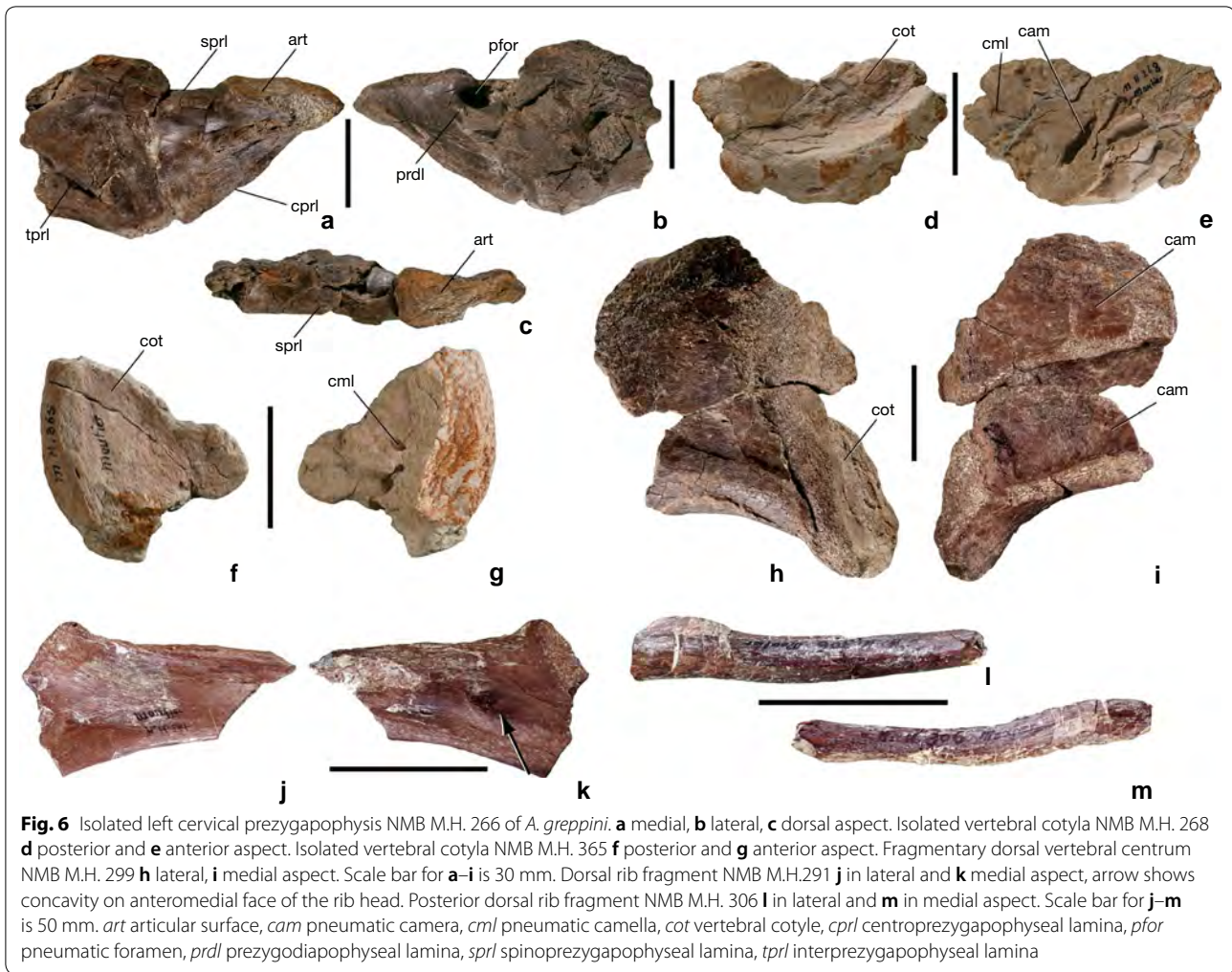


Fig. 5 Cervical vertebra NMB M.H. 267 of *A. greppini*. Left lateral view **a** as photograph and **b** as drawing with indication of visible anatomical details. Right lateral view **c** as photograph and **d** as drawing with indication of visible anatomical details. **e** Selected computed tomographic images of vertebra, (E1–E7) levels of transverse tomographic sections through the vertebra. Scale bar is 20 mm. Drawings by Serafin Padzera. *ar diap* area of attachment of diapophysis, *cam* pneumatic camera, *cml* pneumatic camella, *lam* lamina, *parap* parapophysis, *pfor* pneumatic foramen, *pfos* pneumatic fossa, *prz ped dext* right prezygapophyseal pedestal, *vcond* vertebral condyle

margin of the prezygapophysis forms the centroprezygapophyseal lamina (CPRL), which is anteriorly slightly convex and non-bifid. As such, the CPRL differs from many diplodocoids, wherein this lamina is bifid (Upchurch 1995; Wilson 2002). In its anteriormost part, the CPRL is rugose and bends to the lateral face of the prezygapophyseal pedestal. The prezygapophyseal articular surface is planar and half as long as the whole prezygapophyseal pedestal. It has a rounded rectangular outline with the long axis directed anteroposteriorly. There is no evidence for a pre-epiphysis: its absence might be preservational, but could also reflect the posterior position of NMB M.H.

266 in the cervical sequence. Level with the posterior end of the prezygapophyseal articular surface, a distinct pneumatic foramen pierces the lateral surface (Fig. 6b). Ventral to this foramen, the dorsal part of the rounded prezygodiapophyseal lamina (PRDL) is visible. A comparable foramen characterises the cervical vertebrae of several diplodocoids, as well as the macronarians *Europasaurus* and *Giraffatitan* (Harris 2006; Tschopp and Mateus 2013; Carballido and Sander 2014). The medial face of the prezygapophyseal pedestal is slightly irregular and bears a medial depression in its posterior third. The prezygapophysis divides posteriorly into a medial lamina (TPRL)



and a lateral wall connecting to the vertebral neural arch (Fig. 6a). The base of the spinoprezygapophyseal lamina (SPRL) is preserved, which is transversely wide ventrally, becoming slightly medially bevelled dorsally.

Presacral vertebral cotyle Greppin (1870: p. 339, pl. 1, fig. 4) figured and interpreted two plate-like bone fragments adhered to one another as osteoderms, and concluded that for ‘*Megalosaurus meriani*’: “Le corps était protégé par de grandes plaques, disposées de manière que le bord postérieur de chaque écusson recouvrait la base du suivant” [translation: The body was protected by large bony plates, arranged in a manner that the posterior margin of each plate overlapped with the following]. In the introduction to his description of ‘*C. greppini*’, Huene (1922: p. 80, Fig. 6d, f) mentioned that he was not able to find the figured osteoderms. Apparently, both fragments were prepared and separated from one another before Huene’s visit and were subsequently assigned to different collection numbers (NMB M.H. 268 and NMB M.H.

365). Huene (1922: p. 82) even mentioned NMB M.H. 268 in his work and determined it to be part of a cervical vertebra, but he did not recognize that it was identical to one of the bone fragments in Greppin’s (1870) description. Both fragments are unequivocally determined to be two incomplete vertebral cotyles of the presacral region, representing about one third of the vertebral cotyle (Fig. 6d–g).

In posterior view, the outer rim of the vertebral cotyle is broadened and rugose. The posterior articular surface is strongly concave and forms a bowl-shaped depression in NMB M.H. 268, but is only slightly concave in NMB M.H. 365. In anterior view, the bone surface is drawn out into thin and thick walls bounding small and irregular camellae between them, with the cavity system more complex in NMB M.H. 268 than in NMB M.H. 365 (Fig. 6e, g). This pattern presents the posteriormost extension of the internal pneumatic cavity system of the vertebrae. Both cotylar fragments belong to roughly similarly large vertebral centra (Table 4).

Dorsal vertebra NMB M.H. 299 is the left side of the posterior half of a dorsal vertebral centrum (Fig. 6h, i). It has been strongly compressed mediolaterally. The posterior articular surface is slightly concave and surrounded by a thickened rim of bone (Fig. 6h). Its ventral surface is strongly concave anteroposteriorly, but flat to convex transversely. The lateral, external surface of the centrum is slightly convex and no pneumatic foramina are present, as preserved. In medial view, the wall of the centrum is divided at mid-height by a horizontal bar of bone (Fig. 6i). The two halves each represent the remnant of a pneumatic camera in the interior of the centrum. The ventral camera is ventrally bounded by a thick bone margin. Both camerae extend posteriorly until the indentation of the posterior cotyle. The preserved walls of the pneumatic camerae are smooth.

Dorsal ribs The dorsal ribs of *Amanzia* are only very fragmentarily preserved. NMB M.H. 291 is the proximal part of a left dorsal rib with a small portion of the rib head and the base of the capitulum and tuberculum (Fig. 6j–k, Table 4). The rib head is broad and mediolaterally flattened at the transition to capitulum and tuberculum. Its anterior margin is slightly concave, whereas the posterior margin is nearly straight. Both margins converge distally, causing the rib shaft to taper. The anterolateral face of the rib shaft is slightly vaulted in its distal third. A rugosity extends along the posterior margin. The anteromedial face is medially depressed and bears a shallow groove paralleling the posterior margin. M.H. 291 preserves an elongate concavity situated distal to the capitulotubercular incision on the anteromedial face of the rib (Fig. 6k). This concavity has a diameter of 8 mm and is 2 mm deep. It is bowl-shaped with a flat central third. The cortex within the concavity is not broken. The concavity is interpreted to represent either a pneumatic fossa, or a bite mark, but the structure lacks unambiguous evidence to confirm either hypothesis.

NMB M.H. 307 is another small proximal fragment of a right dorsal rib with only the region of the anterior margin preserved, and is very similar to NMB M.H. 291. The preserved fragments of the rib shafts are very incomplete and often half of the bone is broken off. NMB M.H. 316 shows a complete cross-section of the proximal shaft region, which is D-shaped, with a convex anterolateral and straight posteromedial margin. As is visible on the other rib fragments, the shaft becomes subcircular in cross-section distally. NMB M.H. 293 is a longer, relatively straight shaft fragment that might be from the middle dorsal vertebral region. In contrast, the shaft of NMB M.H. 306 is irregularly curved and might belong to a dorsal rib from the posterior dorsal region (Fig. 6l, m). NMB M.H. 378 is a mediolaterally flattened distal

shaft fragment that is expanded relative to mid-shaft. The anterolateral face of this distal fragment bears some fine vertical striae. None of the rib shafts are plank-like, in contrast to those of titanosauriforms (Wilson 2002).

Anterior caudal vertebrae Twelve vertebrae are preserved from the anterior region of the tail, and might represent a continuous series (Table 1, “individual A”, Table 5). All of the vertebrae have undergone crushing, such that they are strongly anteroposteriorly compressed. The centra are preserved together with remains of the transverse processes (=caudal ribs in the anteriormost caudals) and the bases of the neural arches. Three isolated neural spines are tentatively attributed to three of the most anterior caudal vertebrae based on their size and morphology (Fig. 7d–f).

NMB M.H. 278 is the most anterior caudal vertebra preserved, referred to as Cd1 here (i.e. the first postsacral vertebra). In contrast to the other preserved caudal vertebrae, articular facets for chevrons are absent in this specimen, supporting the interpretation that this is one of the anteriormost caudal vertebrae. Only the centrum and base of the left transverse process are preserved (Fig. 7a–c). The flat articular surfaces of the centrum are incomplete, and the posterior articular surface partially lacks its cortical bone. Even taking into account crushing, the centrum is anteroposteriorly short, approximately one third of its height (Fig. 7c, Table 5). The anterior articular surface is approximately as high as it is wide, and roughly one third larger than its posterior counterpart (Fig. 7a, b). A thickened outer rim, formed by concentric and thin crests, bounds the anterior articular surface. The lateral and ventral faces of the centrum are weakly anteroposteriorly concave with several longitudinal crests. The preserved left transverse process is plate-like and extends laterally from mid-height of the centrum and onto the neural arch. Its ventral margin is not deflected upwards, and it appears that it lacks the wing-like morphology that characterises diplodocoids (Gallina and Otero 2009), although the dorsal margin is not complete enough to be certain. There are no excavations or projections. The ventralmost part of the transverse process is anteroposteriorly broadened and supported by an anterior (acdl) and posterior (pcdl) centrodiapophyseal lamina (Fig. 7c). The presence of these diapophyseal laminae in caudal vertebrae is primarily a feature of diplodocoids (Wilson 2002; Mannion et al. 2011), although an acdl is also present in some ‘basal’ titanosauriforms, including the brachiosaurids *Giraffatitan* and *Vouivria* (Mannion et al. 2017), as well as the somphospondylan *Tastavinsaurus* (Canudo et al. 2008).

A heavily abraded caudal neural spine, NMB M.H. 371 (Fig. 7d–f), possibly belongs to NMB M.H. 278.

Table 5 Measurements of bones of *A. greppini*, from Moutier, Switzerland: Caudal vertebrae

	Bns	CL	Hca	Hcr	Hfn	Hna	Hns	Htp	Lna	Lns	VH	Wca	Wcr	Wfn
M.H. 221	–	–	–	–	27	–	–	–	14 ^a	–	92 ^a	–	–	26
M.H. 238	–	178	–	87 ^a	–	–	–	–	–	–	93 ^a	41 ^a	37 ^a	–
M.H. 239	–	186	–	92 ^a	–	–	–	–	–	–	96 ^a	44 ^a	41 ^a	–
M.H. 240	–	151	29 ^a	33 ^a	–	–	–	–	–	–	37	70 ^a	71 ^a	–
M.H. 242	–	101 ^a	69 ^a	–	–	–	–	–	–	–	83 ^a	26 ^a	–	–
M.H. 243	–	99 ^a	–	64 ^a	–	–	–	–	–	–	67 ^a	–	24 ^a	–
M.H. 244	–	119	16	22	–	–	–	–	61	–	18	59 ^a	–	13 ^a
M.H. 245	–	111	27 ^a	29 ^a	–	–	–	–	50	–	27 ^a	54 ^a	63 ^a	10 ^a
M.H. 248	–	92 ^a	31 ^a	–	–	–	–	–	55 ^a	–	34 ^a	70 ^a	–	–
M.H. 249	–	143 ^a	26 ^a	33 ^a	–	–	–	–	–	–	34 ^a	72 ^a	76 ^a	–
M.H. 250	–	119	50 ^a	63 ^a	–	–	–	–	69 ^a	–	52 ^a	20 ^a	25 ^a	–
M.H. 251	–	146	45 ^a	29 ^a	–	–	–	–	–	–	37 ^a	82 ^a	66 ^a	–
M.H. 252	–	162	29 ^a	30 ^a	–	–	–	–	85	–	39 ^a	69 ^a	85 ^a	11 ^a
M.H. 253	–	115	26 ^a	28 ^a	–	–	–	–	61	–	29 ^a	54 ^a	58 ^a	–
M.H. 254	–	127	28 ^a	29 ^a	–	–	–	–	72	–	24 ^a	72 ^a	77 ^a	–
M.H. 255	–	93	61 ^a	62 ^a	–	–	–	–	44	–	62 ^a	31 ^a	30 ^a	–
M.H. 256	–	118	32 ^a	30 ^a	–	–	–	–	–	–	31 ^a	58 ^a	63 ^a	–
M.H. 257	–	118	71 ^a	73 ^a	–	–	–	–	66	–	74 ^a	42 ^a	33 ^a	11 ^a
M.H. 258	–	122	67 ^a	71 ^a	18 ^a	27	–	–	59	–	88 ^a	32 ^a	41 ^a	7 ^a
M.H. 271	30	39 ^a	–	111 ^a	37	56	33 ^a	99	36 ^a	32 ^a	212 ^a	–	131 ^a	28
M.H. 272	–	20 ^v	–	–	–	–	–	–	–	–	64 ^a	100 ^a	100 ^a	–
M.H. 273	91	45	69 ^a	–	39 ^a	–	–	–	–	–	125 ^a	130 ^a	–	28 ^a
M.H. 274	–	41 ^a	76 ^a	88	–	–	–	64 ^a	27 ^a	–	106 ^a	88	103	23 ^a
M.H. 275	15	41 ^a	62	78	24	34	42 ^a	23	30 ^a	23 ^a	152 ^a	74 ^a	99 ^a	19
M.H. 276	16	29 ^a	59	90	33	48	45 ^a	50	24	29 ^a	149 ^a	73 ^a	89 ^a	26
M.H. 277	16 ^a	44 ^a	102	109 ^a	28 ^a	41 ^a	–	78 ^a	36	18 ^a	178 ^a	123	124 ^a	24 ^a
M.H. 278	–	42	106 ^a	128	–	–	–	103 ^a	26	–	171 ^a	123	137	31
M.H. 279	–	46 ^a	98 ^a	117 ^a	–	–	–	76 ^a	–	–	121 ^a	95 ^a	115 ^a	–
M.H. 280	25	37	99	125	29	38	–	102	–	23	192 ^a	106	138	33
M.H. 286	20/23 ^a	–	–	–	–	–	79 ^a	–	–	47 ^a	–	–	–	–
M.H. 288	–	109 ^a	–	–	–	–	–	–	–	–	25 ^a	–	–	–
M.H. 295	–	40 ^a	74 ^a	–	–	–	–	–	–	–	–	–	–	–
M.H. 297	–	62 ^a	82 ^a	–	–	–	–	–	–	–	–	43 ^a	–	–
M.H. 300	26 ^a /69 ^a	–	–	–	–	–	90 ^a	–	–	29 ^a	–	–	–	–
M.H. 304	7 ^a	–	–	–	–	41 ^a	–	–	71 ^a	29 ^a	–	–	–	–
M.H. 335	–	74 ^a	–	62 ^a	–	–	–	–	36	–	62 ^a	–	25 ^a	–
M.H. 342	–	99	66 ^a	68 ^a	–	–	–	–	–	–	69	24 ^a	–	–
M.H. 353	–	97	–	76	–	–	–	–	41 ^a	–	70 ^a	–	28	–
M.H. 354/355	–	88	72 ^a	67 ^a	–	–	–	–	–	–	65 ^a	27 ^a	24 ^a	–
M.H. 369	28 ^a /58 ^a	–	–	–	–	–	109	–	–	39 ^a	–	–	–	–
M.H. 371	16/62 ^a	–	–	–	–	–	76 ^a	–	–	27 ^a	–	–	–	–
M.H. 449	15 ^a	112	86 ^a	–	26 ^a	26	–	–	64 ^a	–	102 ^a	34 ^a	–	9 ^a
M.H. 450	17/18 ^a	–	–	–	–	–	73 ^a	–	–	41	–	–	–	–

Bns breadth of neural spine at the base/dorsalmost breadth, *CL* centrum length, *Hca* height of caudal articular surface, *Hcr* height of cranial articular surface, *Hfn* height of foramen neuralis, *Hna* height of neural arch, *Hns* height of neural spine, *Htp* height of caudal rib or transverse process, *Lna* length of neural arch, *Lns* length of base of neural spine, *VH* total vertebral height, *Wca* width of caudal articular surface, *Wcr* width of cranial articular surface, *Wfn* width of foramen neuralis. All measurement are in mm

^a Indicates that the measurements refers only to preserved dimension at the incomplete bone

The neural spine apex is at least 2.5 times as wide as it is anteroposteriorly long and has a convex dorsal margin (Fig. 7d). In anterior and posterior views, the neural spine expands rapidly towards its apex, to about four times its basal width, giving it a ‘club’-like appearance. In this regard, the neural spine is similar to several ‘basal’ macronarians, including *Aragosaurus*, *Camarasaurus*, and *Tastavinsaurus* (Canudo et al. 2008; Royo-Torres et al. 2014). The anterior and posterior surfaces of NMB M.H. 371 are strongly rugose, but there are no distinct prespinal or postspinal laminae. The lateral face of the apex is dorsally rugose, but becomes smooth and slightly concave ventrally (Fig. 7e). On the right lateral side of the neural spine, this concavity is medially divided by a remnant of the spinoprezygapophyseal lamina (SPRL) (Fig. 7d).

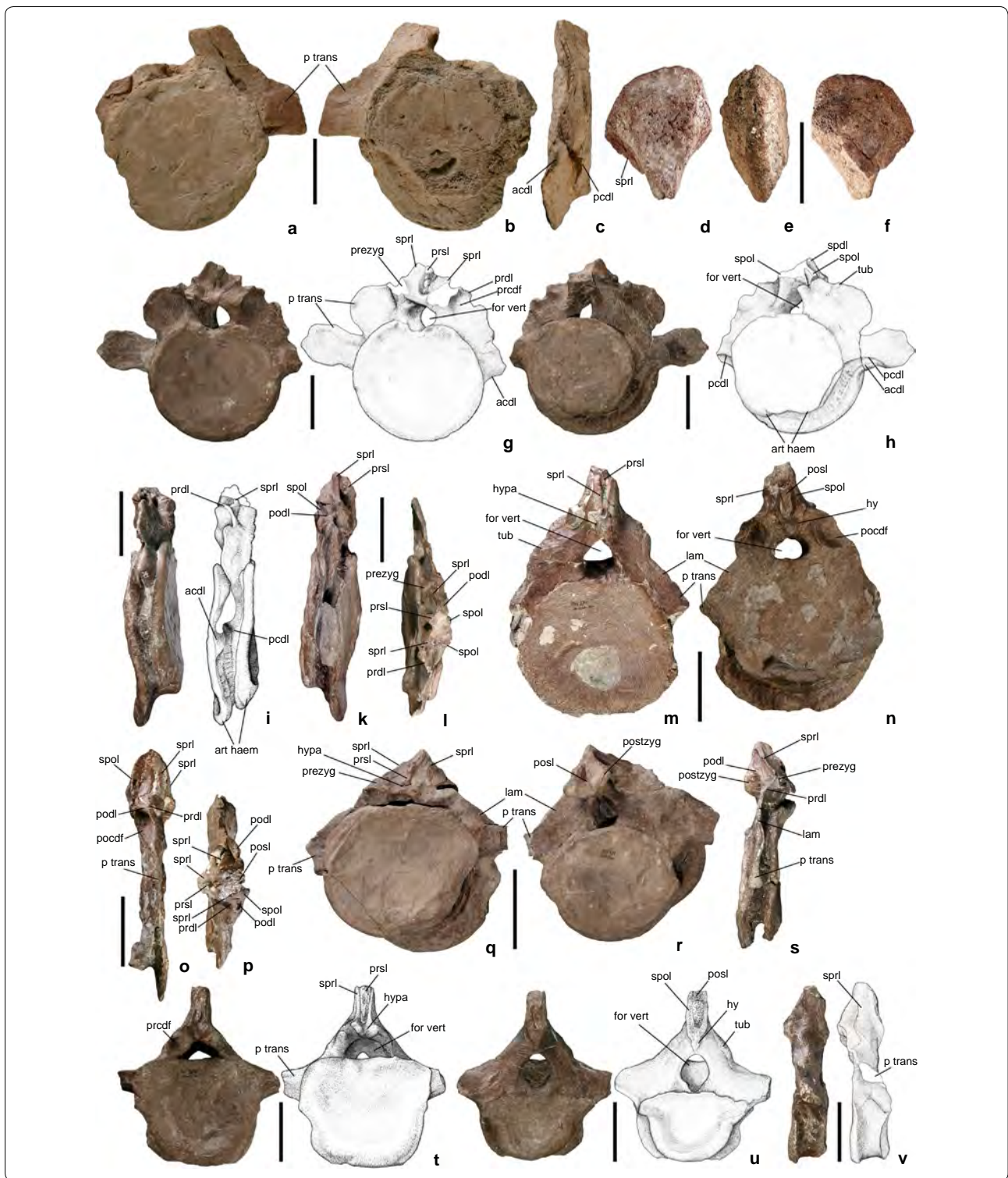
For simplicity, we refer to the subsequent eleven caudal vertebrae as Cd2–12 here. The centra of these vertebrae have similar lengths as NMB M.H. 278 (Fig. 7, Table 5). Consequently, centrum length increases relative to height along the sequence, such that the length of Cd12 (NMB M.H. 275) is 50% that of its height. In NMB M.H. 275–280, the articular surfaces of the centra are nearly circular in outline (Fig. 7). The anterior articular surfaces are approximately one third larger than their posterior counterparts (Fig. 7). All centra are slightly amphicoelous to amphiplatyan. Anterior articular surfaces of proximal caudal centra are distinctly concave in their central two-thirds, with the depth of this concavity decreasing distally. The posterior articular surfaces of Cd2 (NMB 280), Cd4 (NMB M.H. 277) and Cd7 (NMB M.H. 279) are essentially flat. Both articular surfaces are surrounded by an outer margin comprising rounded, concentric crests; these are broadest in Cd11 (NMB M.H. 276, Fig. 7t, u) and Cd12 (NMB M.H. 275). Haemapophyseal articular surfaces (chevron facets) are preserved in NMB M.H. 275 (Cd12), 279 (Cd7), and 280 (Cd2). Each haemapophyseal articulation is separated from its partner along the midline by a broad indentation, which suggests that chevrons were probably proximally unbridged. In lateral view, the haemapophyseal articulations also project posterovertrally (Fig. 7h, i). Both the ventral and lateral surfaces of

the anterior caudal centra are slightly concave, although there is no distinct ventral midline furrow. Towards the anterior and posterior margins, the ventral and lateral surfaces are rugose, with short, longitudinally directed crests. A few nutrient foramina are irregularly distributed on the ventral and lateral vertebral surfaces.

Fragmentary transverse processes are preserved in NMB M.H. 280 (Cd2), NMB M.H. 271 (Cd3), NMB M.H. 277 (Cd4), NMB M.H. 274 (Cd9), NMB M.H. 276 (Cd11), and NMB M.H. 275 (Cd12). Cd2 (NMB M.H. 280) preserves the most complete transverse process of the series, on its right side. This transverse process projects laterally and extends from the dorsal third of the centrum to the base of the neural arch. It has a simple, triangular shape in anterior/posterior views, with a horizontal ventral margin. The ventral part of the transverse process is broadened, but dorsally thins out to a plate-like structure. Both parts are separated from each other by a shallow indentation of the lateral margin of the transverse process (Fig. 7g, h). The transverse process is ventrally buttressed by an undivided anterior (acdl) and a posterior (pcdl) centrodiapophyseal lamina, with a shallow depression between them (Fig. 7g–i). At its dorsal end, the transverse process divides into a prezygodiapophyseal lamina (prdl) and a short but distinct postzygodiapophyseal (podl) lamina (Fig. 7g–l). A prdl is present in the caudal vertebrae of an array of eusauropods (Chure et al. 2010; Mannion et al. 2013), but a podl is much less common: it is otherwise known only in diplodocines, rebbachisaurids, and titanosaurs, as well as the non-neosauropod eusauropod *Wamweracaudia* (Wilson 2002; Mannion et al. 2019). The transverse processes of Cd3 (NMB M.H. 271) and Cd4 (NMB M.H. 277) are not divided horizontally: they form a rounded triangular lateral projection without distinct acdl and pcdl at the vertebral centrum, from which a laminar part (the reduced version of the plate-like structure of NMB M.H. 280) ascends (Fig. 7m, n, q, r). As in NMB M.H.280, a prdl and a short, but distinct, podl are visible in both vertebrae (Fig. 7m–p). In Cd11 (NMB M.H. 276) and Cd12 (NMB M.H. 275), the transverse processes are laterally directed rod-like structures (Fig. 7t–v)

(See figure on next page.)

Fig. 7 Anterior caudal vertebrae of *A. greppini*. 1st caudal vertebra NMB M.H. 278, **a** anterior, **b** posterior and **c** left lateral aspect. Isolated caudal neural spine NMB M.H. 371, possibly belonging to 1st caudal vertebra **d** anterior, **e** lateral and **f** posterior aspect. Photograph and interpretative drawings of 2nd caudal vertebra NMB M.H. 280, **g** anterior, **h** posterior, **i** right lateral, **k** left lateral and **l** dorsal aspect. 3rd caudal vertebra NMB M.H.271 **m** anterior, **n** posterior, **o** right lateral, and **p** dorsal aspect. 4th caudal vertebra NMB M.H. 277 **q** anterior, **r** posterior and **s** left lateral aspect. Photograph and interpretative drawing of 11th caudal vertebra NMB M.H. 276, **t** anterior, **u** posterior and **v** right lateral aspect. Scale bar is 50 mm. Drawings by Serafin Padzera. *acdl* anterior centrodiapophyseal lamina, *art haem* articular surface for haemal arch, *for vert* vertebral foramen, *hy* hyposphene, *hypa* hypantrium, *lam* lamina, *pcdl* posterior centrodiapophyseal lamina, *pcpdf* postzygapophyseal centrodiapophyseal fossa, *podl* postzygodiapophyseal lamina, *posl* postspinal lamina, *postzyg* postzygapophysis, *prcdf* prezygapophyseal centrodiapophyseal fossa, *prezyg* prezygapophysis, *prsl* prespinal lamina, *p trans* transverse process, *spdl* spinodiapophyseal lamina, *spol* spinopostzygapophyseal lamina, *sprl* spinoprezygapophyseal lamina, *tub* tuberosity



that extend from the dorsal part of the vertebral centrum to the base of the neural arch. In NMB M.H. 221, NMB M.H. 275, NMB M.H. 276 and NMB M.H. 280, an oval tuberosity is present on the dorsal margin of the

transverse process, close to the neural arch (Fig. 7m, u). A comparable tubercle has been documented in a wide array of eusauropod taxa (D’Emic et al. 2013; Propat et al. 2016; Mannion et al. 2019).

The neurocentral suture is not visible in any of the anterior caudal vertebra. The anterior opening of the neural canal is nearly circular in outline, whereas the posterior opening has a dorsoventrally tall oval shape. In NMB M.H. 271, NMB M.H. 277 and NMB M.H. 280, the bases of the prezygapophyses are preserved. Postzygapophyses are preserved in NMB M.H. 277 (Fig. 7r) but they are strongly distorted mediolaterally. Their articular surfaces are transversely oval in outline and planar. A prezygapophyseal centrodiapophyseal fossa (prcdf) is preserved ventrolateral to each prezygapophysis in Cd2 (NMB M.H. 280), Cd6 (NMB M.H. 273) and Cd11 (NMB M.H.276) and roofed by the prezygodiapophyseal lamina (prdl) (Fig. 7g). A postzygapophyseal centrodiapophyseal fossa (pocdf) is only present ventrolateral to each postzygapophysis in Cd3 (NMB M.H.271). From the dorsal margin of the prezygapophysis, a well-developed spinoprezygapophyseal lamina (sprl) extends posterodorsally and is exposed on the lateral side of the neural spine (Fig. 7k, o, s, v), although this might have been affected by crushing. The bases of spinopostzygapophyseal laminae (spol) are also preserved.

The bases of a narrow and dorsally directed neural spine are preserved in NMB M.H. 271, NMB M.H. 275, NMB M.H. 276, NMB M.H. 277, and NMB M.H. 280. The base of the neural spine is square-shaped, i.e., it is mediolaterally as wide as it is anteroposteriorly long. In NMB M.H. 271, NMB M.H. 277 and NMB M.H. 280, the base of the neural spine is buttressed by the spinoprezygapophyseal lamina (sprl) anterolaterally and by the spol and the postzygodiapophyseal lamina (podl) posterolaterally (Fig. 7h). A prominent midline rugosity, the prespinal lamina (prsl), extends along the anterior surface of the neural spine, and is laterally bounded on either side by the low and rounded spinoprezygapophyseal lamina (sprl). The development of this prsl is variable. In some specimens it is a distinct ridge, comparable to the morphology in many diplodocoids, titanosaurs, and *Giraffatitan*, whereas in others it has little anterior relief, as is the condition in most eusauropods (Mannion et al. 2013). Ventrally, the prsl ends level with the base of the prezygapophyses in a smooth pit or hollow; the latter roofs the neural canal and might represent a hypantrum (Fig. 7m, q, t). The posterior face of the neural spine bears a median groove with a rugose postspinal lamina (posl) between the spinopostzygapophyseal laminae (spol). The posl ends ventrally in a median, rounded triangular peg that reaches the roof of the neural canal and might represent a 'block'-like hyposphene. The hyposphene is best observed in NMB. M.H. 271, NMB M.H. 221, and NMB M.H.276 (Fig. 7n).

Two apices of neural spines (NMB M.H. 300 and NMB M.H. 369) are tentatively assigned to Cd3 (NMB M.H.

271), and Cd4 (NMB M.H. 277). These two neural spines are relatively similar in their morphology to that of the anteriormost caudal vertebra NMB M.H. 371 (see above). The partly preserved neural spines of Cd11 (NMB M.H. 276) and Cd12 (NMB M.H. 275) are anteroposteriorly two and three times, respectively, as long as they are mediolaterally wide. In lateral aspect, the neural spines taper dorsally, but their apices are not preserved.

Middle to posterior caudal vertebrae Several vertebrae from the region posterior to the 12th caudal vertebra are preserved. According to their size, some of them possibly belong to the same tail sequence as the anterior caudal vertebrae described above (see also "Discussion. Assignment to individuals" and Table 1. "Individual A"); however, exact determination of the position in the tail is uncertain. Based on comparisons with eusauropod taxa with complete tails [e.g., *Apatosaurus louisae*, (Gilmore 1936); *Camarasaurus lentus*, (Gilmore 1925); *Dicraeosaurus hansemanni*, (Janensch 1929); *Diplodocus carnegii*, (Hatcher 1901); *Malawisaurus dixeyi*, (Gomani 2005); *Mamenchisaurus hochuanensis*, (Young and Zhao 1972)], and taking into account that some vertebrae must be missing within this series, these caudal vertebrae reach terminally the position of at least the 28th caudal vertebra. Three of the caudal vertebrae (NMB M.H. 242, NMB M.H. 248 and NMB M.H. 256) bear regions with abnormal neoplastic bone growth, which will be described elsewhere. These vertebrae are rather similar in size and therefore could belong to the same individual. The remaining caudal vertebrae are either too large or too small to fit into the series and probably belong to other individuals, but similarities in proportions and morphology make it probable that they derived from a similar region of the tail, between the 15th and the 30th caudal vertebrae (Tables 1, 5).

All of the vertebrae are either dorsoventrally or mediolaterally compressed, and the neural arches are broken off at their bases. Centra are cylindrical and slightly hourglass-shaped in dorsal/ventral view (Fig. 8g, k). The centra become proportionally longer and lower along the tail: the length-to-height ratio ranges from 1.7 in the middle caudal vertebrae (e.g. NMB M.H. 449, Fig. 8a) to 2.8 in the most posterior caudal vertebrae (e.g. NMB M.H. 253, NMB M.H. 254, Fig. 8g, k). In contrast, the length-to-width ratio is relatively constant at around 2.4.

All of the centra are amphicoelous, with concave anterior and posterior articular surfaces (Fig. 8). Both the ventral and lateral surfaces of the centra are slightly concave and smooth; however, they become rugose lateral and ventral to the articular surfaces. The articular surfaces are surrounded by three to four concentric rings of denser bone, which are most strongly developed

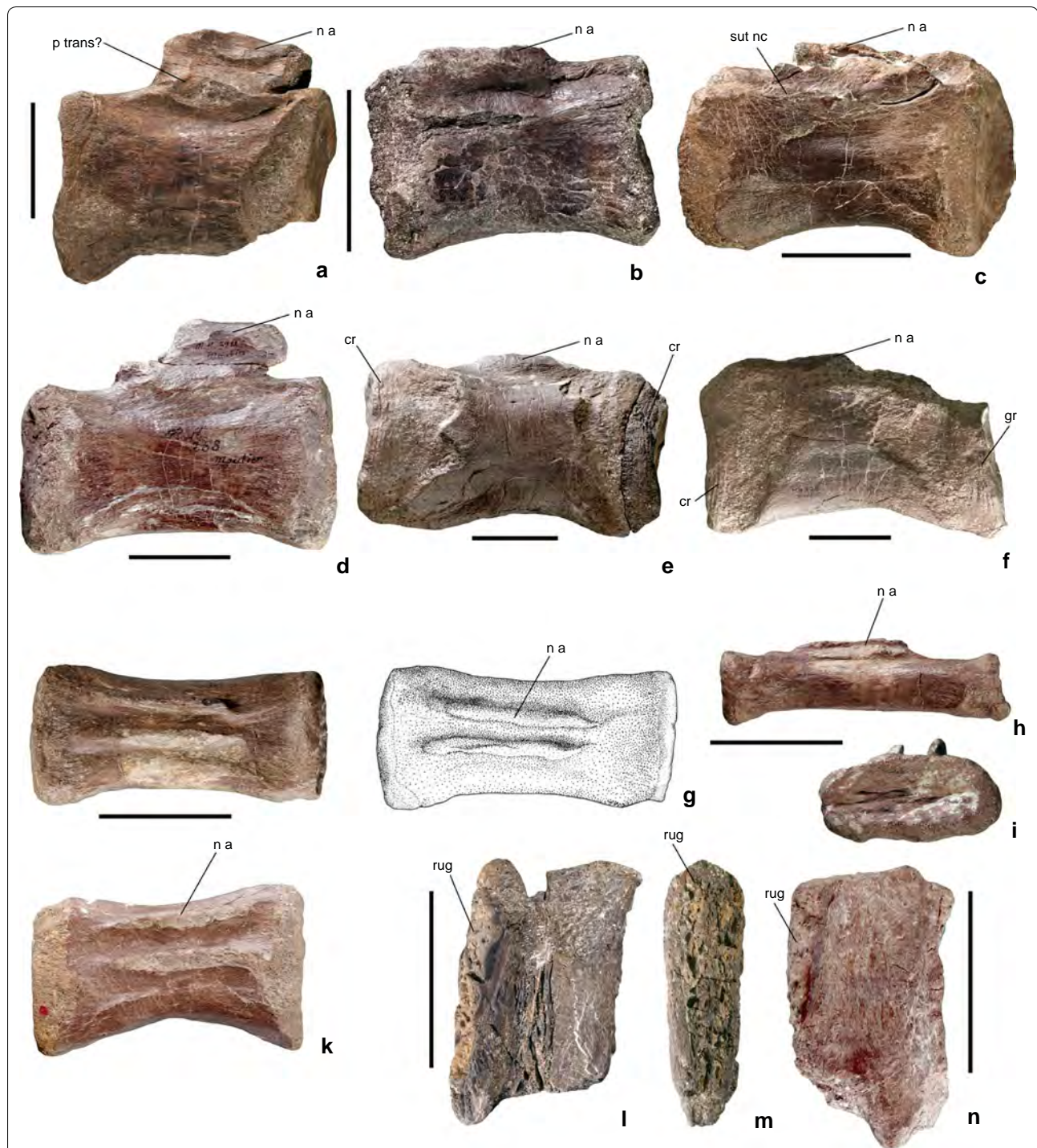


Fig. 8 Middle and posterior caudal vertebrae of *A. greppini*. **a** NMB M.H. 449, middle caudal vertebra in right lateral aspect. **b** NMB M.H. 255, middle caudal vertebra in left lateral aspect. **c** 19th (?) caudal vertebra NMB M.H. 257 in right lateral aspect, showing remnant of neurocentral suture. **d** 21st (?) caudal vertebra NMB M.H. 258 in lateral aspect. **e** Mid-caudal vertebra NMB M.H. 238 in lateral aspect. **f** Mid-caudal vertebra NMB M.H. 239 in lateral aspect. 26th (?) caudal vertebra NMB M.H. 253, **g** photograph and interpretative drawing in dorsal aspect, **h** photograph in left lateral aspect, **i** photograph in anterior aspect showing vertebral cotyle. **k** caudal vertebra NMB M.H. 254 in dorsal aspect. Mid-caudal neural spine NMB M.H. 286 **l** in left lateral, **m** in anterior aspect. **n** NMB M.H. 450, mid-caudal neural spine in left lateral aspect. Scale bar is 50 mm. Drawings by Serafin Padzera. *cr* crest, *gr* growth ring, *na* neural arch, *p trans* transverse process, *rug* rugosity, *sut nc* neurocentral suture

in the largest vertebrae (Fig. 8e, f). In damaged areas, these rings of dense bone continue as layers transversely through the bone, parallel to the articular surface, making it likely that they represent growth lines of the articular region of the vertebrae. Only one of the caudal vertebrae, NMB M.H. 249, bears laterally at the neural arch an area of broken bone that probably represent a remnant of a transverse process (Fig. 8a). The exact position of the vertebra within the tail cannot be determined, but according to its proportions a position between the 15th and 20th caudal vertebra is plausible. None of the other preserved middle and more posterior caudal vertebrae bear traces of transverse processes or lateral ridges at the vertebral centra. The base of the neural arch extends for approximately half of the length of the vertebral centra, with an anterior bias in the more anterior caudal vertebrae (Fig. 8a–c) and a slight anterior bias in the middle caudal vertebrae (Fig. 8d), whereas the posterior caudal vertebrae have no bias of the neural arch (Fig. 8g, h, k). A strong anterior bias of the neural arch characterises the middle caudal vertebrae of titanosauriforms (Calvo and Salgado 1995; Upchurch 1995), as well as some turiasaurs (Royo-Torres et al. 2017). As such, the middle caudal vertebrae of *Amanzia* have an intermediate condition between that of titanosauriforms and other sauropods. All of the neural arches are completely fused to their respective centra. A fused, or synostosed, remnant of the neurocentral suture is visible in NMB M.H. 257 as a slightly jagged and thickened line (Fig. 8c).

Two isolated neural spines (NMB M.H. 286 and NMB M.H. 450) from the proximal middle caudal vertebrae are preserved. These neural spines are twice as long anteroposteriorly as they are transversely wide (Fig. 8l–n, Table 5). In anterior and posterior views, the apices of the neural spines are slightly broadened (Fig. 8m). The anterior and posterior surfaces of the neural spines each bear a strong median rugosity, but these do not form distinct

pre- and postspinal laminae. In lateral view, the neural spines are rectangular, with straight anterior and posterior margins. The lateral surface is slightly concave and smooth.

Scapula Two incomplete scapular blades are preserved. Along with the coracoid (see below), they are described with the long-axis of the blade held horizontally. NMB M.H. 344 is a right scapula (Table 6) that is missing its dorsal margin (Fig. 9a, b). The ventral margin is concave. Both the lateral and medial surfaces are smooth, but they are also slightly compressed and distorted. Whereas the lateral surface of the scapula is slightly convex, the medial surface is flat, resulting in a D-shaped cross-section, as is the case in most eusauropods, except titanosaurs (Wilson 2002). NMB M.H. 368 comprises the distal part of a left scapular blade (Fig. 9c, d), and demonstrates that there was some distal expansion.

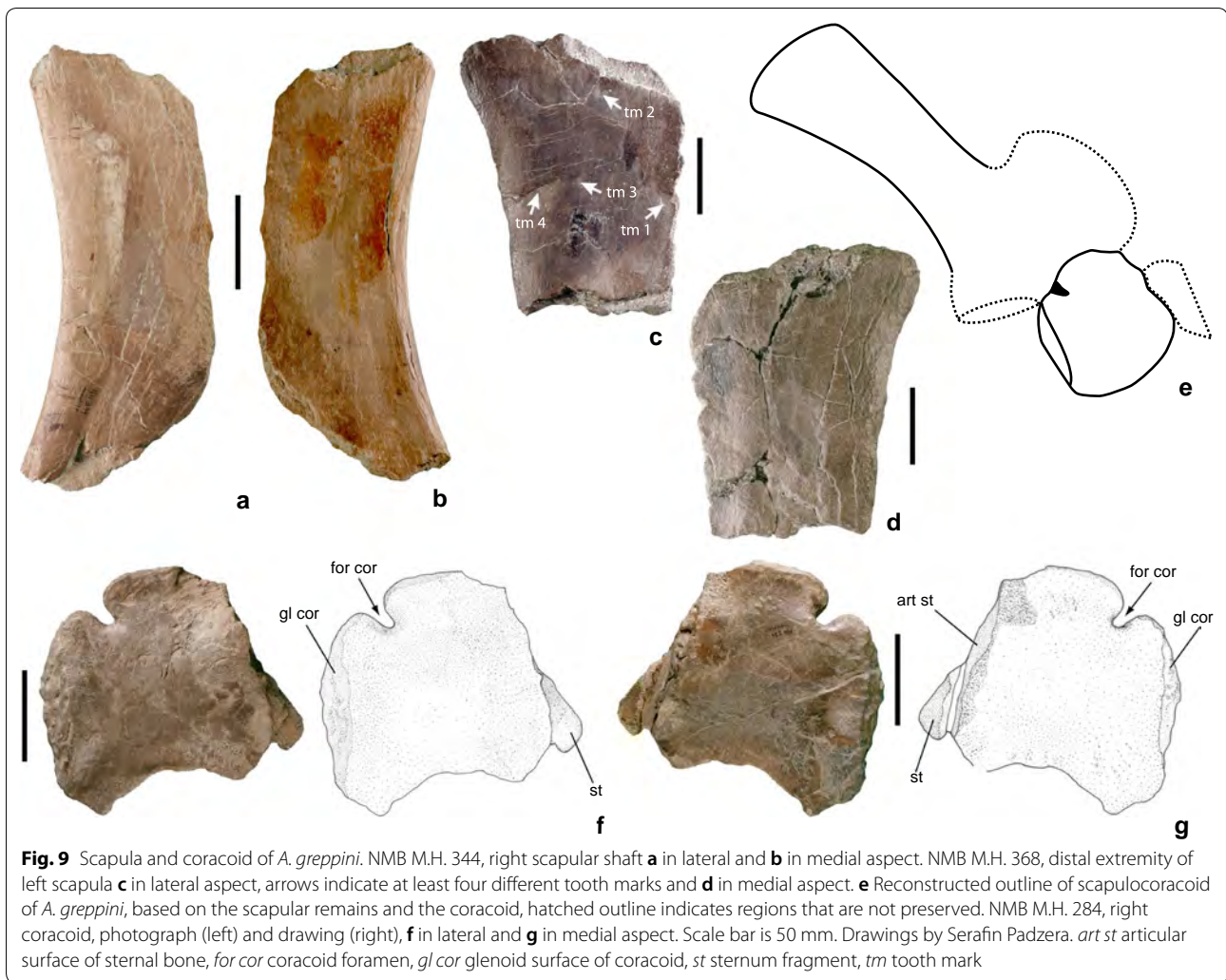
NMB M.H. 368 (Table 6) bears several unstriated tooth marks (tm) on its lateral surface. Tm 1, a small, subcircular concavity or pit (sensu D'Amore and Blumenschine 2009) is situated close to the ventral margin (Fig. 9c). Its largest (transverse) diameter is 11 mm and its depth is 3 mm. The middle third of the concavity is flat. Around the concavity, the cortical bone is broken into three concentric rings. A similar pit, tm 2, is present at the preserved distal end of the scapula. Additionally, two large impressions are positioned at the middle of NMB M.H. 368 (tm 3) and close to the dorsal margin (tm 4) (Fig. 9c). Both are roughly similar in size and oval in outline, representing probable furrows (sensu D'Amore and Blumenschine 2009), with a maximum diameter of 22 mm and depth of 4 mm. These furrows are asymmetrical, becoming steeper along their dorsal third. The cortical bone is broken at the deepest point of the concavity, as well as in a semi-circular line around the steeper dorsal flange of the concavity.

Table 6 Measurements of bones of *A. greppini*, from Moutier, Switzerland: Girdles

	DW	GL	LBS	LDO	LG	PW
M.H. 284, left coracoid	111 ^a	119	–	–	102	94 ^a
M.H. 344, right scapula	–	244 ^a	79 ^a	–	–	–
M.H. 346, left pubis	–	283 ^a	92 ^a	–	–	88 ^a
M.H. 347, left pubis	–	267 ^a	61 ^a	–	–	96 ^a
M.H. 359, left pubis	–	87 ^a	–	36	–	76 ^a
M.H. 358, left ischium	72 ^a	226 ^a	72 ^a	–	–	165 ^a
M.H. 368, left scapula	131 ^a	182 ^a	92 ^a	–	–	–

DW width of distal end = ventral end of pubis and ischium, dorsal end of scapula/dorsoventral height of coracoid, GL greatest length/craniocaudal length of coracoid, LBS least width of shaft, LDO largest diameter of obturator foramen (applies only to pubis), LG length of glenoid (applies only to scapula and coracoid), PW width of proximal end/at coracoid length of sternal articular surface

^a Indicates that the measurements refers only to preserved dimension at the incomplete bone



Coracoid. A right coracoid, NMB M.H. 284, is missing parts of its anterior margin (Fig. 9f, g). This element was interpreted as a metatarsal by Huene (1922). It is plausible that it comes from a similar-sized individual as the scapular blade NMB M.H. 344 (Table 6). The lateral surface of the coracoid is gently convex and thickened along the glenoidal part, whereas the anterior part is much thinner. The medial surface is fairly flat, and there are no tubercles or rugosities present on either surface. The glenoid articular surface is oval shaped and strongly rugose, extending onto the lateral surface. The coracoid foramen is situated at approximately midheight and is posteriorly open. This might indicate that the coracoid comes from a juvenile individual; however, the size of the element, coupled with information from other remains from the locality (see “Discussion”), argues against that interpretation. *Euhelopus* and several titanosaurs have foramina that are very close to the scapulo-coracoid suture, but they are not fully open (Curry

Rogers 2005); as such, this might be a genuinely unusual feature of *Amanzia*, and a possible autapomorphy. A small piece of bone, possibly from the right sternal plate is attached to the preserved anterodorsal corner of the coracoid. The articular surface for the sternal plate is exposed in medial aspect, where it extends along the anterior two-thirds of the dorsal margin. The coracoid is too incomplete anteriorly to determine whether or not there was a ventral notch.

Humerus A right humerus, NMB M.H. 260, is nearly complete, missing only a small medial portion and its proximolateral corner (Table 7). It has also been compressed anteroposteriorly. A larger left humerus, NMB M.H. 341 (Table 7), is preserved without most of its proximal articular surface; it also has a heavily eroded distal extremity and a distorted shaft, it was also originally mentioned by Huene (1922).

Table 7 Measurements of bones of *A. greppini*, from Moutier, Switzerland: Forelimb bones

Specimen number	DH	DTW	GL	GWdpc	Ldct	MSW	PH	PTW
M.H. 259, right ulna	–	–	394	–	–	59 ^a	–	119 ^a
M.H. 260, left humerus	–	156	534	19	298	97	–	–
M.H.264, left radius	–	–	242 ^a	–	–	55	–	–
M.H. 269, pollex claw	19	9	68 ^a	–	–	–	29 ^a	17
M.H. 340, left ulna	–	–	397 ^a	–	–	50	–	–
M.H. 341, right humerus	–	138	474 ^a	–	337	102	–	141 ^a

DH distal height (applies only to ungual phalanges), DTW distal transverse breadth, GL greatest length, GWdpc greatest width of deltopectoral crest (applies only to humerus), Ldct distance from distal end to start of dpc (applies only to humerus), MSW minimum shaft width, PH proximal height (applies only to ungual phalanges), PTW proximal transverse breadth. All measurement are in mm

^a Indicates that the measurements refers only to preserved dimension at the incomplete bone

The shaft of the humerus is slightly constricted mediolaterally and widens proximally and distally (Fig. 10). The medial margin of the midshaft is concave in anterior view, whereas the lateral margin is straight. In NMB M.H. 260, the proximal end of the humerus is transversely expanded to approximately twice the minimum shaft width, although most of this expansion occurs along the medial margin, meaning that the humerus lacks the hourglass shape that characterises most sauropods, with the exception of titanosauriforms and some turiasaurs (Tschoop et al. 2015; Poropat et al. 2016). Relative to humeral length, the midshaft is mediolaterally broad (ratio of 0.18). The distal end is approximately 1.5 times the minimum shaft width.

The humeral head has a nearly straight proximal margin, although the anteromedial corner is rounded. The anterolateral corner is too incomplete to determine its morphology. The deltopectoral crest is a low and rounded ridge restricted to the proximal half of the humerus (Fig. 10b). It projects primarily anteriorly, and does not thicken distally. It is also covered by striae oriented concentrically around the apex of the crest. A subtle, rounded tuberosity on the anterior surface of the proximal end likely represents the attachment site for *M. coracobrachialis* (Fig. 10b).

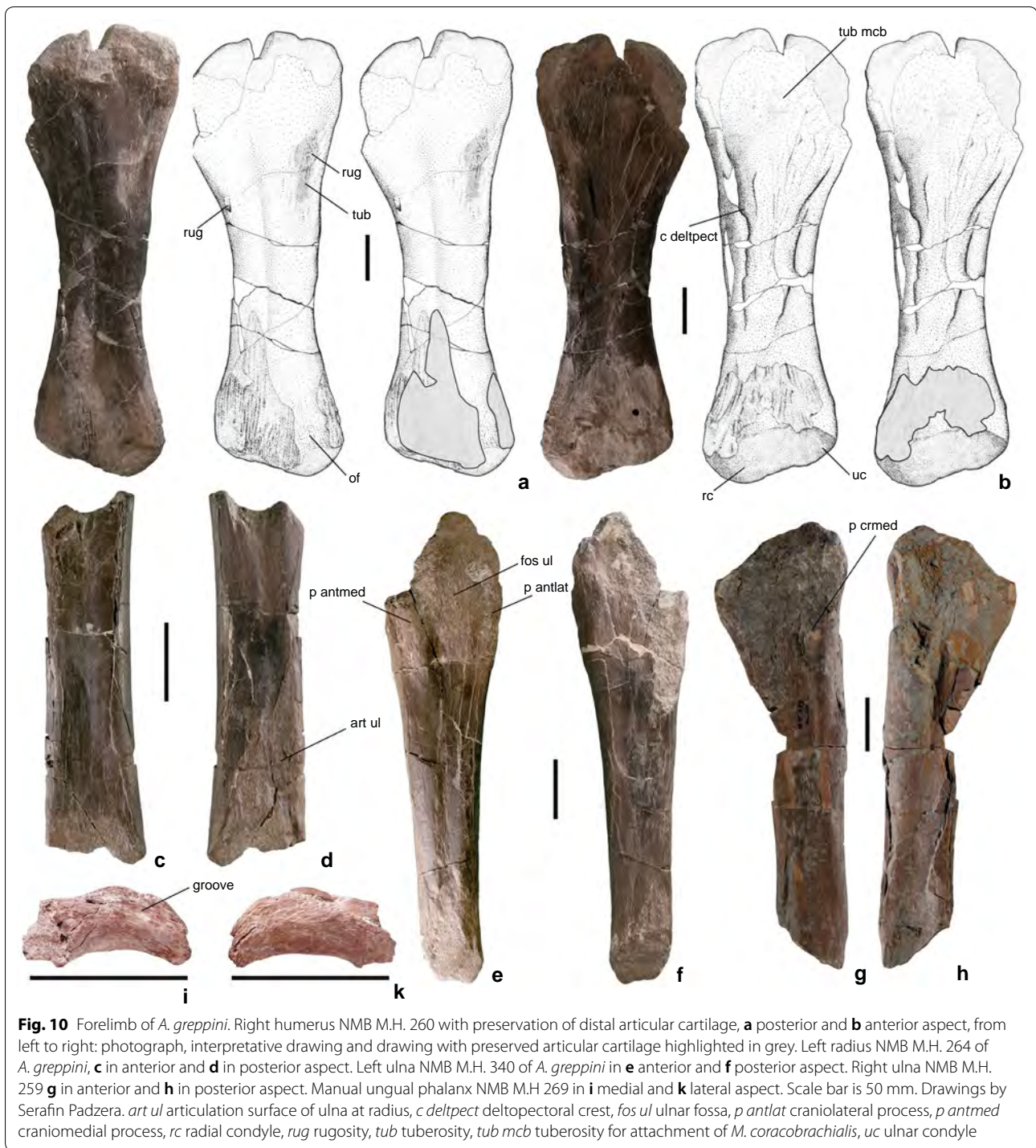
The posterior surface of the humeral shaft bears a central groove along its middle third. A prominent longitudinally oval tuberosity is developed on the lateral margin of the posterior surface, level with the deltopectoral crest (Fig. 1A). Proximally, this tuberosity continues as a rugosity. It is paralleled by a rugosity on the medial margin of the posterior humeral surface that is covered by proximodistally oriented striae (Fig. 10a). Although not as well developed as those taxa, the posterolateral tuberosity is reminiscent of muscle attachment sites documented in many titanosaur taxa (Otero 2010; Upchurch et al. 2015), as well as the turiasaur *Zby* (Mateus et al. 2014). The posteromedial rugosity is potentially also an unusual feature

of *Amanzia*, and we regard it as an autapomorphy of the genus.

At the distal articular surface of the humerus, the radial (lateral) condyle is larger and extends further distally than the ulnar (medial) condyle, giving the humerus a strongly bevelled distal margin in anterior/posterior view (Fig. 10b). The ulnar and radial articular surfaces are separated from each other by a shallow median groove, expanding onto the posterior surface as a shallow olecranon fossa. The laterally positioned epicondyle is roughened. Most of the distal extremity of NMB M.H. 260 is covered by remnants of the distal articular cartilage (Schwarz et al. 2007c) (Fig. 10), which means that we cannot determine whether or not the lateral condyle is divided. Similar, but smaller patches of articular cartilage are preserved on NMB M.H. 341.

Radius Huene (1922) interpreted an anteroposteriorly compressed long bone shaft fragment (NMB M.H. 264) as a metacarpal. However, based on both its morphology and size (Table 7), we identify this element as a distal left radius instead (Fig. 10c, d). The anteroposteriorly compressed shaft has relatively straight lateral and medial margins. At the distalmost preserved part, the radius is as wide as the shaft of the ulna, NMB M.H. 340. The posterior surface is slightly mediolaterally convex and bears a rugosity, which represents the ulnar articular surface. Distally, this rugosity covers the whole width of the posterior surface, tapering proximally towards the medial margin of the radius shaft.

Ulna A left (NMB M.H. 340) and a right (NMB M.H. 259) ulna are preserved (Fig. 10e–h; Table 7). In both ulnae, the proximal and distal articular surfaces are broken away. NMB M.H. 259 is strongly compressed and fragmentary. NMB M.H. 259 was originally interpreted by Huene (1922) to be either a radius or tibia, but our comparison with NMB M.H. 340 suggests identification as a right ulna.



The ulna has a straight shaft and tapers distally to at least half of its proximal width (Fig. 10e, f). The shaft is approximately 60% of the proximal width of the ulna, so that the bone is proportionally gracile (Table 7). The preserved part of the proximal ulnar extremity shows a weak division into anterolateral and anteromedial processes,

with a medial ulnar fossa in between (Fig. 10e, f). This fossa is better preserved in NMB M.H. 240 (Fig. 10e).

Manual phalanx I-2 NMB M.H. 269 is a left manual ungual phalanx of digit I, and represents a manus claw with the proximal articular surface broken off (Fig. 10i–k,

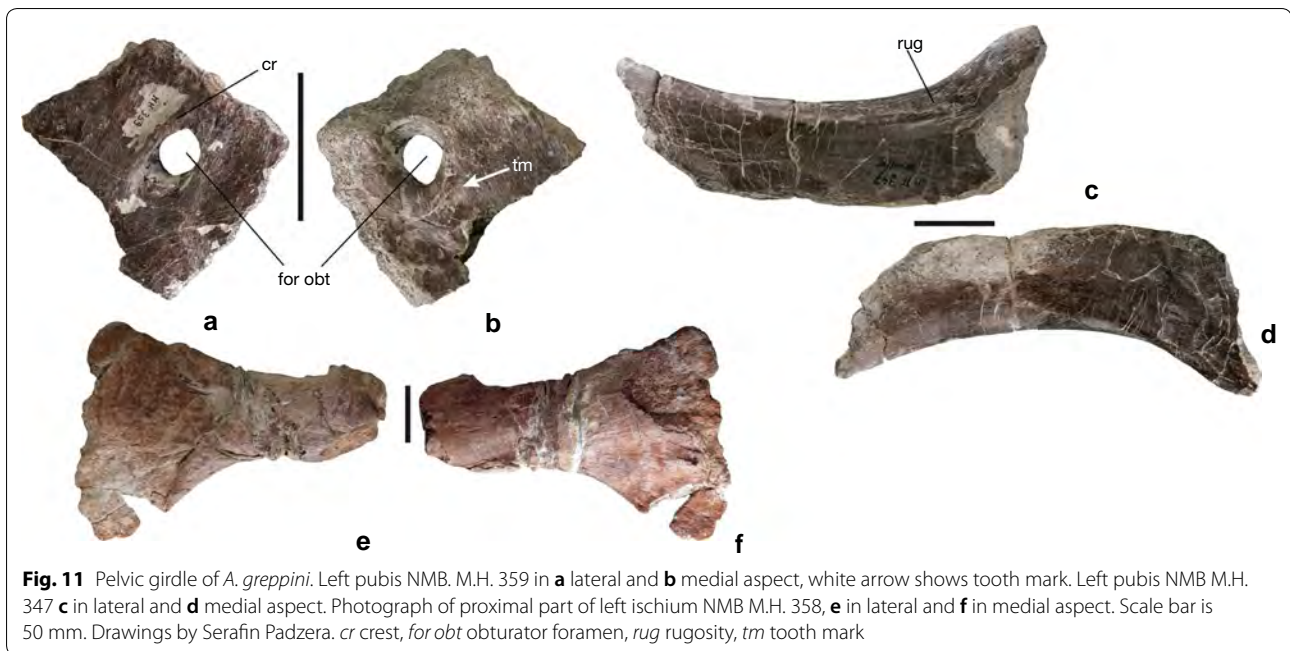


Fig. 11 Pelvic girdle of *A. greppini*. Left pubis NMB. M.H. 359 in **a** lateral and **b** medial aspect, white arrow shows tooth mark. Left pubis NMB M.H. 347 **c** in lateral and **d** medial aspect. Photograph of proximal part of left ischium NMB M.H. 358, **e** in lateral and **f** in medial aspect. Scale bar is 50 mm. Drawings by Serafin Padzera. *cr* crest, *for obt* obturator foramen, *rug* rugosity, *tm* tooth mark

Table 7). The phalanx I-2 is sickle-shaped in medial/lateral view, but only slightly recurved, and ends in a dull tip. The phalanx bears a weak medial groove, and a regular lateral surface.

Pubis Fragments of three pubes are preserved, comprising a left ischiadic peduncle and obturator foramen (NMB M.H. 359), and two proximal parts of left pubic shafts of similar size (NMB M.H. 346 and NMB M.H. 347) (Table 6). No articular surfaces are preserved in NMB M.H. 359, although the obturator foramen is completely surrounded by bone. Approximately 2.5 cm of bone separate the obturator foramen and the approximate position of the ischial articular surface. The foramen is oval with its long axis oriented posterodorsal-to-anteroventral. The obturator foramen is accompanied by an anteroventrally directed fossa on the lateral, and a posterodorsally directed fossa on the medial face of the pubis (Fig. 11a, b). On the lateral surface, the foramen is bounded dorsally by a small, rounded crest with the same long-axis as the foramen. The rest of the lateral surface is irregular, whereas the medial surface is flat. NMB M.H. 359 possesses a circular concavity on its medial surface, anteroventral to the obturator foramen (Fig. 11b), which we interpret as a tooth mark. This bowl-shaped concavity measures 6 mm in diameter and is 2 mm deep, and the cortical bone has been abraded from its walls.

The pubic shaft has a slightly concave anterior margin (Fig. 11c, d), which thickens proximally, and the lateral surface is gently convex anteroposteriorly. Posteriorly,

the pubic shaft decreases in thickness to form a slightly medially canted lamina, of which only the medial-most part is preserved in NMB M.H. 346. In the distal-most preserved part of the pubic shaft of NMB M.H. 346, the lateral surface is rugose. Proximally, the lateral surface of the shaft of NMB M.H. 347 bears a rugosity that runs parallel to the anterior margin (Fig. 11d). The medial surface of the pubic shaft is slightly concave.

Ischium A fragmentary proximal part of a left ischium (NMB M.H. 358) is preserved (Table 6). None of the articular surfaces are preserved in the ischiadic fragment. NMB M.H. 358 is a flattened bone fragment with a more spatulate proximal part that distally is more narrow and rounded to form the most proximal part of the shaft.

Another specimen, NMB M.H. 387, has been described and figured as a right ischium by Huene (1922) with reference to the collection number NMB M.H. 386, whereas he mentioned a left tibia as bearing the collection number NMB M.H. 387 (see also below). The tibia could not be located and it is currently unclear if it was lost after Huene's work and the catalogue number NMB M.H. 387 was erroneously ascribed to the bone in question later, or if Huene himself made a mistake in twice referring to this bone under different collection numbers, identifying it as both an ischium (NMB M. H. 386) and a tibia (NMB M. H. 387). Nevertheless, a well-defined proximal triangular muscle scar and a potential lateral trochanter makes it much more likely that NMB M.H. 387 is a strongly compressed and deformed fibula instead (see below).

Femur NMB M.H. 262 is a fragmentary right femoral shaft (Fig. 12f, g) that belongs to the same size class (Table 8), and possibly to the same individual, as the humerus NMB M.H. 260 (Table 1). NMB M.H. 349 is a left femoral shaft, of which the lateral half is broken away (Fig. 12c–e). The most complete femoral bone is the left femur NMB M.H. 372, which is missing only the femoral head (Fig. 12a, b). The length of the incomplete femur NMB M.H. 262 is estimated on the basis of NMB M.H. 372 and is used for comparison with the humerus NMB M.H. 260. The humerus NMB M.H. 260 reaches about 70% of the estimated length of the femur NMB M.H. 262 (Tables 7, 8).

NMB M.H. 372 is relatively straight and slender (Fig. 12a, b). Its femoral shaft is not constricted and the lateral and medial margins of the shaft are nearly straight in anterior/posterior views (Fig. 12). In cross-section, the femoral shaft is elliptical, with the transverse diameter about 1.4 times that of the anteroposterior diameter. Based on the most proximally preserved portion of the femur, it appears that the lateral margin was not medially deflected, although we cannot be certain. The distal extremity is 1.5 times as wide as the femoral shaft and slightly twisted medially in relation to the long axis of the shaft (Table 8).

Proximally, the lateral surface of the shaft bears a proximodistally striated rugosity, but it is not drawn out into a distinct lesser trochanter (Fig. 12b). This rugosity also extends onto the anterior and posterior surfaces of the femur. The 4th trochanter is positioned close to the medial margin of the posterior surface; and if the proportions of the femoral head are correctly reconstructed in the figure, it was probably restricted to the proximal half of the femur (Fig. 12a). It is a broad, low and roughened ridge, extending for an estimated one-fifth of the total femoral length. In contrast to a number of eusauropods (e.g. *Haplocanthosaurus*, *Camarasaurus*, most brachiosaurids (Whitlock 2011; Mannion et al. 2013)), the 4th trochanter is not visible in anterior view. Lateral to the distal end of the 4th trochanter, there is a proximodistally oval and rugose paratrochanteric fossa. A small rugosity is also present lateral to the proximal end of the 4th trochanter (Fig. 12a).

At the distal end, the lateral and medial condyles are almost completely abraded on the anterior surface, but are better preserved posteriorly. There is no distinct bevelling of the condyles relative to the long axis of the femur. The lateral (fibular) condyle is about 1.5 times the mediolateral width of the medial (tibial) condyle (Fig. 12a), which is a feature otherwise known primarily in titanosauriforms (Wilson 2002; Poropat et al. 2016). The intercondylar fossa on the posterior surface is slightly rugose and perforated by an oval foramen (Fig. 12a). The

lateral epicondyle of the distal femoral extremity is a prominent and proximodistally striated area that merges with the lateral femoral margin (Fig. 12a).

NMB M.H. 349, a left femoral fragment, bears multiple tooth marks on its posterior surface around and on the 4th trochanter (Fig. 12c, d). The 4th trochanter bears two large impressions but, due to its abrasion, neither the cortical bone, nor the exact shape is preserved. These oval impressions can be estimated to be around 30 mm in long-axis diameter and 5 mm in depth. Another large and circular concavity (tm1) is positioned in the dorsalmost preserved part of the bone (Fig. 12d). It is bowl-shaped and 38 mm in diameter. The medial three-fourths of this concavity are planar, and the concavity is about 6 mm deep. The cortical bone is broken around and within the walls of the concavity into three concentric breakage lines that also irregularly grow out in between. Anteriorly adjacent to this concavity are two further subcircular concavities (tm2, tm3), each with a diameter of 14 mm and a depth of 2 mm. They are bowl-shaped and similar to the large neighbouring concavity, but possess only one concentric breakage zone of the cortex. Between the 4th trochanter and these proximal concavities are several smaller concavities (tm), which are relatively weakly depressed with a depth of 2 mm. The smaller concavities are subcircular to proximodistally slightly oval in outline, and have diameters between 7 and 10 mm. The cortex within and around these concavities is not broken.

Tibia A right (NMB M.H. 339) and a left (NMB M.H. 342) tibia are preserved (Fig. 13a–d). Huene (1922) described a third (left) tibia with the specimen number NMB M.H. 387 (see ischium section above) and a bone length of 52 cm, but this could not be relocated in the NMB. The right tibia NMB M.H. 339 has an incomplete cnemial crest, but is figured in Huene (1922) with a complete crest. In the left tibia, NMB M.H. 342 (Fig. 13a, b), the proximalmost part of the cnemial crest and the posteriormost part of the distal extremity are both broken off. Neither tibia exceeds 60% of the length of the left femur (NMB M.H. 272).

Proximally, the tibia is strongly expanded mediolaterally, such that it reaches 1.8 times that of the shaft width (Fig. 13a, b, Table 8). The distal end is expanded to 1.3 times of the shaft width. The tibial shaft tapers from proximal to distal, and has a nearly straight medial and a slightly concave lateral margin. In anterior view, the proximal margin is nearly straight. The proximal articular surface seems to have been transversely oval in outline, although it is strongly compressed anteroposteriorly.

The cnemial crest is well developed and projects laterally, with a strongly convex lateral margin (Fig. 13a, b). It extends along the proximal quarter of the tibial length

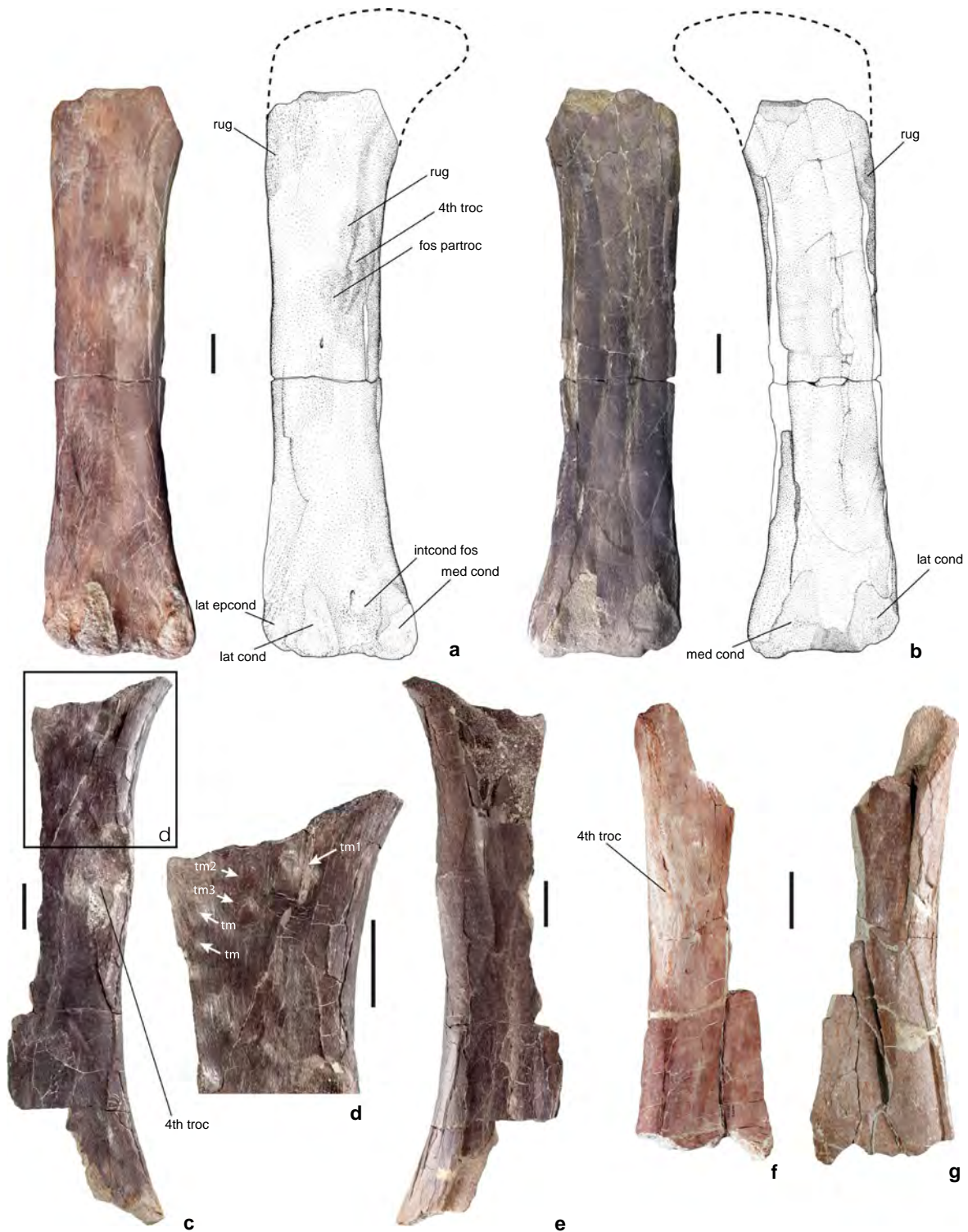


Fig. 12 Femora of *A. greppini*. Left femur NMB M.H. 372, photograph and interpretative drawing in **a** posterior and **b** anterior aspect, hatched line shows reconstructed supposed outline of femoral head. Left femur NMB M.H. 349 in **c** posterior aspect with box indicating **d** enlarged detail of posterior face of proximal femur with bite marks, some of them indicated by white arrows, **e** anterior aspect. Right femur NMB M.H. 262 in **f** posterior and **g** anterior aspect. Scale bar is 50 mm. Drawings by Serafin Padzera. *fos partrroc* fossa paratrochanterica, *intcond fos* intercondylar fossa, *lat cond* lateral condyle, *lat epcond* lateral epicondyle of femur, *med cond* medial condyle, *rug* rugosity, *tm* tooth mark, *4th troc* fourth trochanter of femur

Table 8 Measurements of bones of *A. greppini*, from Moutier, Switzerland: Hindlimb bones

Specimen number	DH	DTW	GL	Ltroc/Lcn	MSW	PH	PTW
M.H. 262, right femur	–	–	406 ^a	–	–	–	–
M.H. 282, left fibula	–	–	374 ^a	–	69 ^a	–	–
M.H. 294, metapodium	–	–	64 ^a	–	26	–	–
M.H. 323, metapodium	–	–	67 ^a	–	29 ^a	–	–
M.H. 339, left tibia	–	108	523	158	79 ^a	–	168 ^a
M.H. 342, right tibia	–	119	516	108 ^a	83 ^a	–	183 ^a
M.H. 345, right fibula	–	–	248 ^a	–	44 ^a	–	–
M.H. 349, left femur	–	–	599 ^a	295 ^a	130	–	–
M.H. 372, left femur	–	189	731 ^a	402	143	–	–
M.H. 373, left fibula	–	66 ^a	468 ^a	–	52	–	91 ^a
M.H. 387m left fibula	–	98 ^a	534 ^a	–	57 ^a	–	101 ^a
M.H. 246, right MTIII	–	34	108 ^a	–	26	–	37
M.H. 270, pedal unguis phalanx cast	21 ^a	12 ^a	101 ^a	–	23 ^a	58 ^a	16 ^a

DH distal height (applies only to unguis phalanges), DTW distal transverse breadth, GL greatest length, Ltroc/Lcn distance from distal end to 4th trochanter (applies only to femur)/length of cnemial crest (applies only to tibia), MSW minimum shaft width, PH proximal height (applies only to unguis phalanges), PTW proximal transverse breadth. All measurements are in mm

^a Indicates that the measurements refers only to preserved dimension at the incomplete bone

and its anterior and posterior surfaces are covered by proximodistally oriented wrinkles. There is no ‘tuberculum fibularis’ on the posterior surface of the cnemial crest, contrasting with several flagellicaudatans (Harris 2007; Tschoop et al. 2015) and some ‘basal’ macronarians (Mannion et al. 2017). Poor preservation of the proximal end does not allow us to determine whether a ‘second cnemial crest’ (Bonaparte et al. 2000; Mannion et al. 2013) was present.

The distal articular surface of the tibia is separated by a narrow notch at the midline, and forms lateral and medial condyles that extend mainly onto the posterior surface of the distal extremity. The medial condyle extends slightly further distally than the lateral condyle, resulting in the distal articular surface having an oblique margin in anterior/posterior views (Fig. 13b). The posterior astragalar fossa is not visible, because this area is not preserved.

Fibula A left fibula, NMB M.H. 373 (Fig. 13e, f), is preserved without its proximal- and distal-most articular ends. Another fibular fragment, NMB M.H. 282, is very incomplete and can only be identified by the preserved portion of the fibular (lateral) trochanter. NMB M.H. 282 was identified by Huene (1922) as a femoral fragment, presumably because he interpreted the fibular trochanter as a 4th (femoral) trochanter. NMB M.H. 345 is a distal fragment of a right fibula, similar in size to NMB M.H. 373. NMB M.H. 387 (Fig. 13g, h) has been determined as another, strongly flattened and diagenetically distorted left fibula, although this bone was originally identified as an ischium (Huene 1922). NMB M.H. 387 consists of two glued fragments, which were formerly given separate

(and now invalid) numbers (NMB M.H. 374 and M.H. 386).

The fibula of *Amanzia* is slender and approximately as long as the left tibia, NMB M.H. 339 (Fig. 13e, f, Table 8). The proximal and distal extremities of the fibula are moderately expanded anteroposteriorly and reach 1.5 times that of the mid-shaft width. In medial/lateral view, the fibular shaft is sigmoidal, as is the case in several titanosauriforms (Canudo et al. 2008). A distinct triangular tibial articular scar occupies nearly the entire, slightly concave medial surface of the proximal end (Fig. 13e, g). In lateral view, the proximal fibular extremity is slightly convex anteroposteriorly and bears a series of close-standing, proximodistally oriented striae. The medial surface of the middle third of the fibular shaft bears a midline groove, whereas the corresponding region of the lateral surface is characterised by a midline ridge. The fibular (‘lateral’) trochanter is a well developed and proximodistally oval rugosity formed from two vertically eongate, parallel ridges. The fibular trochanter is positioned slightly dorsal to mid-height of the shaft, and anterior to the aforementioned midline ridge (Fig. 13f, h). As such, this morphology is comparable to that of many titanosauriforms, in which the lateral trochanter has been described as being formed from two parallel ridges (Upchurch 1998). The distal fibular condyle is only partially preserved and provides no anatomical details. The lateral surface of the distal fibular extremity is irregularly rugose.

Metapodials NMB M.H. 246 was misidentified by Huene (1922) as a distal caudal centrum, and formed the basis



Fig. 13 Elements of crus and pes of *A. greppini*. Left tibia NMB M.H. 342 as photograph and interpretative drawing in **a** posterior and **b** anterior aspect. Right tibia NMB M.H. 339 in **c** anterior and **d** posterior aspect. Left fibula NMB M.H. 373 as photograph and interpretative drawing with reconstructed supposed outline of fibular head (hatched line) in **e** medial and **f** lateral aspect. Photograph and interpretative drawing of left fibula NMB M.H. 387 in **g** lateral and **h** medial aspect. Presumed 4th metatarsal NMB M.H. 246 in **i** dorsal, **k** ventral and **l** lateral aspect. Cast of pedal ungual phalanx NMB M.H. 270 **m** in lateral aspect and **n** in medial aspect. Scale bar is 50 mm. Drawings by Serafin Padzera. *cond* condyle, *cr cn* cnemial crest, *fib troc* fibular trochanter, *lat cond* lateral condyle, *med cond* medial condyle, *rug* rugosity, *t art* tibial articular surface of fibula

for his reconstruction of a “whiplash-like” distal tail of *Amanzia*. The morphology and apparent lack of bilateral long-axis symmetry in NMB M.H. 246 makes a centrum identification unlikely and we instead interpret this element to be a nearly complete metapodial, possibly a left metatarsal IV (Table 8). In dorsal/ventral views, it has a slightly mediolaterally constricted shaft, with the proximal end approximately 1.5 times the width at mid-shaft (Fig. 13i–l). Proximally, the lateral margin bears a proximodistally oval rugosity (Fig. 13i). The proximal and distal articular surfaces are strongly compressed dorsoventrally and incomplete, but a slightly convex condyle can be traced on the distal articular face (Fig. 13i). The dorsal face of the metatarsal bears a rounded ridge situated along the distal half of the specimen (Fig. 13i).

NMB M.H. 294 and NMB M.H. 323 are shaft fragments belonging to slightly transversely constricted, proximally and distally expanded metapodials (Table 8). NMB M.H. 323 bears a small, longitudinally oval concavity on the distal half of its ventral surface. The cortical bone is broken into concentric rings around the concavity. No further anatomical details can be gleaned from these remains.

Pedal ungual phalanx The ungual phalanx NMB M.H. 270 was figured by Greppin (1870), but was subsequently lost, with Huene (1922) describing only the surviving cast. The cast of this ungual phalanx, NMB M.H. 270, is about twice as large as NMB M.H. 269 (manual phalanx I-1), and is much more strongly recurved (Fig. 13m, n). Its ventral margin is concave, and the medial groove is weakly developed. NMB M.H. 270 likely represents a pedal ungual phalanx (Table 8). Its proximal articular surface is bevelled relative to the long axis of the element, as is the case in most derived eusauropods (Wilson and Upchurch 2009). There is no evidence for the ventral tuberosity seen in the pedal unguals of many titanosauriforms (Canudo et al. 2008; Mannion et al. 2013).

3.2 Bone histology

The cortex tissue, comprising the area of the outer cortex to the center of the medullary cavity (including remodelled inner parts), in the thin section of the long bone fragment NMB M.H. 261 (Fig. 14) has a total thickness of 5–11 mm. Similar to all non-dwarfed sauropod long bones studied so far (Klein and Sander 2008), the dominant tissue in the section is primary laminar fibrolamellar bone (sensu Francillon-Vieillot et al. (1990) but see Stein and Prondvai (2013). Relatively wide laminae (high ratio of vascular space to bone tissue) occur in the inner and middle cortex. Vascular space is rare in the outer cortex. Here, vascularity changes to a dominance of longitudinal canals, resulting in the absence of laminae (sensu

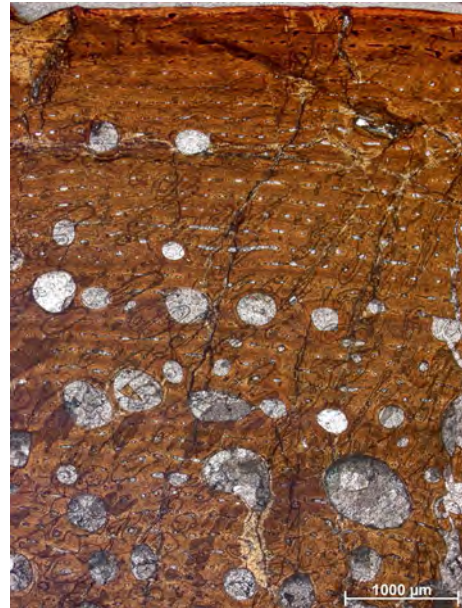


Fig. 14 Thin section of NMB M.H. 261 showing laminar fibrolamellar bone tissue with several secondary osteons and no clear lines of arrested growth

Hofmann et al. 2014). In contrast to these observations in the thin section, the polished cross-section shows wide canals in the outermost cortex.

Remodelling is evident through the presence of a number of immature secondary osteons, scattered mainly in the inner half of the cortex, and almost all of which are only partially filled with bone tissue (Fig. 14). Towards its outer margin, the cortex shows a transition from type D to type E bone tissue (Klein and Sander 2008), with the latter being far more common. The specimen can thus be attributed to Histologic Ontogenetic Stage 9 (HOS-9) sensu Klein and Sander (2008). The outer cortex shows a few faint growth marks. The cross-section reveals only three complete annual cycles, but no clear lines of arrested growth (LAGs), no signs of “polished lines” sensu Sander (1999, 2000), and no evidence of an external fundamental system (EFS), despite a smooth and complete bone surface (Fig. 14). The inner part of the bone (medullary cavity) consists of cancellous bone which is crushed as a result of compaction during diagenesis. All of the bone tissues show diagenetic cracks, which have been subsequently infilled by calcite and pyrite.

3.3 Additional vertebrate material from the locality of Moutier

SAURISCHIA Seeley, 1887b
THEROPODA Marsh, 1881

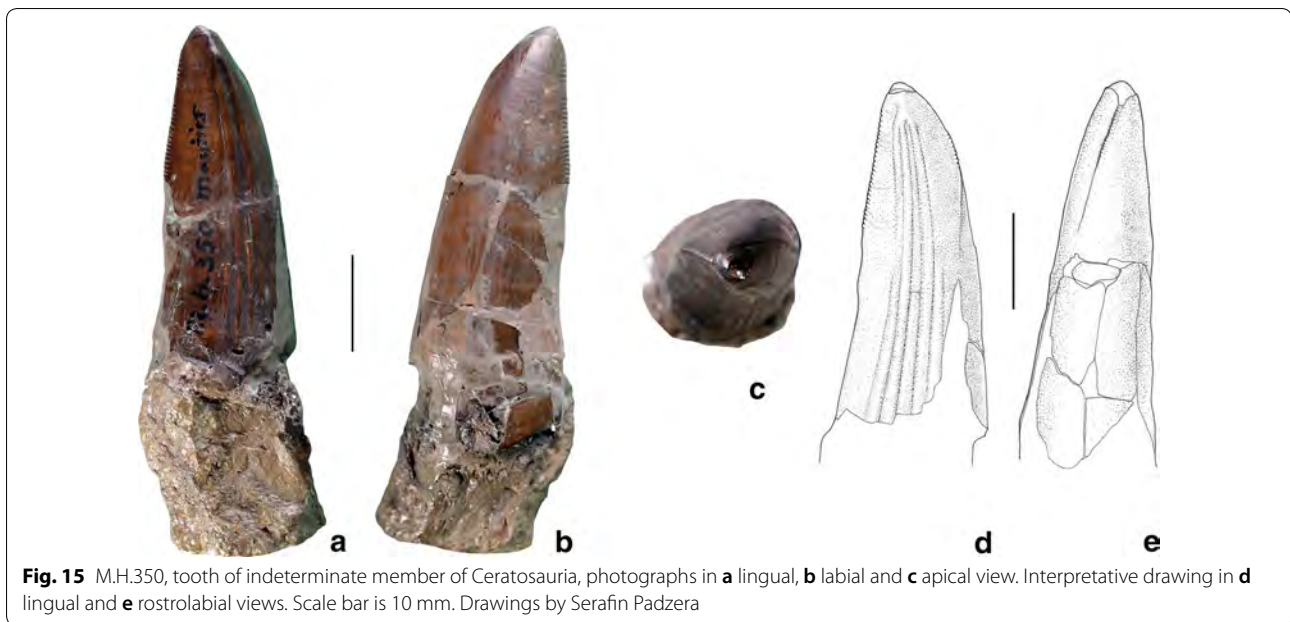


Fig. 15 M.H.350, tooth of indeterminate member of Ceratosauria, photographs in **a** lingual, **b** labial and **c** apical view. Interpretative drawing in **d** lingual and **e** rostralabial views. Scale bar is 10 mm. Drawings by Serafin Padzera

NEOTHEROPODA Bakker, 1986

CERATOSAURIA Marsh, 1884

CERATOSAURIA indet.

Synonymy:

v * 1870 *Megalosaurus meriani* Greppin: p. 118, p. 339, Pl. I fig. 1a–c (nom. dub.)

v 1920 *Labrosaurus* Janensch 1920: p. 233

v 1922 *Labrosaurus* Huene 1922: p. 80

v 1926 *Labrosaurus meriani* Huene 1926: p. 81

v 1970 *Antrodemus* Steel 1970: p. 29

1978 *Allosaurus meriani* Olshevsky 1978 (nom. dub.)

v 1991 ?*Allosaurus meriani* Olshevsky 1991: p. 111

Material NMB M.H. 350, tooth from the rostral snout region.

Description NMB M.H. 350 is almost complete, though only parts of the root are preserved and are embedded in sediment. It exhibits a fairly typical theropod tooth morphology (Fig. 15, Table 9). The apex of the crown is well worn and polished. The apical part of the slightly labiolingually compressed and distally curved crown is slightly twisted, such that the crown is asymmetrical (Fig. 15c). In apical view, the tooth crown also exhibits a slight curvature to the lingual side. As a result of the slightly twisted apex, the mesial and distal carinae are not parallel to each other. The well-developed distal carina bears 10 denticles per 5 mm (Fig. 15b, d). The basal half of this distal serration shows wear. In contrast, serration of the mesial

carina is weakly developed along its basal half and curves to the lingual side. A prominent feature of the tooth is the presence of five longitudinal enamel ridges, which are centred on the lingual face (Fig. 15a, d). In contrast, the more convex, labial surface of the tooth crown is smooth. The base of the tooth crown is subcircular. Because of its rounded base and only slight curvature of the tooth crown, the preserved tooth can be placed in the rostral-most part of the skull or the mandible.

Remarks In his original erection of the taxon *Megalosaurus meriani*, Greppin (1870) considered the single tooth NMB M.H. 350 to belong to the same taxon as the other dinosaur remains. The tooth was later mentioned by Janensch (1920), who referred it to the genus *Labrosaurus*. Following Janensch (1920), Huene (1922, 1926) designated the tooth as *Labrosaurus meriani*, whereas the majority of the preserved bones from Moutier were identified as belonging to a sauropod, therein named *Ornithopsis greppini*. Steel (1970) subsequently referred the tooth to the genus *Antrodemus*, although did not comment upon any species assignment. However, *Antrodemus* is a junior synonym of *Allosaurus*, and Olshevsky (1991) consequently determined the tooth as belonging to *Allosaurus meriani*. The latter classification was doubted by Glut (1997), who placed the tooth outside the genus *Allosaurus*. Neither *Megalosaurus meriani*, nor any of its subsequent recombinations, is considered to be a valid, diagnostic taxon, and it has been considered a nomen dubium by all recent authors (e.g. Molnar et al. 1990; Glut 1997; Holtz et al. 2004).

Table 9 Measurements of bones of other fossil vertebrates from Moutier, Switzerland: Crocodylomorpha and Theropoda

	CL	Hca	Hcr	Lna	VH	Wca	Wcr	B	L
M.H. 247, caudal vertebra	52 ^a	56 ^a	–	–	33 ^a	62 ^a	–		
M.H. 351, caudal vertebra	98	–	–	–	28 ^a	–	64 ^a		
M.H. 352, dorsal vertebra	61	64 ^a	63	44 ^a	66 ^a	55 ^a	50 ^a		
M.H. 329, articular	–	–	–	–	–	–	–	31 ^a	58 ^a
M.H. 303, skull fragment	–	–	–	–	–	–	–	25 ^a	56 ^a
M.H. 309, skull fragment	–	–	–	–	–	–	–	26 ^a	50 ^a
M.H. 370, skull fragment	–	–	–	–	–	–	–	45 ^a	98 ^a

M.H. 350, theropod tooth: total preserved height = 48.8 mm; length (mesiodistal) at base = 18.1 mm; length at apex = 2–3 mm; breadth (labiolingual) at base = 15.5 mm; breadth at apex = 3 mm; length of complete serrated edge = 19 mm

B preserved breadth or width of skull fragments, CL centrum length, Hca height of caudal articular surface, Hcr height of cranial articular surface, L preserved length of skull fragments, Lna length of neural arch, VH total vertebral height, Wca width of caudal articular surface, Wcr width of cranial articular surface. All measurement are in mm

^a indicates that the measurements refer only to preserved dimension at the incomplete bone

A detailed description and taxonomic analysis of the tooth was presented by Chure (2000), who stated that the tooth closely resembles the first premaxillary tooth of *Ceratosaurus* in the presence of a short mesial denticle row. According to Chure (2000), the tooth differs from the teeth of *Allosaurus* by the characteristic lingual ridges on the tooth enamel. Among Theropoda, exclusively lingual ridges on rostral teeth have been reported from *Ceratosaurus* (Madsen 1976; Madsen and Welles 2000; Britt 1991; Bakker and Bird 2004; Soto and Perea 2008), “*Labrosaurus*” *stechowi* (Janensch 1925) and “*Labrosaurus*” *sulcatus* (Marsh 1896). However, “*Labrosaurus*” *stechowi* possesses lingual ridges on the teeth of the lateral side of the jaws and not the premaxillary teeth (Chure 2000), and “*Labrosaurus*” *sulcatus* is most probably a junior synonym of *Ceratosaurus* (Soto and Perea 2008; Chure 2000). According to Madsen and Welles (2000), lingual grooves typically occur in the rostral-most teeth of *Ceratosaurus*; however, these teeth do not show differences at the species level. Madsen and Welles (2000) therefore determined that the tooth from Moutier belongs to *Ceratosaurus*, but did not assign it to any species. Most recently, Carrano et al. (2012) assigned NMB M.H. 350 to an indeterminate member of Ceratosauria based on its overall similarity to the anterior teeth of *Ceratosaurus*, a determination which we follow here.

CROCODYLOMORPHA Walker, 1970 (sensu Clark 1986)

THALATTOSUCHIA Fraas, 1901

TELEOSAURIDAE Geoffroy, 1831

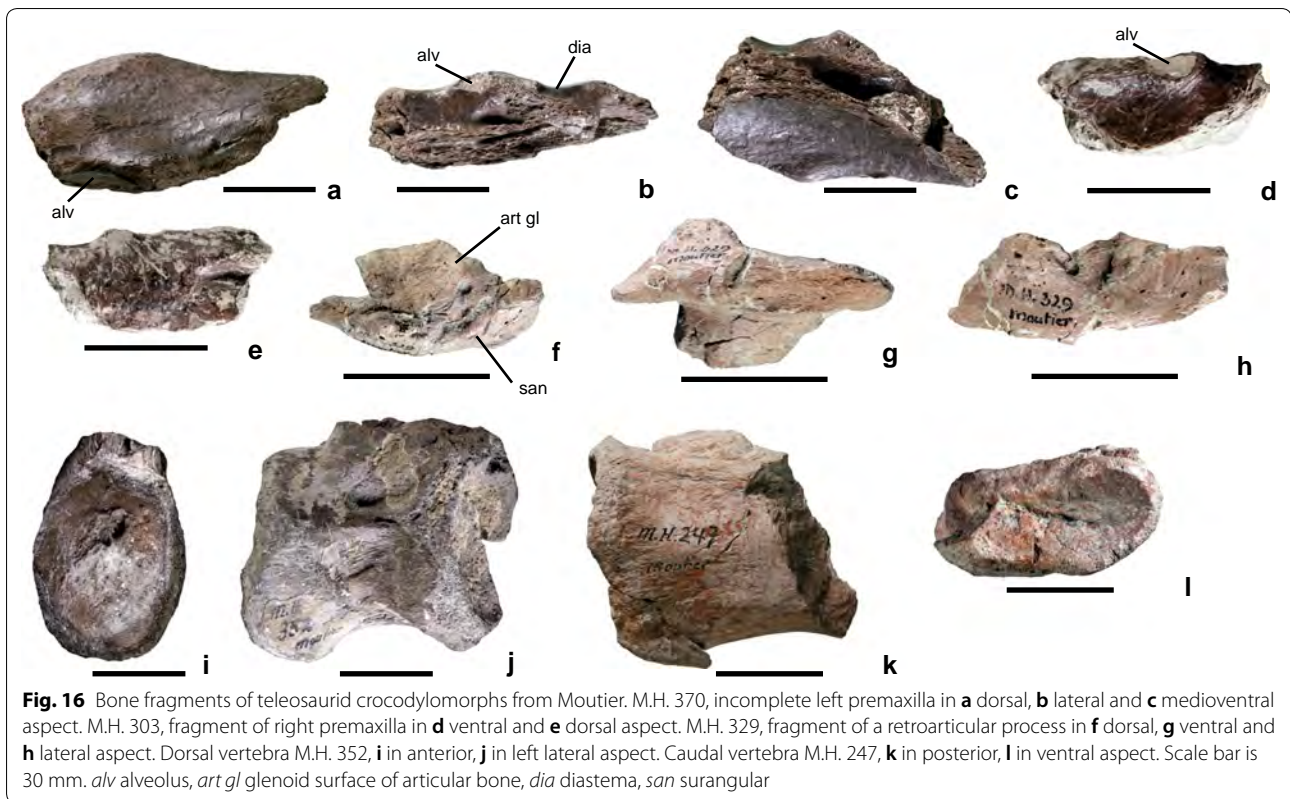
Teleosauridae indet.

Material. NMB M.H. 303, right premaxilla fragment; NMB M.H. 370, left premaxilla; NMB M.H. 309

undetermined skull fragment; NMB M. H. 329, fragment of articular; NMB M.H. 352, dorsal vertebra; NMB M.H. 247, caudal vertebra; NMB M.H. 351, caudal vertebra.

Description NMB M.H. 370 is a partial left premaxilla (Fig. 16a–c), preserved with the main premaxillary body and parts of its anteriormost extension. The dorsal surface of the bone is smooth without any trace of sculpturing. The medial margin of the premaxilla, forming the contact to the nasal, is straight in its posterior half and bends obliquely laterally in its anterior half. The medial-most part of the premaxilla is broken off and no trace of the outline of the external nares is visible. Laterally, the posteriormost part of the margin forms a slight indentation, which represents a diastema to the posteriorly adjacent maxilla. Directly anterior to the diastema lies a small, circular premaxillary alveolus, with another indentation from the lateral premaxillary margin anterior to this alveolus. In ventral view, the premaxillary bone is slightly concave and smooth. In medial view, a canal between the ventral and dorsal parts of the premaxilla is visible, which represents the anteriormost extent of the nasal passage and the secondary palate. A smaller fragment of a right premaxilla of similar size, NMB M.H. 303, is identical in shape to NMB M.H. 370, and also preserves a circular premaxillary alveolus anterior to a diastemal indentation (Fig. 16d, e).

NMB M.H. 329 is a fragment of a retroarticular process with the glenoid preserved (Fig. 16f–h). In dorsal view, a weakly visible suture between the glenoid process and the laterally adjacent bone wall marks a division between the articular (forming the glenoid and medial wall of the preserved bone) and surangular (forming the lateral wall of the preserved bone) (Fig. 16g, h). The glenoid surface is nearly circular and medially expanded, and continues anteriorly with the dorsal margin of the articular;



however, its cortical bone surface is destroyed. The ventral margin of the preserved retroarticular fragment is convex. In lateral view, the preserved part of the surangular is very weakly sculptured (Fig. 16f). The posterior part of the retroarticular process is not preserved.

NMB M.H. 352 preserves a transversely compressed centrum, and was originally described by Huene (1922) as a cervical vertebra. It is likely that Huene (1922) mistook a part of abraded bone on the posterior side of the vertebral body as a parapophysis, whereas the vertebra shows neither traces of a parapophysis nor diapophysis. As such, given the absence of a parapophysis, we consider it most likely that the vertebral centrum represents a dorsal vertebra instead. The centrum is as long as it is high (Tables 3, 4, 5, 6, 7, 8, 9), and its articular surfaces are concave and bowl-shaped (Fig. 16i). A distinct, rugose rim surrounds each articular surface. The broadened ventral face of the vertebral centrum is separated from the lateral face by a rounded edge, and is concave in lateral view (Fig. 16j). Fine, longitudinal striae excavate the ventral surface. The lateral face of the centrum is also slightly rugose and bears longitudinal striae. A prominent longitudinal ridge is developed at mid-height of the centrum; the lateral surface dorsal and ventral to this ridge is weakly concave. The neurocentral suture is completely fused, but is visible on the right side of the vertebra as a

weakly convex, jagged and thickened line. Only the base of the neural arch is preserved, and is situated along the posterior two-thirds of the centrum.

An anterior caudal vertebra, NMB M.H. 351, preserves the ventral half of its centrum. It is broad and stout, and bears concave articular surfaces. The ventral surface of the centrum is concave and broad, and is separated from the lateral face by a prominent ridge-like edge. The lateral side of the centrum is smooth, becoming slightly concave dorsally. On the right side, the base of a posteriorly-directed transverse process is preserved, situated on the anterior third of the centrum, at approximately mid-height. The internal surface of the centrum is compact bone. NMB M.H. 247 (Fig. 16k, l) is a posterior half of an anterior caudal vertebra, with a strongly concave articular surface, and similar morphology as NMB M.H. 351. NMB M.H. 309 is another possible vertebral fragment of a crocodylomorph; however, it is too fragmentarily preserved to be identified further.

Remarks The material preserved can be unambiguously determined to belong to a medium-sized crocodylomorph. Huene (1922) determined the vertebra NMB M.H. 352 to be a cervical vertebra of (?) *Dacosaurus* sp., whereas the caudal vertebra NMB M.H. 351 was determined to belong to the tail of the same individual. He

also assigned the two vertebral centra NMB M.H. 254 and NMB M.H. 355 to (?) *Dacosaurus* sp., but these specimens have been revised here to represent caudal vertebrae of *Amanzia* instead (see above). The general proportions of the amphicoelous vertebrae, along with the morphology of the premaxillary fragment with a diastema, strongly resemble those of teleosaurid thalattosuchians (Delfino and Dal Sasso 2006; Fraas 1901; Pierce and Benton 2006; Westphal 1962; Buffetaut 1982; Krebs 1962, 1967a, b, 1968; Sauvage 1874; Hua 1997, Young et al. 2014). With its short vertebral centrum with high-oval articular surfaces, the dorsal vertebra (NMB M.H. 352) closely resembles the dorsal vertebrae of *Machimosaurus* (Krebs 1967b). However, the absence of taxonomically informative remains, such as teeth or more readily identifiable snout fragments, makes determination at the genus level impossible. Teleosaurid thalattosuchians have previously been reported from the Upper Jurassic of Switzerland (Krebs 1962, 1967b; Huene 1925, Young et al. 2014a, b), and thus their presence in Moutier is not unexpected.

4 Discussion

4.1 Assignment to individuals, skeletal reconstruction, and ontogenetic age

The bones attributed to *A. greppini* were found together but not articulated. The significant size differences between the individual bones (Tables 3, 4, 5, 6, 7, 8, 9), in addition to the presence of duplicated elements, demonstrates that more than one individual of *Amanzia* was present in the deposit. Huene (1922) suggested that there were between 2 and 3 individuals, but we conclude that at least four individuals were present (Table 1). However, because of the disarticulated nature of the material, assignment of the bones to discrete individuals is difficult, and it is plausible that even more individuals were present. Furthermore, there are many additional elements that cannot be attributed by size or morphology to any of these individuals.

The cranial remains, one of the cervical vertebrae, most of the caudal vertebrae, scapula and coracoid, the left humerus, left pubis and partial left ischium, a fragmentary left femur, both tibiae, the left fibula, the metapodials, and one ungual phalanx, comprise one size class and therefore possibly belonged to one individual, labelled in this work as “individual A”. A second fragmentary left pubis of similar size to individual A indicates the presence of another individual, labelled as “individual B”. As individuals A and B were similar in size, the attribution of single bones (except the duplicated left pubis) to one of these individuals is uncertain, but for convenience we attribute most of the material to individual A. “Individual C” comprises caudal vertebrae, a right humerus, a right

and a left ulna, a left radius, both femora, and a left fibula and is approximately 15% larger than individuals A and B, based on the femora. Size differences in the cervical and caudal vertebrae allow the recognition of a fourth individual, which is labelled here as “individual D” and was at least 20% smaller than individuals A and B.

All identifiable remains of *A. greppini* were used for the skeletal reconstruction, with individual A providing information on the proportions of the animal (Fig. 17). The cranial remains do not provide information on the skull shape, and the two incomplete cervical vertebrae provide no information on their neural spine morphology. The number of missing caudal vertebrae was estimated based on comparisons with other sauropod caudal series (e.g. Upchurch et al. 2004) and a total of at least 45 caudal vertebrae with a proportional decrease in size posteriorly is likely, based on proportions of the tail vertebrae. As the numbers of vertebrae are not known, the total length of the reconstructed individual is speculative and might consequently be over- or underestimated. Taking this into account, a body length of between 7 and 8 m is estimated for individuals A and B, with individual C approaching a length between 9 and 10 m. Thus, *A. greppini* can be reconstructed to have been a relatively small sauropod that was probably not more than 10 m in body length.

Ontogenetically, with the possible exception of the open coracoid foramen (see Description), none of the skeletal remains bear indications of a juvenile status. Indicators for an adult ontogenetic stage of the individuals are the generally fully closed, synostosed (i.e., absent) neurocentral sutures, the obturator foramen of the pubis completely surrounded by bone, the strongly rugose articular ends of the appendicular bones, and the very strongly developed insertion scars for soft-tissues on the appendicular bones (Ikejiri 2004; Ikejiri et al. 2005a; b).

Because of the fragmentary nature of NMB M.H. 261, which was used for the histological section, it cannot be unambiguously assigned to any of these individuals representing different ontogenetic stages, or even to a size class. In the thin section, the low number of growth marks and the absent EFS indicate a still growing individual, although the growth rate has already decreased based on tissue organization and vascular density. The wide canals in the outermost cortex, visible in the bone cross-section, are another indication of ongoing growth. The laminar fibrolamellar tissue is typical for sauropods. The low number of secondary osteons speaks for a low remodeling stage (RS) sensu Mitchell et al. (2017) and thus against a senescent age. Following Klein and Sander (2008), bone tissue types D and E have been identified, which confirms the relatively fast growing tissue of young, still growing adults (Klein and Sander 2008). This

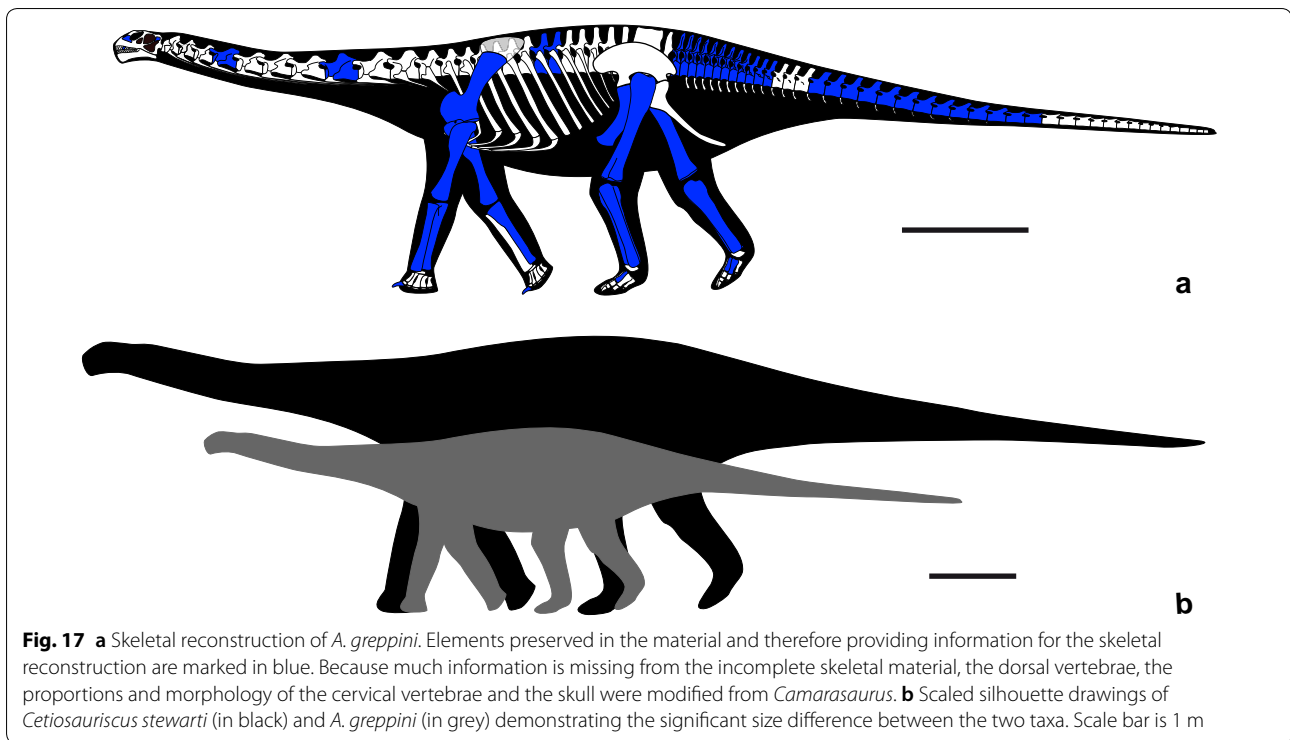


Fig. 17 **a** Skeletal reconstruction of *A. greppini*. Elements preserved in the material and therefore providing information for the skeletal reconstruction are marked in blue. Because much information is missing from the incomplete skeletal material, the dorsal vertebrae, the proportions and morphology of the cervical vertebrae and the skull were modified from *Camarasaurus*. **b** Scaled silhouette drawings of *Cetiosauriscus stewarti* (in black) and *A. greppini* (in grey) demonstrating the significant size difference between the two taxa. Scale bar is 1 m

so-called HOS-9 stage of the bone tissue indicates a successive slow-down in the initial growth rate of a not yet fully-grown individual, which nevertheless would still have achieved a substantial gain in body size if not for its premature death: HOS-9 occurs in animals of up to 75% of maximum adult size (Klein and Sander 2008; Sander et al. 2006). A combination of unfinished neurocentral closure in the vertebrae and the presence of HOS-9 as in *Amanzia* is also reported for the diplodocid *Galeamopus pabsti* (Tschopp and Mateus 2017) and the titanosaurid *Bonitasaurus* (Gallina and Apesteguía 2011, 2015). However, as it is not possible to say from which individual of *Amanzia* the sampled bone derived, any conclusion about the implications of these characters for maturity stages would be ambiguous.

The different sizes of the adult individuals of *A. greppini* can be explained in at least three ways. Firstly, the different sizes might have been affected by environmental factors, such as climate or food availability, as has been proposed for the basal sauropodomorph *Plateosaurus* (Sander and Klein 2005). In *Plateosaurus*, fully-grown individuals were apparently distributed in a large spectrum, ranging from 5 to 10 m in body length, which was attributed to a high developmental plasticity by different environmental factors. However, such a developmental plasticity does not seem to have been present in more derived sauropodomorphs (Sander and Klein 2005). A

second interpretation would be to attribute the size variation to sexual dimorphism. Unfortunately, the minimum number of preserved individuals is too low to determine a clear bimodal size distribution, and the material shows a gradual size increase across three body size classes instead (Tables 3, 4, 5, 6, 7, 8, 9). The third interpretation, and the one we prefer, is that the different body sizes might be the result of different ontogenetic ages, with the smallest individual representing the youngest, and the largest individual representing the oldest. This hypothesis is supported by the presence of a smaller cervical vertebra (NMB M.H. 267: individual A or D), which is less pneumatized than the cervical vertebra NMB M.H. 265 (individual A); the degree of internal pneumatization increases strongly during ontogeny (Wedel 2005; Schwarz et al. 2007b). The histological section, indicating a still growing individual, further supports this interpretation.

4.1.1 Interpretation of tooth marks

Tooth marks have been detected on five bones of *Amanzia*. Four of these bones (NMB M.H. 291, NMB M.H. 323, NMB M.H. 349, and NMB M.H. 359) are of comparable size to one another and therefore might belong to the same individual, whereas the remaining element (NMB M.H. 368) probably belonged to a larger individual. The tooth marks occur mainly on appendicular bones, with

the exception of a putative tooth mark on a dorsal rib. The size of the tooth marks ranges from 6 to 38 mm in diameter, and their depth does not exceed 6 mm.

The majority of the tooth marks are circular and bowl-shaped. There are also two oval tooth marks with steeper bone walls. Both types are present in the two size classes. These tooth marks are morphologically consistent with those described in the literature for theropod dinosaurs and crocodylomorphs (e.g., Buffetaut 1983; Fiorillo 1991; Erickson and Olson 1996; Fowler and Sullivan 2006; Njau and Blumenschine 2006). The circular, bowl-shaped tooth marks can be interpreted as puncture marks, and are particularly similar to those puncture marks reported as feeding traces from extant and fossil crocodylomorphs (e.g. Avilla et al. 2004; Njau and Blumenschine 2006). The more groove-like tooth marks closely resemble puncture marks described for theropod dinosaurs (Fowler and Sullivan 2006; Carpenter 1998), but also for extant crocodylians (Njau and Blumenschine 2006).

Given that there is evidence for both a fossil crocodylomorph and a theropod dinosaur in the same locality as *Amanzia* (see above), these taxa are likely candidates for having produced these traces. The crocodylomorph remains most likely belonged to a teleosaurid thalattosuchian, such as *Machimosaurus*, which had stout conical teeth and has been reconstructed as being able to feed on harder prey (Young et al. 2014b). Teeth of *Machimosaurus* can exceed 10 mm in diameter, and are a close fit to the puncture marks. A *Machimosaurus*-like animal is thus likely to have scavenged on *Amanzia*. The theropod has been identified as a ceratosaur (Chure 2000), which would have likely both preyed and scavenged on other dinosaurs. The larger and oval puncture marks in the remains of *Amanzia* are a close fit with the preserved ceratosaur tooth, although such an animal could have produced some of the round puncture marks as well.

4.2 Taxonomic assignment

4.2.1 Generic separation of “*Cetiosauriscus*” *greppini* from *Cetiosauriscus stewarti*

The genus name *Cetiosauriscus* was erected by Huene (1927b) for a late Middle Jurassic (Callovian) sauropod specimen from the British lower Oxford Clay of Peterborough, Cambridgeshire, that was originally assigned to “*Cetiosaurus leedsi*” (Woodward 1905). In the same year, Huene (1927a) also included the Swiss sauropod “*Ornithopsis*” *greppini* into his new genus, which thus comprised the two species *Cetiosauriscus* “*leedsi*” and “*Cetiosauriscus*” *greppini*. The taxonomic history of these included specimens, however, is complex and complicated (see also “Introduction”). NHMUK R3078, the type specimen for the genus and species *C. stewarti*, is the only skeletal remains available for a generic comparison

with *A. greppini*. Huene’s (1922: p. 122) diagnosis of *Cetiosauriscus* was “dorsal and caudal vertebrae much shorter than in *Cetiosaurus*, broad neural spines. Fore leg much shorter relatively than in *Cetiosaurus*. Low ilium and slender femur as in *Haplocanthosaurus*”. However, none of these features are unique to *Cetiosauriscus* and all characterize a wide array of sauropods. There have been no further attempts to diagnose the genus based on both the UK and Swiss species. Here, we compare elements of the two species to provide further information about their taxonomic assignment.

NHMUK R3078 consists of four partial dorsal vertebrae, sacral neural spines, four anterior caudal vertebrae, 27 middle caudal vertebrae, several haemapophyses, a right scapulocoracoid, humerus and antebrachium, parts of the right and left ilium, and left hind limb (Woodward 1905). It comprises one individual of at least 15 m body length, whereas the Swiss remains are from at least four different, smaller-bodied individuals. The largest preserved individual (C) of *Amanzia* has an estimated maximum body length of 10 m, just two-thirds the size of the British taxon (see above and Figs. 13, 18), and yet evidence from histology (see above) suggests that this animal was close to being fully grown. This suggests that ontogeny is unlikely to be the reason for the morphological differences described below, and indicates that size difference of a factor of at least 1/3 is a distinguishing characteristic between *C. stewarti* and *A. greppini*.

The four anterior caudal vertebrae of *C. stewarti* are incompletely preserved and re-modelled with plaster, and comparison is mainly based on the 4th caudal vertebra (5.F.) (Fig. 18a–c). The anterior caudal vertebrae of *C. stewarti* differ from those of *Amanzia* in several aspects. The anterior articular surface of the vertebral bodies is completely concave in *C. stewarti*, whereas in *Amanzia* the concavity is restricted to the dorsal two-thirds of the articular surface and is generally more weakly developed (Fig. 18a). Additionally, the posterior articular surface is mildly convex in *C. stewarti*, but flat in *Amanzia* (Fig. 18b). The anterior articular surface in *C. stewarti* is nearly circular, and the posterior articular surface is mediolaterally compressed. In contrast, the anterior articular surface in anterior caudal centra of *Amanzia* is slightly wider than tall, and the posterior articular surface is nearly circular. As the vertebrae of *Amanzia* are only anteroposteriorly compressed taphonomically, these differences are probably not the result of distortion.

The rib of the 4th caudal vertebra of *C. stewarti* is laterally drawn out and extends from the dorsal third of the vertebral body to the base of the neural spine at the ventral end of the postzygapophysis. At its ventral end, the transverse process forms a laterally directed process, with a subcircular cross-section. In contrast, the ventral part

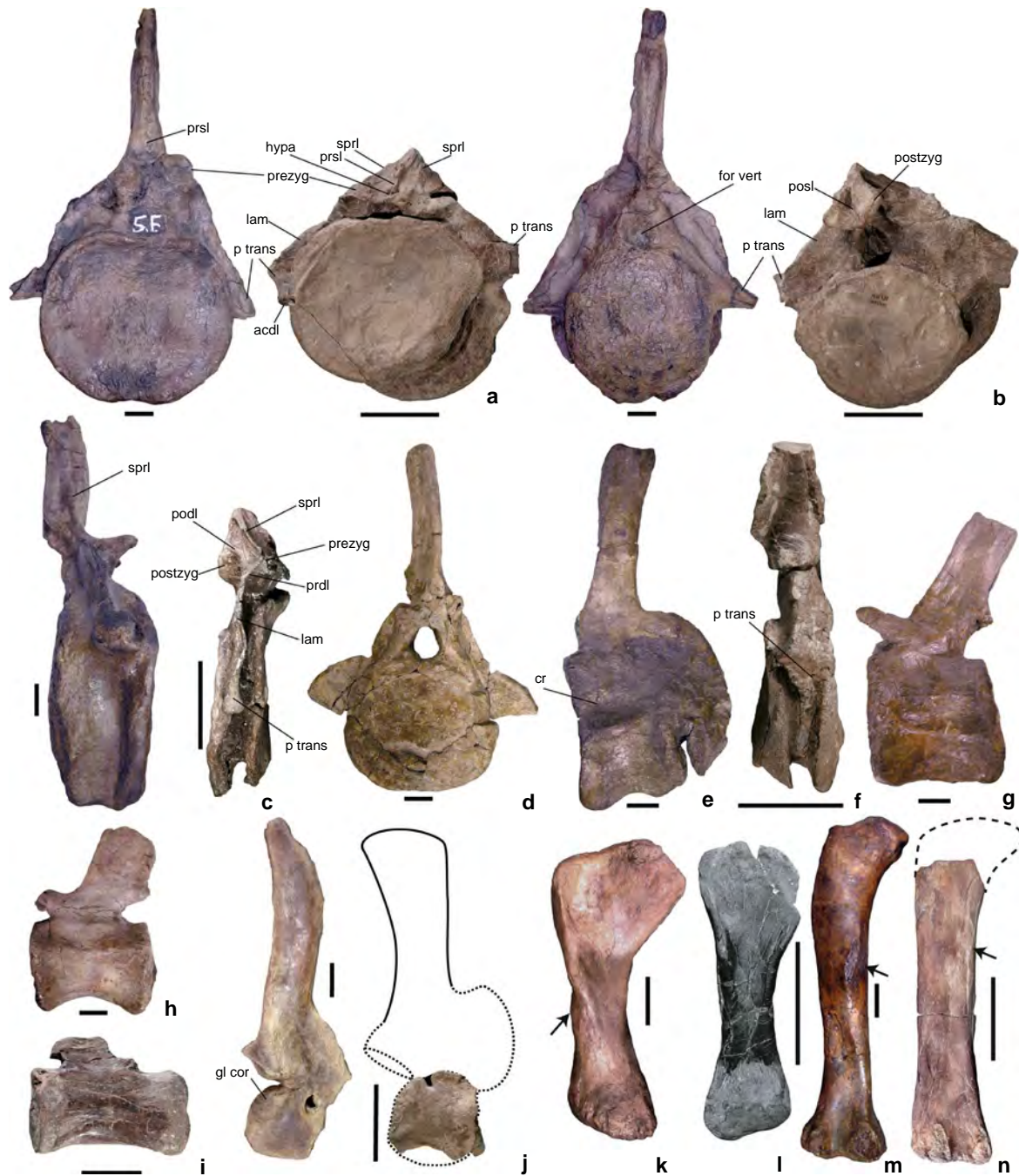


Fig. 18 Comparison of caudal vertebrae of *Cetiosauriscus stewarti* (BMNH R3078) and “*Cetiosaurus leedsii*” (BMNH R1984) with those of *Amanzia greppini*. 4th caudal vertebra “5.F.” of *C. stewarti* and NMB M.H.277 of *A. greppini* **a** in anterior, **b** in posterior and **c** in lateral aspect. **d** Anterior caudal vertebra of “*Cetiosaurus leedsii*” (BMNH R1984) in anterior aspect. **e** 11th caudal vertebra “7” of *C. stewarti* in lateral aspect. **f** 12th caudal vertebra M.H.275 of *A. greppini* (mirrored view for better comparison) in lateral aspect. **g** “F.14” ?17th caudal vertebra of *C. stewarti* in lateral aspect. **h** “18” 21st caudal vertebra of *C. stewarti* in lateral aspect. **i** NMB M.H. 258, 21st caudal vertebra of *A. greppini* in lateral aspect. **j** Right scapulocoracoid of *Cetiosauriscus stewarti* (BMNH R3078) (above) and left coracoid NMB M.H. 284 (below) with hypothetical scapula reconstruction in lateral aspect. **k** Right humerus of *Cetiosauriscus stewarti* (BMNH R3078) in anterior aspect with arrow indicating bulge laterally to deltopectoral crest. **l** Right humerus NMB M.H. 260 of *A. greppini* in anterior aspect. **m** Left femur of *Cetiosauriscus stewarti* (BMNH R3078) in posterior aspect, arrow indicating fourth trochanter. **n** Left femur of NMB M.H. 372 of *A. greppini* in posterior aspect, arrow indicating fourth trochanter. Scale bar for **a–j** is 100 mm, scale bar for **k–n** is 200 mm. *acdi* anterior centrodiapophyseal lamina, *cr* crest, *for vert* vertebral foramen, *gl cor* glenoid surface of coracoid, *hypo* hypantrum, *lam* lamina, *podl* postzygodiapophyseal lamina, *posl* postspinal lamina, *postzyg* postzygapophysis, *prezyg* prezygapophysis, *prsl* prespinal lamina, *p trans* transverse process, *sprl* spinoprezygapophyseal lamina

of the transverse processes in *Amanzia* forms a higher process, extending over the dorsal third of the vertebral centrum to the dorsal end of the postzygapophysis, and has a triangular cross-section (Fig. 18a–c). With the exception of a weakly developed anterior centrodiapophyseal lamina (acd1) on the 4th caudal vertebra, none of the preserved transverse processes and transverse processes of *C. stewarti* possess distinct ventral diapophyseal laminae, whereas well developed anterior and posterior centrodiapophyseal laminae are present in *Amanzia* (Fig. 18a–c). The anterior caudal vertebrae of *Amanzia* also exhibit a postzygodiapophyseal lamina (pod1), which is absent in *C. stewarti*. In the 4th caudal of *C. stewarti*, the postzygapophyses are positioned far dorsally to the neural canal, at the base of the neural arch, but in the 4th caudal of *Amanzia*, the postzygapophyses sit directly dorsal to the neural canal. The sacral and the anterior caudal neural spines of *C. stewarti* are only moderately broadened at their apex, such that their long-axis is orientated anteroposteriorly (Fig. 18). Additionally, the neural spine apices have an anteroposteriorly concave dorsal margin in lateral view, which was described as an autapomorphy by Upchurch et al. (2004). In contrast, the isolated neural spine apices from the anterior caudal region of *Amanzia* are strongly expanded mediolaterally, such that they are four times the width at the base of the neural spine, and are wider mediolaterally than anteroposteriorly (Fig. 7).

Another difference is the more anterior reduction in transverse process length in *C. stewarti*, with the transverse processes being present only in the form of a ridge by approximately the 11th caudal vertebra (F.7). In contrast, distinct transverse processes are present in *Amanzia* until approximately the 15th caudal vertebra (Fig. 18e, f).

Between the ?16th and the ?25th caudal vertebrae of *C. stewarti*, the length-to-height ratio of the vertebral centra changes from 1.2 to 1.4. Thus, the middle caudal vertebrae of *C. stewarti* have proportionally shorter vertebral centra than those of *Amanzia*, in which the vertebral centra have a length-to-height range between 1.7 and 2.8 in the same tail region (Figs. 8, 18g, h). Even the most posteriorly preserved caudal vertebra (~35th) of *C. stewarti* has a length-to-height ratio of only 2.5, although it cannot be excluded that more posterior caudal vertebrae would become longer. The differences in (proportional) lengths of the tail vertebrae mean that it is also possible that *Amanzia* had a longer tail than *C. stewarti*. The proximal middle caudal vertebrae of *C. stewarti* possess three distinct longitudinal ridges, one separating the lateral from the ventral face of the vertebral body, one along the dorsal third of the lateral vertebral body, and one along the dorsal margin of the vertebral body. In contrast, none

of these ridges are present in any middle caudal vertebrae of *Amanzia* (Fig. 18g–i). The two isolated caudal neural spines (NMB M.H. 286 and NMB M.H. 450) of *Amanzia* differ from the ?16th and ?17th caudal neural spines (F.13 and F.14) of *C. stewarti* (Fig. 18g) in their broader anterior and posterior faces, with a more strongly developed median rugosity and more prominent paired pre- (prsl) and postspinal (posl) laminae.

The coracoid of *C. stewarti* has a rounded rectangular outline with a dorsoventrally longer axis and a straight anterior margin. Its glenoid surface is restricted to the dorsal half of the posterior coracoid margin, and has a rounded triangular outline with a laterally expanding part (Fig. 18j). In contrast, the coracoid of *Amanzia* has a rounded square outline. Its glenoid surface occupies the whole posterior coracoid margin and is longitudinally oval in outline. The coracoid foramen of *Amanzia* is narrow and slit-like, whereas it is large and rounded in *C. stewarti* (Fig. 18j). The humerus of *C. stewarti* has a strongly medially directed head (Fig. 18k), with a convex proximal margin, which is in contrast to the straight and nearly 'shovel'-like head of the humerus of *Amanzia* (Fig. 18l). In *C. stewarti*, the proximolateral corner of the humeral head above the deltopectoral crest is much more rounded than that of *Amanzia*, which is almost rectangular. The fourth trochanter on the femur of *C. stewarti* (Fig. 18m) is situated almost at equal distance from the proximal and distal ends, whereas in *Amanzia* it is probably restricted to the proximal third of the femur (Fig. 18n). Finally, the distal articular end of the femur of *Amanzia* possesses a relatively wider intercondylar fossa than that of *C. stewarti*.

In summary, *C. stewarti* (NHMUK R3078) and *A. greppini* differ from each other in several characters, namely: (1) differences in the presence of distinct diapophyseal laminae and neural spine morphology of the anterior caudal vertebrae; (2) the length-to-height proportion in the middle caudal centra; (3) the presence or absence of ridges and crests on the middle caudal centra; (4) the shape and proportions of the coracoideal glenoid surface and coracoid foramen; (5) the head of the humerus; and (6) the differences in the position of the 4th trochanter and the width of the distal intercondylar fossa of the femur. There is also a significant body size difference between both taxa. Finally, a stratigraphic age difference is present between the two taxa, with *C. stewarti* belonging to the Middle Jurassic (Callovian; 163.5 ma) Oxford Clay, and *A. greppini* belonging to the Late Jurassic (early Kimmeridgian; 157.3 ma) Reuchenette Formation. The sum of these characters makes it unlikely that *C. stewarti* and *A. greppini* are congeneric, and supports placement of *A. greppini* in a different genus.

4.2.2 *Sauropod diversity in the Late Jurassic of Europe*

Our recognition of *A. greppini* as a distinct genus adds to the Late Jurassic diversity of eusauropods in western Europe. Including *Amanzia*, twelve species are currently considered valid by most authors. Three of these are members of the non-neosauropod eusauropod clade Turiasauria (Royo-Torres et al. 2006), and consist of *Zby atlanticus*, from the late Kimmeridgian of Portugal (Mateus et al. 2014), as well as *Losillasaurus giganteus* and *Turiasaurus riodevensis* from the Kimmeridgian–Tithonian of Spain (Royo-Torres et al. 2006). *Amanzia* and *Zby* both possess a prominent tuberosity on the posterolateral surface of the humerus, a short distance above midshaft (Mateus et al. 2014). This feature is otherwise known only in derived titanosaurs (Otero 2010). No features of *Amanzia* are considered unique to Turiasauria, although the general morphology of the humerus, in particular, is similar to the European members of the clade. A number of characteristics of *Amanzia* support a non-neosauropod position that would be in keeping with a close relationship with Turiasauria, although these are symplesiomorphies. These include: (1) the absence of a preantorbital fenestra; and (2) the spatulate morphology of the tooth crown.

Dinheirosaurus lourinhanensis (*Supersaurus lourinhanensis*, according to Tschopp et al. 2015) from the late Kimmeridgian of Portugal (Bonaparte and Mateus 1999), is a diplodocine diplodocid, and Europe's only unambiguous pre-Cretaceous representative of Diplodocoidea (Mannion et al. 2012). Anatomical features that potentially unite *Amanzia* with Diplodocoidea consist of: (1) the retention of a full suite of diapophyseal laminae in anterior caudal vertebrae (Wilson 2002); and (2) elongate middle–posterior caudal centra.

The remaining seven Late Jurassic European sauropod genera are all members of Macronaria. *Lourinhasaurus alenquerensis* (late Kimmeridgian–early Tithonian of Portugal) and *Galveosaurus herreroi* (Kimmeridgian–Tithonian of Spain) appear to lie outside of Titanosauriformes (Carballido et al. 2011; Mannion et al. 2013; Mocho et al. 2014), whereas *Vouivria dampariensis* (middle–late Oxfordian of France) and *Lusotitan atalaiensis* (late Kimmeridgian–early Tithonian of Portugal) both seem to be brachiosaurids (Mannion et al. 2013, 2017; Mocho et al. 2017). *Europasaurus holgeri* (late Kimmeridgian of Germany) is either a non-titanosauriform macronarian (e.g. Carballido and Sander 2014) or brachiosaurid (D'Emic 2012; Mannion et al. 2017), whereas *Duriatitan humerocristatus* (late Kimmeridgian of the UK) is too incomplete to determine its position within Macronaria (Barrett et al. 2010; Mannion et al. 2013). *Oceanotitan dantasi*, from the late Kimmeridgian–early Tithonian of Portugal, is an

additional macronarian that might represent a member of Somphospondyli (Mocho et al. 2019). An isolated anterior caudal vertebral centrum has been described from the Tithonian of Cognac, France, and tentatively been determined to belong to an unidentified camarasaurid (LeLoeuff et al. 1996). Although the specimen resembles *Amanzia* in the general proportions of the vertebral centrum and its anteroposterior compression, it differs from the latter by lacking a distinct acdl and pcdl ventral to the transverse process. Another large and anteroposteriorly compressed caudal vertebral centrum from the Late Jurassic of Riodeva, Spain, was described and determined to be morphologically rather similar to *Amanzia*, *C. stewarti* and the vertebral centrum from Cognac (Royo-Torres and Cobos 2005). However, similar to the French sauropod vertebral centrum, the Spanish vertebral centrum lacks distinct anterior and posterior centrodiapophyseal laminae (acdl and pcdl), so that neither of these two vertebrae can be assigned to *Amanzia*. *Amanzia* shares a number of anatomical features with 'basal' macronarians, comprising: (1) the presence of camellae in one cervical vertebra; and (2) a club-like anterior caudal neural spine. It also displays some characteristics more usually associated with titanosauriforms, consisting of: (1) the anterior bias of some middle caudal neural arches; (2) a much broader fibular than tibial condyle on the distal femur; and (3) the lateral muscle scar of the fibula consisting of two parallel ridges. Finally, one feature of *Amanzia* is otherwise primarily restricted to the titanosauriform clade Somphospondyli. This pertains to the sigmoidal shape of the fibula shaft in lateral view, whereas the shaft is straight in other sauropods. *Oceanotitan* also shares this feature (Mocho et al. 2019).

4.3 Phylogenetic affinities of *Amanzia greppini*

Our detailed redescription of the Swiss material demonstrates that it is distinct from *C. stewarti*, and represents a new genus. *Amanzia greppini* is characterized by a unique combination of plesiomorphic and derived features, making qualitative assessment of its placement within Eusauropoda difficult. To try to resolve the phylogenetic affinities of *Amanzia*, we incorporated it into the eusauropod-focussed data matrix of Mannion et al. (2019), which comprises 117 eusauropod taxa scored for 542 characters, and includes nearly all Late Jurassic to mid-Cretaceous sauropods, as well as *C. stewarti*.

We were able to score *Amanzia* for 94 characters (Additional files 1, 2). Following Mannion et al. (2019), 18 characters (11, 14, 15, 27, 40, 51, 104, 122, 147, 148, 195, 205, 259, 297, 426, 435, 472, and 510) were treated as ordered multistate characters, and seven unstable and fragmentary taxa were excluded from the analyses

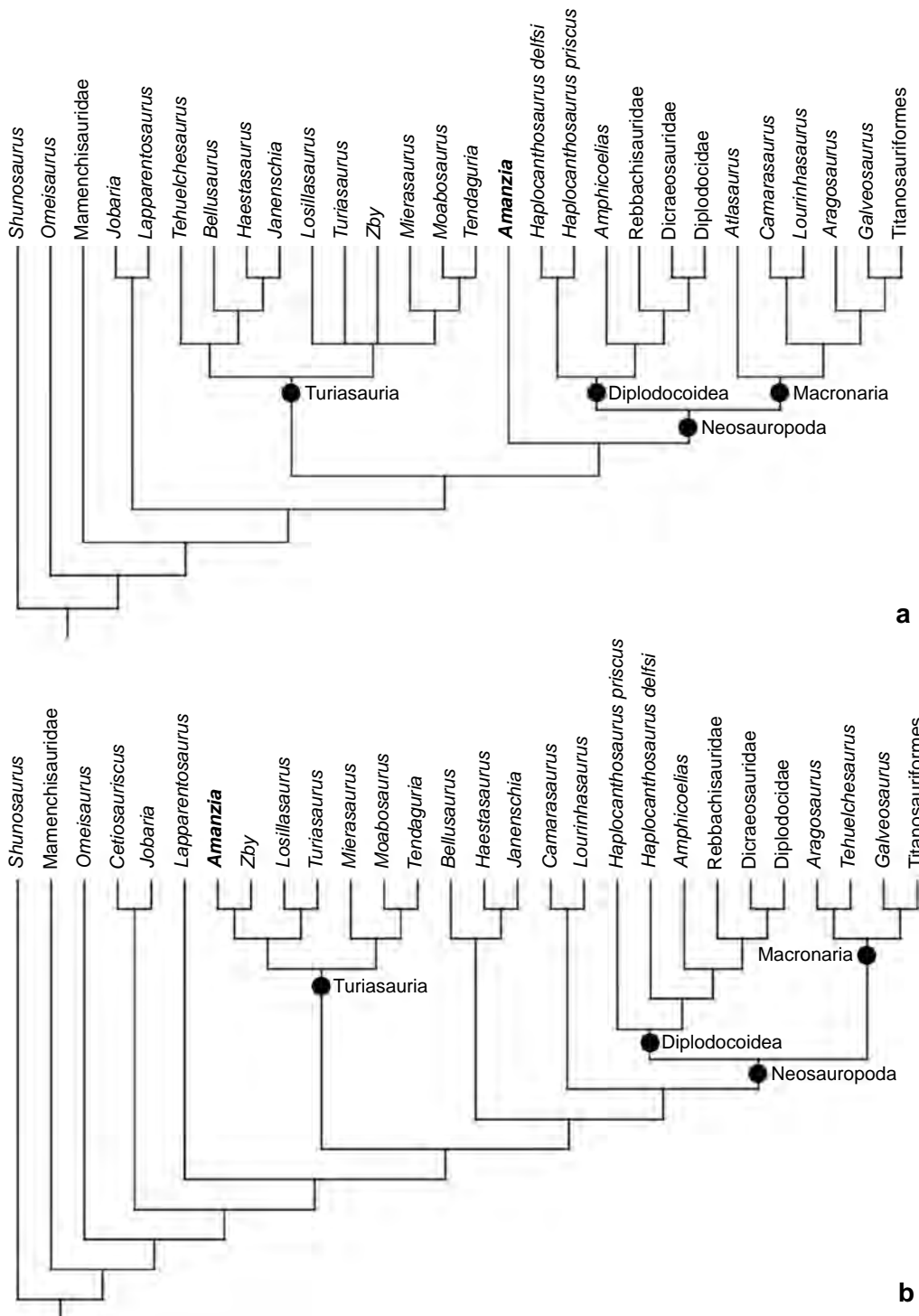


Fig. 19 Strict consensus cladogram showing the position of *Amanzia greppini* using **a** equal weights, and **b** extended implied weights. Several clades are collapsed for simplicity. Note that *Cetiosauriscus* is recovered within *Dicraeosauridae* in the equal weights analysis

a priori (*Astrophocaudia*, *Australodocus*, *Brontomerus*, *Fukuititan*, *Fusuisaurus*, *Liubangosaurus*, *Malarguesaurus*). This pruned data matrix was analysed via Parsimony, using the ‘Stabilize Consensus’ option in the ‘New Technology Search’ in TNT v.1.5 (Goloboff et al. 2008; Goloboff and Catalano 2016). Searches employed sectorial searches, drift, and tree fusing, with the consensus stabilized five times, prior to using the resultant trees as the starting topologies for a ‘Traditional Search,’ utilizing Tree Bisection-Reconstruction. We ran two versions of the analysis, using: (1) equal weighting of characters (Fig. 19a); and (2) extended implied weighting (Goloboff 2014) (Fig. 19b), with the default settings in TNT (with a k value of 3).

Using equal weighting of characters, our analysis produced 22704 MPTs of length 2573 steps. *Amanzia* is placed as the sister taxon to Neosauropoda, and the remainder of the topology is identical to that presented in Mannion et al. (2019) (Fig. 19). Bremer support for the placement of *Amanzia* is low (1), as is the case for most of the topology. Analysis with extended implied weights recovered 27 MPTs of length 237.4 steps. Other than the inclusion of *Amanzia*, the resulting strict consensus tree is again identical to that presented in Mannion et al. (2019). Here, *Amanzia* is again recovered outside of Neosauropoda, but is instead placed within Turiasauria, as the sister taxon of *Zby*, whereas *C. stewarti* is placed as the sister taxon to *Jobaria* (Fig. 19) and in a more basal position than Turiasauria. As such, both analyses point to a non-neosauropod eusauropod position for *Amanzia*, although its exact placement remains uncertain.

5 Conclusions

A re-examination of the Swiss Late Jurassic material of “*Cetiosauriscus*” *greppini* revealed that the material can be generically separated from *C. stewarti* by a number of osteological differences and consequently is assigned to a new genus, *Amanzia*. Although incomplete and partly damaged, the large number of bones preserved from *A. greppini* belong to at least four individuals and allow description of a large number of osteological characters of most body regions. *Amanzia* augments the growing diversity of Late Jurassic European sauropods. The phylogenetic analysis recovered *Amanzia* to be outside Neosauropoda and comprising a mixed of diplodocoid, macronarian and basal osteological characters. The presence of non-neosauropodan sauropods in the Late Jurassic and Early Cretaceous of Europe is not unusual, and it can be expected that new finds and redescription of historical material will increase their diversity even more. The exact phylogenetic placement of the Swiss sauropod remains unclear, but a thorough reassessment of *C. stewarti* would facilitate to understand character distribution

in *A. greppini* and other basal eusauropods from Europe better.

Although the bone material described in the present paper could no longer be observed in situ, the careful examination of the remaining matrix revealed important information on the paleoenvironment. Caliche concretions with traces of rhizomes combined with possible brackish/freshwater ostracods indicates burial in waterlain sediment that underwent pedogenesis. A nearby marine area is indicated by the presence of marine crocodylomorphs. Furthermore, the existence of fusite in our sample provides for the first time evidence of wild fires in the Late Jurassic of Northern Switzerland.

Until the first European dinosaur megatracksite was reported in 1990, the Late Jurassic carbonates were thought to be fully marine deposits (Meyer 1990). Since then numerous terrestrial fossils and sedimentological features including over 50 individual dinosaur tracksites, dinosaur bones and teeth, pterosaurs and plant remains as well as charophytes have been reported spanning from the Oxfordian to the Berriasian. Dinosaur tracks preserved in charophyte-bearing stromatolites (Vorbourg and Röschenz members; SB OX5; middle Oxfordian) and the remains of *A. greppini* with proof of well drained soils corroborate the idea of emergent landmasses (Meyer 2011; Meyer and Marty 2014; Razzolini et al. 2017; Castanera et al. 2018). They are important for palaeogeographical reconstructions and show the coeval presence of freshwater, soils and dinosaurs on the Jura carbonate platform. The recurrent terrestrial evidence indicates that these emergent areas were able to host large populations of dinosaurs and were—at least temporarily—not islands.

Supplementary information

Supplementary information accompanies this paper at <https://doi.org/10.1186/s00015-020-00355-5>.

Additional file 1. TNT data matrix used in the phylogenetic analysis of *Amanzia greppini* in this paper.

Additional file 2. Mesquite data matrix used in the phylogenetic analysis of *Amanzia greppini* in this paper.

Acknowledgements

We thank W. Tschudin (Dep. of Geology and Palaeontology, University of Basel) for making the thin sections, Antoine Heitz (Natural History Museum Basel) for the preparation of the specimens and S. Padzera for the drawings provided for this work. We are also indebted to Ulla Schudack and the late Michael Schudack (Berlin) for determination of the ostracods, as well as to Nicole Klein (Bonn) for a review of the bone histology section. DS and PDM thank Sandra Chapman and Paul Barrett for access to the material of *Cetiosauriscus stewarti* in the collections of the NHMUK London. We gratefully acknowledge the Willi Hennig Society, which has sponsored the development and free distribution of TNT. PDM’s contribution was supported by a Royal Society University Research Fellowship (UF160216). OW was funded in the *Europasaurus*-Project (grant no. 85 882) by the Volkswagen Foundation within the initiative “Research in Museums”. The publication of this article was funded by the Open Access Fund of the Leibniz Association.

Authors' contributions

DS collected the data, provided the osteology, discussion and figures, drafted the manuscript, PDM contributed major parts of osteology and discussion and conducted the phylogenetic analysis and figures, OW collected data for the histology and interpreted and wrote histology section and figures, CAM provided general and historical information about the specimen, wrote the geology section and provided most of the systematic paleontology and figures, DS, PDM, OW and CAM discussed all parts of the manuscript and contributed to the draft as well as to the revision. All authors read and approved the final manuscript.

Competing interests

The authors declare that they have no competing interests.

Author details

¹ Museum für Naturkunde, Leibniz Institute for Evolution and Biodiversity Science, Invalidenstraße 43, 10115 Berlin, Germany. ² Department of Earth Sciences, University College London, London WC1E 6BT, UK. ³ Martin Luther University Halle-Wittenberg, Natural Sciences Collections, Domplatz 4, 06108 Halle (Saale), Germany. ⁴ Department of Environmental Sciences, University of Basel, Bernoullistrasse 32, 4056 Basel, Switzerland.

Received: 18 June 2019 Accepted: 17 November 2019

Published online: 24 February 2020

References

- Avilla, L. S., Fernandes, R., & Ramos, D. F. B. (2004). Bite marks on a crocodylomorph from the Upper Cretaceous of Brazil: Evidence of social behaviour? *Journal of Vertebrate Paleontology*, *24*, 971–973.
- Bakker, R. T. (1986). *The Dinosaur Heresies*. New York: Morrow.
- Bakker, R. T., & Bird, G. (2004). Dinosaur crime scene investigations: Theropod behavior at Como Bluff, Wyoming, and the evolution of birdness. In B. P. Currie, E. B. Koppelhus, M. A. Shugar, & J. L. Wright (Eds.), *Feathered dragons: studies on the transition from dinosaurs to birds* (pp. 301–342). Bloomington: Indiana University Press.
- Barrett, P. M., Benson, R. B. J., & Upchurch, P. (2010). Dinosaurs of Dorset: Part II, the sauropod dinosaurs (Saurischia, Sauropoda) with additional comments on the theropods. *Proceedings of the Dorset Natural History and Archaeological Society*, *131*, 113–126.
- Berman, D. S., & McIntosh, J. S. (1978). Skull and relationship of the Upper Jurassic sauropod *Apatosaurus* (Reptilia, Saurischia). *Bulletin of the Carnegie Museum of Natural History*, *8*, 1–35.
- Bonaparte, J. F., Heinrich, W. D., & Wild, R. (2000). Review of *Janenschia* Wild with the description of a new sauropod from the Tendaguru beds of Tanzania and a discussion on the systematic value of procoelous caudal vertebrae in the Sauropoda. *Palaeontographica Abteilung A*, *256*, 25–76.
- Bonaparte, J. F., & Mateus, O. (1999). A new diplodocid, *Dinheirosaurus lourinhanensis* gen. et sp. nov., from the Late Jurassic beds of Portugal. *Revista del Museo Argentino de Ciencias Naturales 'Bernardino Rivadavia' e Instituto Nacional de Investigación de las Ciencias Naturales. Paleontología*, *5*, 13–29.
- Britt, B. B. (1991). Theropods of Dry Mesa Quarry (Morrison Formation, Late Jurassic), Colorado, with emphasis on the osteology of *Torvosaurus tanneri*. *Brigham Young University Geology Studies*, *37*, 1–72.
- Buffetaut, E. (1982). Le crocodylien *Machimosaurus* von Meyer (Mesosuchia, Teleosauridae) dans le Kimmeridgien de l'Ain. *Bulletin trimestre de la Société Géologique de la Normandie et Amis du Muséum du Havre*, *LXIX*, pp. 17–26.
- Buffetaut, E. (1983). Wounds on the jaw of an Eocene mesosuchian crocodylian as possible evidence for the antiquity of crocodylian intraspecific fighting behaviour. *Paläontologische Zeitschrift*, *57*, 143–145.
- Calvo, J. O., & Salgado, L. (1995). *Rebbachisaurus tessonei* sp. nov. a new Sauropoda from the Albian-Cenomanian of Argentina; new evidence on the origin of the Diplodocidae. *Gaia*, *11*, 13–33.
- Canudo, J. I., Royo-Torres, R., & Cuenca-Bescós, G. (2008). A new sauropod: *Tastavinsaurus sanzi* gen. et sp. nov. from the Early Cretaceous (Aptian) of Spain. *Journal of Vertebrate Paleontology*, *28*, 712–731.
- Carballido, J. L., Rauhut, O. W. M., Pol, D., & Salgado, L. (2011). Osteology and phylogenetic relationships of *Tehuelchesaurus benitezii* (Dinosauria, Sauropoda) from the Upper Jurassic of Patagonia. *Zoological Journal of the Linnean Society*, *163*, 605–662.
- Carballido, J. L., & Sander, P. M. (2014). Postcranial axial skeleton of *Europasaurus holgeri* (Dinosauria, Sauropoda) from the Upper Jurassic of Germany: implications for sauropod ontogeny and phylogenetic relationships of basal Macronaria. *Journal of Systematic Palaeontology*, *12*(3), 335–387.
- Carpenter, K. (1998). Evidence of predatory behavior by carnivorous dinosaurs. *Gaia*, *15*, 135–144.
- Carrano, M. T., Benson, R. B. J., & Sampson, S. D. (2012). The phylogeny of Tetanurae (Dinosauria: Theropoda). *Journal of Systematic Palaeontology*, *10*, 211–300.
- Castanera, D., Belvedere, M., Marty, D., Paratte, G., Lapaire-Cattin, M., Lovis, C., et al. (2018). A walk in the maze: variation in Late Jurassic tridactyl dinosaur tracks from the Swiss Jura Mountains (NW Switzerland). *PeerJ*, *6*, e4579.
- Charig, A. J. (1980). A diplodocid sauropod from the Lower Cretaceous of England. In L. L. Jacobs (Ed.), *Aspects of vertebrate history. Essays in Honor of Edwin Harris Colbert* (pp. 231–244). Flagstaff: Museum of Northern Arizona Press.
- Charig, A. J. (1993). Case 2876: *Cetiosauriscus* von Huene, 1927 (Reptilia, Sauropodomorpha): proposed designation of *C. stewarti* Charig, 1980 as the type specimen. *Bulletin of Zoological Nomenclature*, *50*, 282–283.
- Chure, D. (2000). *A new species of Allosaurus from the Morrison Formation of Dinosaur National Monument (UT-CO) and a revision of the theropod family Allosauridae*. Unpublished Ph.D. thesis, Columbia University.
- Chure, D., Britt, B. B., Whitlock, J. A., & Wilson, J. A. (2010). First complete sauropod dinosaur skull from the Cretaceous of the Americas and the evolution of sauropod dentition. *Naturwissenschaften*, *97*, 379–391.
- Clark, J. M. (1986). *Phylogenetic relationships of the crocodylomorph archosaurs*. Unpublished Ph.D. dissertation, University of Chicago.
- Curry Rogers, C. (2005). Titanosauria: a phylogenetic overview. In K. A. Curry Rogers & J. A. Wilson (Eds.), *The sauropods: evolution and paleobiology* (pp. 50–103). Berkeley: University of California Press.
- D'Amore, D. C., & Blumenschine, R. J. (2009). Komodo monitor (*Varanus komodoensis*) feeding behavior and dental function reflected through tooth marks on bone surfaces, and the application to ziphodont paleobiology. *Paleobiology*, *35*(4), 525–552.
- D'Emic, M. D. (2012). The early evolution of titanosauriform sauropod dinosaurs. *Zoological Journal of the Linnean Society*, *166*, 624–671.
- D'Emic, M. D., Mannion, P. D., Upchurch, P., Benson, R. B. J., Pang, Q., & Cheng, Z. (2013). Osteology of *Huabeisaurus allocotus* (Sauropoda: Titanosauriformes) from the Upper Cretaceous of China. *PLoS ONE*, *8*, e69375.
- Delfino, M., & dal Sasso, C. (2006). Marine reptiles (Thalattosuchia) from the early Jurassic of Lombardy (northern Italy). *Geobios*, *39*, 346–354.
- Erickson, G. M., & Olson, K. H. (1996). Bite marks attributable to *Tyrannosaurus rex*: Preliminary description and implications. *Journal of Vertebrate Paleontology*, *16*, 175–178.
- Fiorillo, A. R. (1991). Prey bone utilization by predatory dinosaurs. *Palaeogeography, Palaeoclimatology, Palaeoecology*, *88*, 157–166.
- Fowler, D. W., & Sullivan, R. M. (2006). A ceratopsid pelvis with toothmarks from the Upper Cretaceous Kirtland Formation, New Mexico: Evidence of Late Campanian tyrannosaurid feeding behavior. *New Mexico Museum of Natural History and Science Bulletin*, *35*, 127–130.
- Fraas, E. (1901). Die Meerkrokodile (Thalattosuchia n.g.) eine Sauriergruppe der Juraformation. *Jahreshefte des Vereins für vaterländische Naturkunde Württemberg*, *57*, 409–418.
- Francillon-Vieillot, H., de Buffrénil, V., Castanet, J., Géraudie, J., Meunier, F. J., Sire, J. Y., et al. (1990). Microstructure and mineralization of vertebrate skeletal tissues. In J. G. Carter (Ed.), *Skeletal biomineralization: patterns, processes and evolutionary trends* (Vol. 1, pp. 471–530). New York: Van Nostrand Reinhold.
- Gallina, P. A., & Apesteguía, S. (2011). Cranial anatomy and phylogenetic position of the titanosaurian sauropod *Bonitasaurus salgadoi*. *Acta Palaeontologica Polonica*, *56*, 45–60.
- Gallina, P. A., & Apesteguía, S. (2015). Postcranial anatomy of *Bonitasaurus salgadoi* (Sauropoda, Titanosauria) from the Late Cretaceous of Patagonia. *Journal of Vertebrate Paleontology*, *35*, 1–22.
- Gallina, P. A., & Otero, A. (2009). Anterior caudal transverse processes in sauropod dinosaurs: morphological, phylogenetic and functional aspects. *Ameghiniana*, *46*(1), 165–176.

- Geoffroy Saint-Hilaire, É. (1831). Recherches sur de grands sauriens trouvés à l'état fossile aux confins maritimes de la Basse-Normandie, attribués d'abord au crocodile, puis déterminés sous les noms de *Teleosaurus* et *Steneosaurus*. *Mémoires de l'Académie royale des Sciences (Paris)*, 12, 1–138.
- Gilmore, C. W. (1925). A nearly complete articulated skeleton of *Camarasaurus*, a saurischian from the Dinosaur National Monument, Utah. *Memoirs of the Carnegie Museum*, 10(3), 347–384.
- Gilmore, C. W. (1936). Osteology of *Apatosaurus*, with special references to specimens in the Carnegie Museum. *Memoirs of the Carnegie Museum*, 11(4), 1–136.
- Glut, D. F. (1997). *Dinosaurs*. The Encyclopedia. Jefferson: McFarland & Company Inc.
- Goloboff, P. A. (2014). Extended implied weighting. *Cladistics*, 30, 260–272.
- Goloboff, P. A., & Catalano, S. A. (2016). TNT version 1.5, including a full implementation of phylogenetic morphometrics. *Cladistics*, 32, 221–238.
- Goloboff, P. A., Farris, J. S., & Nixon, K. C. (2008). TNT, a free program for phylogenetic analysis. *Cladistics*, 24, 1–13.
- Gomani, E. M. (2005). Sauropod dinosaurs from the Early Cretaceous of Malawi. *Africa. Palaeontologia Electronica*, 8, 37.
- Greppin, J. P. (1870). Description géologique du Jura bernois et de quelques districts adjacents. *Matériaux pour la carte géologique de la Suisse*, 8, 1–357.
- Harris, J. D. (2006). The significance of *Suuwassea emilieae* (Dinosauria: Sauropoda) for flagellicaudatan intrarelationships and evolution. *Journal of Systematic Palaeontology*, 4(2), 185–198.
- Harris, J. D. (2007). The appendicular skeleton of *Suuwassea emilieae* (Sauropoda: Flagellicaudata) from the Upper Jurassic Morrison Formation of Montana (USA). *Geobios*, 40(4), 501–522.
- Hatcher, J. B. (1901). *Diplodocus* (Marsh): its osteology, taxonomy, and probable habits, with a restoration of the skeleton. *Memoirs of the Carnegie Museum*, 1, 1–63.
- Hofer, C. (2005). Osteologie und Taxonomie von *Cetiosauriscus greppini* (Huene 1927a, b) aus dem späten Jura von Moutier (Reuchenette Formation) [Osteology and taxonomy of *Cetiosauriscus greppini* (Huene 1927a, b) from the Late Jurassic of Moutier (Reuchenette Formation)]. Unpublished Diploma thesis, University of Basel, p. 70.
- Hofmann, R., Stein, K., & Sander, P. M. (2014). Constraints on the lamina density of laminar bone architecture of large-bodied dinosaurs and mammals. *Acta Palaeontologica Polonica*, 59(2), 287–294.
- Holland, W. J. (1924). The skull of *Diplodocus*. *Memoirs of the Carnegie Museum*, 9, 379–403.
- Holtz, T. R. J., Molnar, R. E., & Currie, P. J. (2004). Basal Tetanurae. In D. B. Weishampel, P. Dodson, & H. Osmólska (Eds.), *The Dinosauria* (2nd ed., pp. 71–110). Berkeley: University of California Press.
- Hua, S. (1997). *Adaptations des crocodiliens mesosuchiens au milieu marin*. Unpublished Ph.D. thesis, Sciences de la Terre de l'Université Pierre et Marie Curie de Paris.
- Huene, F. V. (1922). Ueber einen Sauropoden im obern Malm des Berner Jura. *Eclogae Geologicae Helveticae*, 17, 80–94.
- Huene, F. V. (1925). Die Saurierfauna des Portlandkalkes von Solothurn. *Eclogae Geologicae Helveticae*, 19, 584–603.
- Huene, F. V. (1926). The carnivorous Saurischia in the Jura and Cretaceous formations, principally in Europe. *Revista del Museo de La Plata*, 29, 35–167.
- Huene, F. V. (1927a). Short review of the present knowledge of the Sauropoda. *Memoirs of the Queensland Museum*, 9, 121–126.
- Huene, F. V. (1927b). Sichtung der Grundlagen der jetzigen Kenntnis der Sauropoden. *Eclogae Geologicae Helveticae*, 20, 444–470.
- Huene, F. V. (1932). Die fossile Reptil-Ordnung Saurischia, ihre Entwicklung und Geschichte. *Monographien zur Geologie und Paläontologie*, 1, 4.
- Ikejiri, T. (2004). *Anatomy of Camarasaurus lentus (Dinosauria: Sauropoda) from the Morrison Formation (Late Jurassic), Thermopolis, central Wyoming, with determination and interpretation of ontogenetic, sexual dimorphic, and individual variation in the genus*. Unpublished Master thesis, Fort Hays State University.
- Ikejiri, T., Schwarz, D., & Breithaupt, B. H. (2005a). A nearly complete skeleton of a baby sauropod from the Lower Morrison Formation of the Howe Stephens Quarry, Wyoming: "little steps" into diplodocid ontogeny and taxonomy. *Journal of Vertebrate Paleontology*, 25, 73A.
- Ikejiri, T., Tidwell, V., & Trexler, D. L. (2005b). New adult specimens of *Camarasaurus lentus* highlight ontogenetic variation within the species. In V. Tidwell & K. Carpenter (Eds.), *Thunder-lizards. The sauropodomorph dinosaurs* (pp. 154–179). Bloomington: Indiana University Press.
- Janensch, W. (1920). Ueber *Elaphrosaurus bambergi* und die Megalosaurier aus den Tendaguru-Schichten Deutsch-Ostafrikas. *Sitzungsberichte der Gesellschaft Naturforschender Freunde zu Berlin*, 1920, 225–235.
- Janensch, W. (1925). Die Coelurosaurier und Theropoden der Tendaguru-Schichten Deutsch-Ostafrikas. *Palaeontographica, Supplement*, 7(1), 1–93.
- Janensch, W. (1929). Die Wirbelsäule der Gattung *Dicraeosaurus*. *Palaeontographica, Supplement*, 7(1), 1–34.
- Jank, M. (2004). New insights into the development of the Late Jurassic Reuchenette Formation of NW Switzerland (Late Oxfordian to Late Kimmeridgian, Jura Mountains). Unpublished PhD, Universität Basel.
- Jank, M., Wetzel, A., & Meyer, (2006). A calibrated composite section for the Late Jurassic Reuchenette Formation of northwestern Switzerland (?Oxfordian, Kimmeridgian sensu gallico, Ajoie Region). *Eclogae Geologicae Helveticae*, 99(2), 175–191.
- Klein, N., & Sander, P. M. (2008). Ontogenetic stages in the long bone histology of sauropod dinosaurs. *Paleobiology*, 34, 247–263.
- Krebs, B. (1962). Ein *Steneosaurus*-Rest aus dem Oberen Jura von Dielsdorf, Kt. Zürich, Schweiz. *Schweizerische Paläontologische Abhandlungen*, 79, 1–28.
- Krebs, B. (1967a). Der Jura-Krokodilier *Machimosaurus* H. v. Meyer. *Paläontologische Zeitschrift*, 41, 46–59.
- Krebs, B. (1967b). Zwei *Steneosaurus*-Wirbel aus den Birnenstorfer Schichten (Ober-Oxford) vom "Weissen Graben" bei Mönthal (Kt. Aargau). *Eclogae Geologicae Helveticae*, 60, 689–695.
- Krebs, B. (1968). Le crocodilien *Machimosaurus*. *Memória dos Servicos Geológicos de Portugal*, 14, 21–53.
- LeLoeuff, J., Buffetaut, E., & Merser, C. (1996). Découverte d'un dinosaure saurope de tithonien dans la région de Cognac (Charente). *Géologie de la France*, 2, 79–81.
- Madsen, J. H. J. (1976). A second new theropod from the Late Jurassic of east central Utah. *Utah Geology*, 3, 51–60.
- Madsen, J. H. J., Mcintosh, J. S., & Berman, D. S. (1995). Skull and atlas-axis-complex of the Upper Jurassic sauropod *Camarasaurus* Cope (Reptilia: Saurischia). *Bulletin of the Carnegie Museum of Natural History*, 31, 1–115.
- Madsen, J. H. J., & Welles, S. P. (2000). *Ceratosaurus* (Dinosauria, Theropoda) a revised osteology. *Utah Geological Survey Miscellaneous Publication*, 00–2, 1–80.
- Mannion, P. D., Allain, R., & Moine, O. (2017). The earliest known titanosauriform sauropod dinosaur and the evolution of Brachiosauridae. *PeerJ*, 5, e3217.
- Mannion, P. D., Upchurch, P., Barnes, R. N., & Mateus, O. (2013). Osteology of the Late Jurassic Portuguese sauropod dinosaur *Lusitan atalaiensis* (Macronaria) and the evolutionary history of basal titanosauriforms. *Zoological Journal of the Linnean Society*, 168, 98–206.
- Mannion, P. D., Upchurch, P., & Hutt, S. (2011). New rebbachisaurid (Dinosauria: Sauropoda) material from the Wessex Formation (Barremian, Early Cretaceous), Isle of Wight, United Kingdom. *Cretaceous Research*, 32, 774–780.
- Mannion, P. D., Upchurch, P., Mateus, O., Barnes, R., & Jones, M. E. H. (2012). New information on the anatomy and systematic position of *Dinheirosaurus lourinhanensis* (Sauropoda: Diplodocoidea) from the Late Jurassic of Portugal, with a review of European diplodocoids. *Journal of Systematic Palaeontology*, 10, 521–551.
- Mannion, P. D., Upchurch, P., Schwarz, D., & Wings, O. (2019). Taxonomic affinities of the putative titanosaurs from the Late Jurassic Tendaguru Formation of Tanzania: Phylogenetic and biogeographic implications for eusauropod dinosaur evolution. *Zoological Journal of the Linnean Society*, 185, 794–909.
- Marsh, O. C. (1878). Principal characters of American Jurassic dinosaurs. Pt. I. *American Journal of Science, Serie 3*, 16, 411–416.
- Marsh, O. C. (1881). A new order of extinct Jurassic reptiles (Coeluria). *American Journal of Science, Series*, 3(21), 339–340.
- Marsh, O. C. (1884). Principal characters of American Jurassic dinosaurs. Part VIII. The order Theropoda. *American Journal of Science, Serie 3*, 27, 329–340.

- Marsh, O. C. (1896). The dinosaurs of North America. U.S. *Geological Survey*, In: sixteenth annual report, pp. 133–415.
- Marty, D., Belvedere, M., Razzolini, N. L., Lockley, M. G., Paratte, G., Cattin, M., et al. (2017). The tracks of giant theropods (*Jurabrontes curtedulensis* ichnogen. & ichnosp. nov.) from the Late Jurassic of NW Switzerland: palaeoecological & palaeogeographical implications. *Historical Biology*, 30, 928–956.
- Mateus, O., Mannion, P. D., & Upchurch, P. (2014). *Zby atlanticus*, a new turiasaurian sauropod (Dinosauria, Eusauropoda) from the Late Jurassic of Portugal. *Journal of Vertebrate Paleontology*, 34(3), 618–634.
- Mcintosh, J. S. (1990). Sauropoda. In D. B. Weishampel, P. Dodson, & H. Osmolska (Eds.), *The Dinosauria* (pp. 345–401). Berkeley: University of California Press.
- Meyer, C. A. (1990). Sauropod tracks from the Upper Jurassic Reuchenette Formation (Kimmeridgian, Lommiswil, Kt. Solothurn) of Northern Switzerland. *Eclogae geologicae Helveticae*, 83(2), 389–397.
- Meyer, C. A. (2011). The hitch-hikers guide to the Late Jurassic and Early Cretaceous—Dinosaur tracks from the Swiss and French Jura mountains in a sequence stratigraphic context. In: Richter, A. & Reich, M. (Eds.) *Dinosaur tracks—an international symposium*, Obernkirchen, p. 43.
- Meyer, C. A., & Hunt, A. (1998). The first stegosaurian dinosaur (Ornithischia: Thyreophora) from the Late Jurassic of Switzerland. *Neues Jahrbuch für Geologie und Paläontologie Monatshefte*, 1998, 141–145.
- Meyer, C. A., & Lockley, M. G. (1996). The Late Jurassic continental fossil record of northern Switzerland: Evidence and Implications. In M. Morales (Ed.), *The Continental Jurassic, Museum of Northern Arizona Bulletin* (pp. 421–426). AZ, USA: Flagstaff.
- Meyer, C. A. & Marty, D. (2014). The recurrent record of terrestrial environments in the Late Jurassic of the Swiss Jura mountains: implications for paleogeographic reconstructions. *SVP Programm and Abstracts*, 187, Berlin.
- Meyer, C. A., & Thüning, B. (2003). Dinosaur of Switzerland. *Comptes Rendus Palevol*, 2, 103–117.
- Mitchell, J., Sander, P. M., & Stein, K. (2017). Can secondary osteons be used as ontogenetic indicators in sauropods? Extending the histological ontogenetic stages into senescence. *Paleobiology*, 43(2), 321–342.
- Mocho, P., Royo-Torres, R., & Ortega, F. (2014). Phylogenetic reassessment of *Lourinhasaurus alenquerensis*, a basal Macronaria (Sauropoda) from the Upper Jurassic of Portugal. *Zoological Journal of the Linnean Society*, 170, 875–916.
- Mocho, P., Royo-Torres, R., & Ortega, F. (2017). New data of the Portuguese brachiosaurid *Lusotitan atalaiensis* (Sobral Formation, Upper Jurassic). *Historical Biology*, 29, 789–817.
- Mocho, P., Royo-Torres, R., & Ortega, F. (2019). A new macronarian sauropod from the Upper Jurassic of Portugal. *Journal of Vertebrate Paleontology*, 39(1), e1578782.
- Molnar, R. E., Kurzanov, S. M., & Dong, Z.-M. (1990). Carnosauria. In D. B. Weishampel, P. Dodson, & H. Osmolska (Eds.), *The Dinosauria* (pp. 169–209). Berkeley: University of California Press.
- Njau, J. K., & Blumenshine, R. J. (2006). A diagnosis of crocodile feeding traces on larger mammal bone, with fossil examples from the Plio-Pleistocene Olduvai Basin, Tanzania. *Journal of Human Evolution*, 50, 142–162.
- Olshevsky, G. (1978). The Archosauria (excluding the Crocodylia). *Mesozoic Meanderings*, 1, 1–49.
- Olshevsky, G. (1991). A Revision of the Parainfraclass Archosauria Cope, 1869, Excluding the Advanced Crocodylia. *Mesozoic Meanderings*, 2, 1–49.
- Otero, A. (2010). The appendicular skeleton of *Neuquensaurus*, a Late Cretaceous saltasaurine sauropod from Patagonia, Argentina. *Acta Palaeontologica Polonica*, 55, 399–426.
- Pierce, S. E., & Benton, M. J. (2006). *Pelagosaurus typus* Bronn, 1841 (Mesoeucrocodylia: Thalattosuchia) from the Upper Lias (Toarcian, Lower Jurassic) of Somerset, England. *Journal of Vertebrate Paleontology*, 26, 621–635.
- Poropat, S. F., Mannion, P. D., Upchurch, P., Hocknull, S. A., Kear, B. P., Kundrát, M., et al. (2016). New Australian sauropods shed light on Cretaceous dinosaur palaeobiogeography. *Scientific Reports*, 6, 34467.
- Razzolini, N. L., Belvedere, M., Marty, D., Paratte, G., Lovis, C., Cattin, M., et al. (2017). *Megalosauripus transjuranicus* ichnosp. nov. A new Late Jurassic theropod ichnotaxon from NW Switzerland and implications for tridactyl dinosaur ichnology and ichnotaxonomy. *PLoS ONE*, 12(7), e0180289. <https://doi.org/10.1371/journal.pone.0180289>.
- Royo-Torres, R., & Cobos, A. (2005). Presencia en Riodeva (Teruel) de la mayor vértebra caudal (Dinosauria, Sauropoda) de Europa. *Geogaceta*, 38, 23–26.
- Royo-Torres, R., Cobos, A., & Alcalá, L. (2006). A Giant European Dinosaur and a new Sauropod Clade. *Science*, 314, 1925–1927.
- Royo-Torres, R., Upchurch, P., Kirkland, J. I., DeBlieux, D. D., Foster, J. R., Cobos, A., et al. (2017). Descendants of the Jurassic turiasaurs from Iberia found refuge in the Early Cretaceous of western USA. *Scientific Reports*, 7, 14311.
- Royo-Torres, R., Upchurch, P., Mannion, P. D., Mas, R., Cobos, A., Gascó, F., et al. (2014). The anatomy, phylogenetic relationships and stratigraphic position of the Tithonian-Berriasian Spanish sauropod dinosaur *Aragosaurus ischiaticus*. *Zoological Journal of the Linnean Society*, 171, 623–655.
- Sander, P. M. (1999). Life history of the Tendaguru sauropods as inferred from long bone histology. *Mitteilungen aus dem Museum für Naturkunde der Humboldt-Universität Berlin, Geowissenschaftliche Reihe*, 2, 103–112.
- Sander, P. M. (2000). Longbone histology of the Tendaguru sauropods: implications for growth and biology. *Paleobiology*, 26, 466–488.
- Sander, P. M., & Klein, N. (2005). Developmental plasticity in the life history of a prosauropod dinosaur. *Science*, 310, 1800–1802.
- Sander, P. M., Mateus, O., Laven, T., & Knötschke, N. (2006). Bone histology indicates insular dwarfism in a new Late Jurassic sauropod dinosaur. *Nature*, 441, 739–741.
- Sauvage, H. E. (1874). Mémoire sur les dinosauriens et les crocodyliens des terrains jurassiques de Boulogne-sur-Mer. *Mémoires de la Société Géologique de France, 2ème série*, 10(2), 1–58.
- Schwarz, D., Ikejiri, T., Breithaupt, B., Sander, P. M., & Klein, N. (2007a). A nearly complete skeleton of an early juvenile diplodocid (Dinosauria: Sauropoda) from the Lower Morrison Formation (Late Jurassic) of North Central Wyoming and its implications for pneumaticity and early ontogeny in Sauropods. *Historical Biology*, 19(3), 225–253.
- Schwarz, D., Wings, O., & Meyer, C. A. (2007b). Super sizing the giants: first cartilage preservation at a sauropod limb joint. *Journal of the Geological Society*, 164, 61–65.
- Schwarz, D., Wings, O., & Meyer, C. A. (2007c). Taxonomische und systematische Revision von *Cetiosauriscus greppini* (Sauropoda). In O. Elicki & J. W. Schneider (Eds.), *Fossile Ökosysteme* (Vol. 36, p. 147). Wissenschaftliche Mitteilungen, Institut für Geologie: Freiberg.
- Seeley, H. G. (1887a). Note on some Dinosaurian Remains in the Collection of A. Leeds, Esq., of Eyebury, Northamptonshire. *Quarterly Journal of the Geological Society of London*, 43, 695–702.
- Seeley, H. G. (1887b). On the classification of the fossil animals commonly called Dinosauria. *Proceedings of the Royal Society London*, 43, 165–171.
- Soto, M., & Perea, D. (2008). A ceratosaurid (Dinosauria, Theropoda) from the Late Jurassic-Early Cretaceous of Uruguay. *Journal of Vertebrate Paleontology*, 28, 439–444.
- Steel, R. (1970). *Saurischia*. Stuttgart: Gustav-Fischer-Verlag.
- Stein, K., & Prondvai, E. (2013). Rethinking the nature of fibrolamellar bone: An integrative biological revision of sauropod plexiform bone formation. *Biological Reviews*, 89, 24–47.
- Tschopp, E., & Mateus, O. (2013). The skull and neck of a new flagellicaudatan sauropod from the Morrison Formation and its implication for the evolution and ontogeny of diplodocid dinosaurs. *Journal of Systematic Palaeontology*, 11(7), 853–888.
- Tschopp, E., & Mateus, O. (2017). Osteology of *Galeamopus pabsti* sp. nov. (Sauropoda: Diplodocidae), with implications for neurocentral closure timing, and the cervico-dorsal transition in diplodocids. *Peer J*. <https://doi.org/10.7717/peerj.3179>.
- Tschopp, E., Mateus, O., & Benson, R. B. J. (2015). A specimen-level phylogenetic analysis and taxonomic revision of Diplodocidae (Dinosauria, Sauropoda). *Peer J*. <https://doi.org/10.7717/peerj.857>.
- Upchurch, P. (1995). The evolutionary history of sauropod dinosaurs. *Philosophical Transactions of the Royal Society of London*, B, 349, 365–390.
- Upchurch, P. (1998). The phylogenetic relationships of sauropod dinosaurs. *Zoological Journal of the Linnean Society*, 124, 43–103.
- Upchurch, P., Barrett, P. M., & Dodson, P. (2004). Sauropoda. In D. B. Weishampel, P. Dodson, & H. Osmolska (Eds.), *The Dinosauria* (2nd ed., pp. 259–322). Berkeley: University of California Press.
- Upchurch, P., Mannion, P. D., & Taylor, M. P. (2015). The anatomy and phylogenetic relationships of "*Pelorosaurus*" *becklesii* (Neosauropoda,

- Macronaria) from the Early Cretaceous of England. *PLoS ONE*, 10(6), e0125819.
- Völkel, H. (1967). Allgemeines über die Anfertigung von Dünnschliffen und Anschliffen. *Der Präparator*, 13, 155–169.
- Walker, A. D. (1970). A revision of the Jurassic reptile *Hallopus victor* (Marsh), with remarks on the classification of crocodiles. *Philosophical Transactions of the Royal Society of London*, B, 257, 323–372.
- Wedel, M. J. (2003). The evolution of vertebral pneumaticity in sauropod dinosaurs. *Journal of Vertebrate Paleontology*, 23, 344–357.
- Wedel, M. J. (2005). Postcranial skeletal pneumaticity in sauropods and its implications for mass estimates. In K. A. Curry Rogers & J. A. Wilson (Eds.), *The sauropods: Evolution and paleobiology* (pp. 201–228). Berkeley: University of California Press.
- Wedel, M. J., Cifelli, R. I., & Sanders, R. K. (2000). Osteology, paleobiology, and relationships of the sauropod dinosaur *Sauroposeidon*. *Acta Palaeontologica Polonica*, 45, 343–388.
- Westphal, F. (1962). Die Krokodilier des deutschen und englischen Oberen Lias. *Palaeontographica Abt. A*, 118, 23–118.
- Whitlock, J. A. (2011). A phylogenetic analysis of Diplodocoidea (Saurischia: Sauropoda). *Zoological Journal of the Linnean Society*, 161(4), 872–915.
- Wilson, J. A. (1999). A nomenclature for vertebral laminae in sauropods and other saurischian dinosaurs. *Journal of Vertebrate Paleontology*, 19, 639–653.
- Wilson, J. A. (2002). Sauropod dinosaur phylogeny: critique and cladistic analysis. *Zoological Journal of the Linnean Society*, 136, 217–276.
- Wilson, J. A., D'Emic, M. D., Ikejiri, T., Macdieh, E. M., & Whitlock, J. A. (2011). A nomenclature for vertebral fossae in sauropods and other saurischian dinosaurs. *PLoS ONE*, 6(2), e17114.
- Wilson, J. A., & Sereno, P. S. (1998). Early evolution and higher-level phylogeny of sauropod dinosaurs. *Journal of Vertebrate Paleontology, Memoir*, 5(18), 1–68.
- Wilson, J. A., & Upchurch, P. (2009). Redescription and reassessment of the phylogenetic affinities of *Euhelopus zdanskyi* (Dinosauria: Sauropoda) from the Early Cretaceous of China. *Journal of Systematic Palaeontology*, 7(2), 199–239.
- Wings, O., Schwarz-Wings, D., & Fowler, D. W. (2011). New sauropod material from the Late Jurassic part of the Shishugou Formation (Junggar Basin, Xinjiang, NW China). *Neues Jahrbuch für Geologie und Paläontologie Abhandlungen*, 262(2), 129–150.
- Woodward, A. S. (1905). On parts of skeleton of *Cetiosaurus leedsi*, a sauropod dinosaur from the Oxford Clay of Peterborough. *Proceedings of the Zoological Society of London*, 1905, 232–243.
- Young, C. C., & Zhao, X. (1972). *Mamenchisaurus*. Institute of Vertebrate Paleontology and Paleoanthropology, Monograph Series I, No. 8, pp. 1–30.
- Young, M. T., Hua, S., Steel, L., Foffa, D., Brusatte, S. L., Thuring, S., et al. (2014a). Revision of the Late Jurassic teleosaurid genus *Machimosaurus* (Crocodylomorpha, Thalattosuchia). *Royal Society Open Science*, 1, 140222.
- Young, M. T., Steel, L., Brusatte, S. L., Foffa, D., & Lepage, Y. (2014b). Tooth serration morphologies in the genus *Machimosaurus* (Crocodylomorpha, Thalattosuchia) from the Late Jurassic of Europe. *Royal Society Open Science*, 1, 140269.

Publisher's Note

Springer Nature remains neutral with regard to jurisdictional claims in published maps and institutional affiliations.

Submit your manuscript to a SpringerOpen[®] journal and benefit from:

- Convenient online submission
- Rigorous peer review
- Open access: articles freely available online
- High visibility within the field
- Retaining the copyright to your article

Submit your next manuscript at ► [springeropen.com](https://www.springeropen.com)
